FEDERAL UNIVERSITY OF MINAS GERAIS
School of Engineering
Electrical Engineering Graduate Program

Lucas Savoi Araujo

Advanced Microgrids: Centralized Control for Coordination of Heterogeneous Converters

Belo Horizonte, MG
2022

FEDERAL UNIVERSITY OF MINAS GERAIS
School of Engineering
Electrical Engineering Graduate Program

Lucas Savoi Araujo

Advanced Microgrids: Centralized Control for Coordination of Heterogeneous Converters

Dissertation presented to the Graduate Program in Electrical Engineering of the School of Engineering of the Federal University of Minas Gerais in partial fulfillment of the requirements for the degree of Doctor in Electrical Engineering.

Advisor: Prof. Danilo Iglesias Brandao, PhD
Co-advisor: Prof. Braz de Jesus Cardoso Filho, PhD

Belo Horizonte, MG
2022

Araújo, Lucas Savoi de.
A663a Advanced microgrids [recurso eletrônico] : centralized control for coordination of heterogeneous converters / Lucas Savoi de Araújo. - 2022.
1 recurso online (126 f. : il., color.) : pdf.

Orientador: Danilo Iglesias Brandão.
Coorientador: Braz de Jesus Cardoso Filho.

Tese (doutorado) - Universidade Federal de Minas Gerais, Escola de Engenharia.

Apêndices: f. 121-126.

Bibliografia: f. 106-120.
Exigências do sistema: Adobe Acrobat Reader.

1. Engenharia elétrica - Teses. 2. Conversores - Teses. 3. Energia elétrica - Distribuição - Baixa tensão - Teses. 4. Geração distribuída de energia elétrica - Teses. I. Cardoso Filho, Braz de Jesus. II. Universidade Federal de Minas Gerais. Escola de Engenharia. III. Título.

CDU: 621.3(043)

Ficha catalográfica elaborada pela Bibliotecária Roseli Alves de Oliveira CRB/6 2121
Biblioteca Prof. Mário Werneck, Escola de Engenharia da UFMG

TESE DE DOUTORADO Nº 414

ADVANCED MICROGRIDS: CENTRALIZED CONTROL FOR COORDINATION OF HETEROGENEOUS CONVERTERS

Lucas Savoi de Araújo

DATA DA DEFESA: 07/10/2022

UNIVERSIDADE FEDERAL DE MINAS GERAIS
ESCOLA DE ENGENHARIA
PROGRAMA DE PÓS-GRADUAÇÃO EM ENGENHARIA ELÉTRICA

FOLHA DE APROVAÇÃO

"ADVANCED MICROGRIDS: CENTRALIZED CONTROL FOR COORDINATION OF HETEROGENEOUS CONVERTERS"

LUCAS SAVOI DE ARAÚJO

Tese de Doutorado submetida à Banca Examinadora designada pelo Colegiado do Programa de Pós-Graduação em Engenharia Elétrica da Escola de Engenharia da Universidade Federal de Minas Gerais, como requisito para obtenção do grau de Doutor em Engenharia Elétrica. Aprovada em 07 de outubro de 2022. Por:

Prof. Dr. Danilo Iglesias Brandão
DEE (UFMG) - Orientador

Prof. Dr. Braz de Jesus Cardoso Filho
DEE (UFMG)

Prof. Dr. José Antenor Pomilio
FEEC (UNICAMP)

Prof. Dr. Sérgio Augusto Oliveira da Silva
DEE (UTFPR)

Prof. Dr. Sidelmo Magalhães Silva
DEE (UFMG)

Prof. Dr. Thiago Ribeiro de Oliveira
(UFMG)

Documento assinado eletronicamente por **Danilo Iglesias Brandao**, **Professor do Magistério Superior**, em 10/10/2022, às 13:43, conforme horário oficial de Brasília, com fundamento no art. 5º do Decreto nº 10.543, de 13 de novembro de 2020.

Documento assinado eletronicamente por **Jose Antenor Pomilio**, **Usuário Externo**, em 10/10/2022, às 14:46, conforme horário oficial de Brasília, com fundamento no art. 5º do Decreto nº 10.543, de 13 de novembro de 2020.

Documento assinado eletronicamente por **Sérgio Augusto Oliveira da Silva**, **Usuário Externo**, em 10/10/2022, às 18:55, conforme horário oficial de Brasília, com fundamento no art. 5º do Decreto nº 10.543, de 13 de novembro de 2020.

Documento assinado eletronicamente por **Thiago Ribeiro de Oliveira**, **Professor do Magistério Superior**, em 11/10/2022, às 10:01, conforme horário oficial de Brasília, com fundamento no art. 5º do Decreto nº 10.543, de 13 de novembro de 2020.

Documento assinado eletronicamente por **Sidelmo Magalhaes Silva**, **Professor do Magistério Superior**, em 11/10/2022, às 16:48, conforme horário oficial de Brasília, com fundamento no art. 5º do Decreto nº 10.543, de 13 de novembro de 2020.

Documento assinado eletronicamente por **Braz de Jesus Cardoso Filho**, **Professor do Magistério Superior**, em 13/10/2022, às 14:04, conforme horário oficial de Brasília, com fundamento no art. 5º do Decreto nº 10.543, de 13 de novembro de 2020.

A autenticidade deste documento pode ser conferida no site https://sei.ufmg.br/sei/controlador_externo.php?acao=documento_conferir&id_orgao_acesso_externo=0, informando o código verificador **1806253** e o código CRC **D7C78335**.

To my grandfather,

Luiz Savoi.

Acknowledgments

The work as a researcher is intrinsically multidisciplinary. In addition to literary research and development activities, it is part of the researcher's routine to write the methodology, results and conclusions in a clear and precise way. Thus, the society and the scientific community may access it and take a step forward in knowledge. The preparation of this material involves a series of skills, such as writing, statistical analysis, drawing, equating, simulating, prototyping, among others.
It is often mostly individual work, in which much of the activities are done by ourselves. However, paradoxically, this work is never done alone. The greater the collaboration and interaction of people involved in the development of the research, the better the quality of the work. During almost five years of my doctorate, many people supported me in my professional and personal formation, and in the development of my research. I met amazing people and made friends that I hope to keep for the rest of my life. I dedicate this space to thank, mainly, the people who were part of this journey.

First and foremost, I would like to thank my advisor Prof. Danilo Iglesias Brandao, who received me very well at the very first meeting, and since then has been guiding me with valuable and enriching contributions that help me to grow professionally as a researcher and as a professor. Prof. Danilo is an example of a great dedicated professional, but also an excellent person with exceptional character. I also thank you for the friendship of these years and for promptly giving me the attention I needed. All the results presented in this dissertation and my doctoral achievements are due to the good relationship during these years.

I would also like to thank everyone who is part of the Tesla Laboratory - Power Engineering, at UFMG, especially Prof. Braz J. Cardoso Filho, my co-advisor, who works hard for the laboratory to have a cutting-edge structure, prospecting projects and who always has rich comments on any topic. Thanks also to Prof. Sidelmo M. Silva, Prof. Igor A. Pires, Prof. Thales A. C. Maia for all interaction and collaboration during the developed research projects and for the development of this dissertation.

Very special and important thanks to my colleagues at the Tesla laboratory who have always collaborated in the development of research projects and in this dissertation. Besides, there were many pleasant moments of relaxation during these year at lunches, cafes and bars in Belo Horizonte. Especially thanks to my dear friends: Antônio Gamaliel, Diogo

Galo, Fernando Amaral, Geovane dos Reis, Gideon Lobato, Gustavo Fontoura, João Henrique Oliveira, Rafael Átila Silva, Reginaldo Vagner Ferreira, Rodrigo Rodrigues Bastos, Tamires Santos de Souza and Thiago Parreiras.

A kind and warm thanks to Arlete Vidal, for always taking care of everything and everyone, and making the laboratory more like a welcoming home in a family environment.

I am thankful to everyone who took part in my doctoral period at the Power Electronics Group of the University of Padova, Italy. Thanks to Prof. Paolo Mattavelli and Prof. Giorgio Spiazzi; and especially to Prof. Tommaso Caldognetto, who is a great person, and received me with great sympathy and taught me so much in just a few months. Thank you for all the interaction during the development of the research, which is always technically enriching and pleasant at the same time. Thank you my friends from the laboratory who, in addition to work, participated in a very nice and important period of my life in Italy, thank you: Stefano Cabizza, Giovanni Bonanno, Ezio Gallo, Ahmed Yahia Farag, Filip Cvejic, Ruzica Cvetanovic and Ivan Petric.

I would like to thank the professors who participated in my doctoral defense: Prof. José A. Pomilio, Prof. Sérgio A. O. da Silva, Prof. Sidelmo M. Silva and Prof. Thiago R. de Oliveira, who enriched the discussion and contributed to the development of this work since the qualification, increasing the quality of this final version.

I thank the institutions: UFMG and PPGEE, all professors, technicians and employees, and for the Oasis Project support; UniPD, for welcoming me; FAPEMIG, for the scholarship support during the doctorate; CAPES, for the sandwich doctorate scholarship support; CNPq; and Petrobras, for the research project support.

Thanks to all those who were not mentioned, but who contributed somehow to the completion of this work.

Thanks to all the people who believe that the development of science is linked to the development of society, and to the Brazilian people who indirectly finance national research.

I thank all my family with my heart, especially my parents, Ernani and Luciana, two great examples of overcoming challenges, who always inspire me in the motivation to live.

And finally, I thank God for life, health and for putting all these special people in my path.

Abstract

Environmental concerns concomitant with the steady growth of energy demand have triggered government guidelines and interventions encouraging renewable-based distributed generators in low-voltage grids. Advanced microgrid (MG) is a promising model for reaching the goal of 100% renewable grid. A complete advanced MG control strategy must steer the power flow in grid-connected mode, regulate voltage/frequency in islanded mode, and perform power sharing between distributed energy resources (DERs) in both modes. Centralized control approaches, such as the power-based control (PBC), are well-known for achieving these three targets. A serious disadvantage of centralized MG structure using PBC approach is the existence of a single central converter to form the islanded MG. Central converter is a single point of failure, which reduces the capability of the MG expansion, and it is an expensive element for implementation of MGs. Thus, the objective of this work is to develop an improved MG structure using PBC together with a droop-based power-loop in voltage-controlled mode (VCM) converters. This allows the MG to operate in both modes without a central converter. The developed strategy achieves grid power flow control, power sharing, unbalanced current compensation, voltage/frequency restoration and smooth transitioning between modes without critical islanding detection. Moreover, the new approach considers single- and three-phase DERs, controlled in VCM or current-controlled mode, and DERs with self-imposed limits, characterizing a heterogeneous MG. Heterogeneous MG is closer to real-world practical application where several sorts of multi-owners converters comprise a coordinated MG to achieve common goals. Theoretical, simulation and hardware-in-the-loop tests are conducted to: first, develop a control for VCM converters to avoid the necessity of central converter; second, develop a centralized control for advanced MGs that considers heterogeneous converters; and, finally, to develop a control approach for harmonics compensation when VCM converters are connected to distorted grids. Real-time hardware-in-the-loop setup is used as primary method for validating the proposed development under several operating conditions. Results support the conclusion that centralized control proves to be a remarkable solution for advanced MG issues.

Keywords: Centralized control, distributed generation, droop control, harmonics, heterogeneous converters, microgrids, smooth transition, unbalance compensation.

Resumo

Preocupações ambientais e o crescimento da demanda de energia elétrica desencadearam diretrizes governamentais, incentivando recursos de energia distribuídos (DERs) de base renovável em redes de baixa tensão. Microrrede (MG) avançada é um modelo promissor para atingir a meta de rede 100% renovável. Uma estratégia de controle completa para MG deve controlar o fluxo de potência no modo conectado à rede, regular a tensão/frequência no modo ilhado e realizar o compartilhamento de potência entre os DERs em ambos os modos. Abordagens de controle centralizado, como o *power-based control* (PBC), são conhecidas por alcançar esses três objetivos. Uma desvantagem da estrutura de MG centralizada que utiliza o PBC é a existência de um único conversor central para formar a MG ilhada. O conversor central é um único ponto de falha, o que reduz a capacidade de expansão da MG, além de ser um elemento caro para a implementação de uma MG. Assim, o objetivo deste trabalho é desenvolver uma estrutura de MG aprimorada, que utiliza o PBC em conjunto com um conversor controlado por tensão (VCM) integrado de uma malha de potência baseada em droop. Isso permite que a MG opere em ambos os modos sem um conversor central. A estratégia desenvolvida realiza controle do fluxo de potência da rede, compartilhamento de potência, compensação de desequilíbrio de corrente, restauração de tensão/frequência e transição suave entre os modos sem detecção de ilhamento crítico. Além disso, a nova abordagem considera DERs monofásicos e trifásicos, controlados por tensão ou por corrente, e DERs com restrições auto-impostas, caracterizando uma MG heterogênea. A MG heterogênea está mais próxima da aplicação prática do mundo real, em que vários tipos de conversores de proprietários diversos formam uma MG coordenada para alcançar objetivos comuns. Estudos teóricos, de simulação e em *hardware-in-the-loop* são conduzidos para: primeiro, desenvolver um controle para conversores VCM a fim de evitar a necessidade de conversor central; segundo, desenvolver um controle centralizado para MGs avançadas que inclua conversores heterogêneos; e, finalmente, desenvolver uma abordagem de controle para compensação de harmônicos quando conversores VCM são conectados a redes distorcidas. Um *setup* em *hardware-in-the-loop* é usado como método principal para validar o desenvolvimento proposto. Os resultados sustentam a conclusão de que o controle centralizado seja uma solução notável para problemas de MG avançadas.

Palavras-chave: Compensação de desequilíbrio, controle centralizado, controle por inclinação, conversores heterogêneos, geração distribuída, microrredes, transição suave.

List of Figures

1.1 Three-phase microgrid structures with a) single- and three-phase distributed units, considering CCM and VCM DERs; b) U.I. and CCM DERs. 27

3.1 MG structure and grid–forming converter electric diagram. 44
3.2 Possible switch S_1 configuration: a) Three-phase contactor; b) Three-phase contactor in parallel with a three-phase solid-state relay (SSR). 44
3.3 Power control loop of the grid–forming converter. 45
3.4 Current and voltage control loops of the grid–forming converter. 46
3.5 Droop curve with external power–loop: a) $P - \omega$; b) $Q - V$. 47
3.6 Model for the inner a) current– and b) voltage–loop controller design. . . . 49
3.7 Simplified grid–connected converter model. 51
3.8 Small-signal model for the external a) active power– and b) reactive power–loop controller design. 52
3.9 Hardware-in-the-loop setup for control validation. 55
3.10 a) Step response of active power; b) Step response of reactive power. . . . 56
3.11 Results of the transition from grid–connected to islanded operation. (Ch1:40V/V; Ch2:12A/A; Ch3:12A/A; Ch4:1Hz/V – 60Hz offset.) 57
3.12 Results of the secondary control in islanded mode. a) Ch1:40V/V; Ch2:16A/A; Ch3: 1Hz/V – 60Hz offset; Ch4: 5V/V – 127V offset. b) Ch1: 2000W/V; Ch2:2000var/V; Ch3:2000W/V; Ch4:2000var/V. 58
3.13 Results of the transition from islanded operation to grid–connected. a) Ch1:40V/V; Ch2:40V/V; Ch3:1Hz/V – 60Hz offset; Ch4:1V/V. b) Ch1:12A/A; Ch2:16A/A; Ch3:12A/A; Ch4:12A/A. 59
3.14 Results of the power control with a) Grid frequency variation (Ch1:12A/A; Ch2:1Hz/V – 60Hz offset; Ch3:2000W/V; Ch4:2000var/V.); and b) Grid voltage variation (Ch1:12A/A; Ch2:5V/V – 127V offset; Ch3:2000W/V; Ch4:2000var/V.). 61
3.15 Results of mode transition from grid–connected to islanded operation with different load conditions. (Ch1:40V/V; Ch2:1Hz/V – 60Hz offset; Ch3:16A/V ; Ch4:12A/V.) 62

3.16 Results of different switch S_1 closing time in the reconnection process. a) Switch S_1 closing time delay of $40ms$. b) Switch S_1 closing time delay of $80ms$. (Ch1: 1V/V; Ch2:12A/A; Ch3:12A/A; Ch4:12A/A). 64
3.17 Results of different signal flag receiving time in the reconnection process. a) DERs currents and flag receiving time. (Ch1: 1V/V; Ch2:1V/V; Ch3:12A/A; Ch4:12A/A) b) Grid and PCC voltages, grid current and MG frequency at reconnection time. (Ch1: 40V/V; Ch2:40V/V; Ch3:1Hz/V; Ch4:12A/A). . 65
3.18 Results of mode transition from grid–connected to islanded operation with different line impedance between converters. (Ch1:2000W/V; Ch2:2000var/V; Ch3:2000W/V ; Ch4:2000var/V.) 66
3.19 Results of mode transition from grid–connected to islanded operation for converters with different power ratings. (Ch1:2000W/V; Ch2:2000var/V; Ch3:2000W/V ; Ch4:2000var/V.). 66

4.1 a) Low-voltage three-phase microgrid. b) MG hierarchical control architecture. 68
4.2 Three-phase Microgrid structure with heterogeneous converters. 70
4.3 Primary control of CCM and VCM DERs. 71
4.4 Power control loop of VCM DERs. 71
4.5 Flowchart of maximum reactive power evaluation. 77
4.6 Restoration Control diagram at Central Controller. 79
4.7 Hardware-in-the-loop setup for control validation. 81
4.8 HIL Results: Grid-connected mode - PBC activation. 82
4.9 HIL Results: Grid-connected mode - performance under grid power step; a) PCC quantities; b) DERs quantities. 82
4.10 HIL Results: Grid-connected 3ϕ-VCM converter operating balanced. 83
4.11 HIL Results: Performance under grid voltage sag. 84
4.12 HIL Results: Performance under grid frequency variation. 84
4.13 HIL Results: Grid-connected mode - performance under load step; a) PCC quantities; b) DERs quantities. 85
4.14 HIL Results: Transition from grid-connected to islanded mode; a) PCC quantities; b) DERs quantities. 86
4.15 HIL Results: Islanded operation mode. 87
4.16 HIL Results: Islanded operation mode - PV withdraw. 88
4.17 HIL Results: Transition from islanded to grid-connected mode; a) PCC quantities; b) DERs quantities. 89

5.1 Simplified model of a grid-connected converter. 92
5.2 Normalized relations between synchronization error and current flow. . . . 93
5.3 Application example of the proposed control. 94

5.4 PCC Measurement System structure. 95
5.5 a) VCI control structure; b) Harmonic compensation block detailed. 96
5.6 Experimental setup for the proposed method validation. 97
5.7 Electrical circuit implemented in HIL. 98
5.8 Results for distorted grid voltage and no load. 99
5.9 Results for distorted grid voltage and RC load. 99
5.10 Results for distorted grid voltage and RL load. 100
5.11 Results for sinusoidal grid voltage and distorted load. 101

A.1 Block diagram of the single-controllable microgrid. 122
A.2 Real installation of the single-controllable microgrid at UFMG, Brazil. . . 123
A.3 Results of the energy time shifting operation: DER power, charged DER energy, discharged DER energy and SOC value during the energy time shift using three different battery banks: lithium-ion (DERab), lead-acid (DERbc) and sodium-nickel (DERca). 126

List of Tables

2.1 Summary of literature review on grid-forming converters. 35
2.2 Evolution of PBC Strategy for MG Application 38

3.1 Maximum and minimum frequency and voltage values in temporary operation 54
3.2 System and Control Parameters 56

4.1 DERs rated power 80
4.2 Line impedances parameters. 80

5.1 System parameters 98
5.2 Performance comparison of the approaches 101

List of abbreviations and acronyms

APF	–	Active power filter
BESS	–	Battery energy storage systems
CC	–	Central Controller
CCM	–	Current-controlled mode
DER	–	Distributed Energy Resource
DOB	–	Disturbance observer
DSO	–	Distribution system operator
EEUFMG	–	School of Engineering at the Federal University of Minas Gerais
EMS	–	Energy Management System
GC	–	Grid-connected
GPS	–	Global positioning system
HCVM	–	Hybrid current and voltage mode
ICT	–	Information and Communication Technology
IS	–	Islanded
LPF	–	Low-pass filter
LV	–	Low-voltage
MAF	–	Moving Average Filter
MG	–	Microgrid
MPPT	–	Maximum Power Point Tracking
MV	–	Medium-voltage
PBC	–	Power-Based Control
PCC	–	Point-of-Common-Coupling
PMS	–	PCC measurement system
PES	–	Primary Energy Source
PLL	–	Phase-Locked Loop
PoC	–	Point of connection
PV	–	Photovoltaic
PWM	–	Pulse Width Modulation
SSR	–	Solid-state relay
UI	–	Utility Interface
UPS	–	Uninterruptible power supply

VCI	–	Voltage-controlled inverter
VCM	–	Voltage-controlled mode
VSG	–	Virtual synchronous generator
THD	–	Total harmonic distortion

Contents

1 Introduction **21**

1.1 Motivation and Relevance 23
1.2 Microgrid Structure and Problem Statement 26
1.3 Objectives 28
1.3.1 Main objective 28
1.3.2 Secondary objectives 28
1.4 Contributions 29
1.5 Publications 30
1.5.1 Journal Papers 30
1.5.2 Conference Papers 31
1.6 Dissertation Outline 31

2 Literature Review **33**

2.1 Introduction 33
2.2 On Grid-forming Converter Control 33
2.3 On Secondary Control for Advanced MGs 36
2.4 On Harmonics Compensation for VCM Converters 39
2.5 Conclusions 41

3 Self–adaptive Control for Grid-forming Converter **42**

3.1 Introduction 42
3.2 Proposed Control for Self–adaptive Grid–forming Converter 43
3.2.1 External power–loop 44
3.2.2 Inner voltage and current control loops 45
3.2.3 System Operation 46
3.3 Design of Control Parameters 49
3.3.1 Inner loops controllers 49
3.3.2 Droop control parameters 50
3.3.3 External power–loop controllers 50
3.3.4 Sizing the Coupling Inductor 52
3.3.5 External power–loop saturators limits 53

3.3.6 Reconnection frequency definition . . . 54
3.4 Real-time Hardware-in-the-loop Results . . . 54
3.4.1 Power-loop controller model verification . . . 55
3.4.2 Seamless grid-connected to islanded operation transition . . . 57
3.4.3 Secondary control in islanded mode . . . 57
3.4.4 Islanded operation to grid-connected transition . . . 59
3.4.5 Power control under grid voltage variation . . . 60
3.4.6 Different load conditions in mode transition . . . 60
3.4.7 Evaluation of delays in the reconnection process . . . 62
3.4.8 Islanded operation under adverse conditions . . . 63
3.5 Conclusions . . . 64

4 Centralized Control for Heterogeneous Converters 67
4.1 Introduction . . . 67
4.2 Hierarchical Control . . . 68
4.3 Microgrid Structure and Converters Control . . . 69
4.3.1 DERs self-imposed limits . . . 71
4.4 Centralized Control for Heterogeneous Distributed Converters . . . 72
4.4.1 Modified Power-based Control . . . 73
4.4.2 3-phase VCM DERs References and Restoration Control . . . 78
4.5 Real-time Hardware-in-the-loop Results . . . 79
4.5.1 Grid-connected operation . . . 80
4.5.2 Transition from grid-connected to islanded operation . . . 85
4.5.3 Islanded operation mode . . . 85
4.5.4 Reconnection transition . . . 87
4.6 Conclusions . . . 88

5 Harmonic Voltage Synchronization for Grid-connected Converters 90
5.1 Introduction . . . 90
5.2 Theoretical Background . . . 91
5.2.1 Phase-mismatch influence in parallel voltage-sources . . . 92
5.3 GPS-based Harmonic Voltage Synchronization . . . 93
5.3.1 PCC Measurement System . . . 94
5.3.2 Voltage-controlled inverter control . . . 95
5.4 Real-time Hardware-in-the-loop Results . . . 97
5.4.1 Distorted grid voltage—No load . . . 98
5.4.2 Distorted grid voltage—RC load . . . 98
5.4.3 Distorted grid voltage—RL load . . . 99
5.4.4 Sinusoidal grid voltage—Distorted load . . . 100
5.5 Conclusions . . . 101

6 Conclusions and Research Perspectives **103**
6.1 Conclusions 103
6.2 Research Perspectives 105

Bibliography **106**

A TESLA-UFMG Microgrid: A Practical Implementation **121**
A.1 Introduction 121
A.2 Microgrid Structure and Control 121
A.2.1 Microgrid structure 121
A.2.2 Control and Organization 123
A.2.3 Communication Infrastructure 123
A.3 Single-Controllable Microgrid Operating Modes 124
A.4 Experimental Results - Energy time shift 125
A.5 Conclusions 125

Chapter 1

Introduction

The electricity supply over the years has been made mainly by large centralized synchronous generators. This scenario has allowed a very important increase in the share of the population with access to electrical energy. However, the generation of electricity has been monopolized and end-users did not have much choice of how to get electrical energy [1]. Recently, government interventions have encouraged renewable-based distributed energy resources (DERs) into the low-voltage (LV) networks. These guidelines are triggered by the steady growth in electricity demand – global electricity demand rose by 4% in 2018 [2] – concomitant with environmental concerns and rising in energy costs. Electricity supply systems, operating on 100% renewable energy with the major proportion from variable renewables, are technically feasible, reliable and affordable for many countries and regions of the world [3]. As an example, Denmark plans to run its entire energy system on renewable energy by 2050, with wind as its main power source [4]; and the European Union targets at least 32% share for renewable energy by 2030 [5]. Reaching the goal of 100% renewable grid requires integration of battery energy storage systems (BESS), electric vehicles and variable renewable energy sources [6]. Besides, DERs owned by end-users will substantially support the cost for greener electric power systems while enhancing their role in the energy market [7]. The increase in electricity generation through low voltage DERs, invested by end-users, is a paradigm shift from previous years.

Renewable energy sources, battery energy storage systems and electric vehicles are connected to the main grid through electronic converters and are characterized as DERs. Areas with heavy penetration of DERs may face some issues (e.g., over-voltage and feeders congestion) that hinder additional installations. However, beyond the ability of active power injection, DERs can offer ancillary services, such as injection of reactive power and reduction of frequency/voltage deviations [8]. Besides, encouraging reactive power markets to promote the participation of DERs in a coordinated way can bring high economical and technical benefits [9].

The microgrid (MG) model is a communication-based solution that enables safe and reliable operation of electric power grids, as well as accommodating the growing

number of DERs. In general, an advanced MG can be defined as a set of loads, generators and storage systems interconnected in a single and controllable electrical system that can operate islanded and connected to the conventional grid [10].

Advanced MGs model not only increases the penetration of renewable sources, but also improves grid power quality, availability, efficiency, hosting capacity and provision of ancillary services through proper coordination of DERs. Three main targets are mandatory for advanced MGs: *i*) operate in grid-connected mode and regulate the power flow with the upstream grid; *ii*) operate in islanded mode and control voltage and frequency; and *iii*) coordinate DERs through power sharing methods, avoiding undesirable current circulation in both grid-connected and islanded modes.

The MG coordinated control allows offering active, reactive, unbalanced and harmonic power sharing between DERs. In addition, allowing power flow control at the point-of-common-coupling (PCC), contributes to the improvement of the system power quality. Moreover, it allows LV MGs to be dynamically controlled and dispatchable [11]. The single-controllable structure steers active and reactive power at the PCC and may contribute to the voltage regulation in the medium–voltage (MV) system [12, 13]. Dispatchable microgrids can support the operations of the electrical distribution networks providing a variety of ancillary services to the utility grid and to the microgrid itself [14]. In this way, other tariff modalities can be created allowing the MG to explore ancillary services markets in a coordinated manner and be compensated for it. Also, exporting energy at times that are beneficial to the utility would free up traditional generators, reducing the use of costly thermoelectric plants that are harmful to the environment.

Although MGs have been extensively studied in recent years [15], several aspects of their management and operation require further study. Among many gaps in literature, forming a flexible structure of MG has gained attention [16]. This structure includes mutually coordinated single- and three-phase converters to perform power sharing, as well as power imbalance compensation functionality. In LV three-phase networks, the random installation of single-phase DERs from residential households, interconnected with unbalanced loads, may cause voltage imbalance and inter-phase power flow circulation among the phases of the network. Thus, the MG model is adopted to accomplish safe and efficient coordination of distributed units.

In addition to the power quality requirements, in a real world scenario a MG must accommodate diverse sorts of DERs in terms of primary energy sources, converters topology, and control scheme. In general, electric vehicles and renewable sources with small batteries are single- or three-phase converters and operate in current-controlled mode (CCM). Large battery storage systems are normally three-phase converters and operate in voltage-controlled mode (VCM). Also, some converters may show self-limitations on processing reactive power, operating unbalanced, or must always track the maximum power point, such as conventional photovoltaic (PV) inverters. The exhaustive development of

the MG structure and control is the first step towards future Smart Grids.

1.1 Motivation and Relevance

Considering that most renewables have intermittent characteristics, energy storage is an indispensable part of MGs, both for storing excess energy when available energy is greater than energy consumed; as to provide power in times of scarcity, where demand exceeds generation [17].

In advanced MGs energy storage can be used to control the power flow from or to the main grid in connected mode. This enables MGs to assist the operation of a stable power grid, providing better power quality and voltage control. In addition, this configuration allows the development of new business models where the MG disconnects or reconnects under the best economic conditions.

The factors driving MG development and deployment in locations with existing electrical grid infrastructure fall into three broad categories: energy security, economic benefits, and clean energy integration [18]. The use of MG technology is already feasible in: areas with high electricity prices – remote locations such as islands that have historically used high cost fuel for electricity; or in facilities such as military bases [19], data centers and hospitals that cannot risk running out of power. The MG market is booming and includes :

- *Remote Microgrid*: Also called off-grid or isolated MG, this type of MG is in geographically remote areas (e.g., islands, rural areas, indigenous villages, offshore platforms, navigation) with little or no interconnection to the main power grid. The main objectives are electricity access, better power quality and reducing costs with fossil fuel. In [20, 21] is shown a successful case of MG implementation in Lençóis Island in Maranhão – Brazil.

- *Commercial and Industrial Microgrid*: This MG may be single or multi-owner. These may be medium voltage companies or industries that wish to use energy from renewable sources and which, together with batteries, may obtain financial and environmental advantages over the use of diesel generators. In [22] and [23], it is shown the feasibility of using battery power for peak-shaving function. In addition, a MG could provide high power quality and uninterruptible power supply (UPS) function. In [24] there are several MG implementation examples around the world, e.g., the Peña Station NEXT which is a 382-acre transit-oriented development adjacent to the Denver International Airport (DEN). The project is a public-private partnership with contributions from a variety of stakeholders, including Xcel Energy, Panasonic, Younicos, and the airport of Denver. The development showcases a variety of smart city and energy technologies, including smart street lighting and electric vehicle

charging stations. This MG features Solar PV Grid Integration, Grid Peak Demand Reduction, Energy Arbitrage, Frequency Regulation and Resilience Through Backup Power.

- *Community Microgrid*: This type of MG is mainly present in urban and rural residential areas. For urban areas in Brazil, LV residential condominiums can obtain benefits using the new tariff *"Tarifa Branca"* [25], offering similar economic advantages of medium-voltage consumers with different on-peak and off-peak consumption tariffs. In rural areas, however, consumers can benefit from existing financing programs for photovoltaic power installation in Brazil [26], and save money by replacing diesel generators with battery-powered microgrids. Thus, enabling more independence of external power supply and independence of electricity costs. [27] presents the architecture, control and operating modes of a MG project under construction in a residential condominium in Fortaleza – CE, Brazil.

- *Utility Microgrid*: This technology allows utilities to manage DERs, enabling increased insertion of renewable sources into distribution grids and improved power quality at the point of installation. The Ameren microgrid installed at the utility's Technology Applications Center in Champaign, Illinois, serves an active utility distribution feeder and can provide more than 1 MW of power to local customers when paralleled with the distribution grid, improving reliability and resiliency [24]. It is one of the few MGs in the world that operates at utility-scale/medium voltages (4-34.5 kV). It also employs a unique military-grade cybersecure MG control system and intelligent automation scheme to seamlessly transition power from islanded mode back to grid-connected mode for the entire distribution circuit. The system features solar, wind, natural gas generator and battery.

- *Institutions and Campi Microgrids*: As the name implies, this type of MG includes buildings with a unique property, such as a campus or institution. The goal is to increase reliability, energy quality and the inclusion of renewable sources. The Shanghai Microgrid Demonstration [28] is a collaboration between Aalborg University in Denmark and Tsinghua University in China. This project developed a "demonstrative, research-oriented platform, which aims to ease integrating distributed generation units, hierarchical and multilevel control strategies, and multiple microgrid configurations with the help of standard-based communication technology, resulting in a set of complete microgrid solutions". The MG includes 136 kW rooftop solar PV, 20 kW (2 x 10 kW) wind turbines, 50 kW energy storage system, Energy Management System (EMS) and smart grid communication technology. [29] presents important design decisions of the TESLA Power Engineering Photovoltaic Experimental Power Plant (37 kWp), connected to the power grid, which is located at the School of Engineering at the Federal University of Minas Gerais (EEUFMG). This PV power plant

is part of a future MG facility that will include three types of battery energy storage system technologies, controlled loads, programmable loads, a PCC central controller and a central converter.

- *Military Microgrid*: The main purpose of this segment focuses on power supply security, so that it is reliable in both grid-connected and islanded modes. Cost savings can also be associated by avoiding the use of diesel generators. The U.S. Army's Fort Bliss located in El Paso, Texas is a military MG example [30]. The 20-foot containerized BESS provided by Princeton Power Systems consists of one 100-kW grid-tied inverter and multiple advanced lead-acid batteries, capable of producing 20 kWh's of energy. In the event of a power outage, the BESS provides enough energy to power the base, thus allowing it to function as an independent energy resource. In addition to seamless transition during grid fault, the BESS also provides valuable support services, including power factor correction and area frequency regulation services to the local electrical system operator while it is connected to the electric grid.

Brazil is among the 10 largest consumers of electricity in the world [31], and around 625,000 people still live without electricity according to [32], mostly in rural areas, islands or isolated indigenous communities with difficult access and natural obstacles [33]. Remote and rural electrification is very expensive mainly due to the distance from centralized generation. An option for increasing access for these people is to use autonomously distributed generation with local renewable energy sources and storage systems in basic MGs, i.e., without grid power flow control.

In this context, even when electricity is available in rural areas of Brazil, it is usually very precarious [34, 35], with demand limitations and quality problems [36]. Brazilian utilities annually pay penalties to consumers due to violations of voltage levels and continuity indicators [37], money that could be used to investments and grid improvement. Thus, MGs appear as a quick, practical and possibly economical solution compared to diesel generators or rural refurbishment to improve the power quality of the rural population, increasing their demand, and considerably reducing the amount paid by utilities.

The commercial development of the MGs is still benefited by some trends, such as: the reduction of the cost of energy storage systems, the increasing accessibility of renewable energy and the constant increase of the electricity tariff by utilities. The price of lithium–ion batteries has reduced 40% from 2010 to 2014 [38] and there are projections that it will continue to decline [39–41]; also solar panels are becoming cheaper [42]. According to a report by Navigant Research [43], in 2018, the global market for remote MGs represented about U$3 billion in implementation expenses, and it is expected to jump to more than U$10.2 billion by 2027.

Therefore, the study and development of MG technology is extremely important,

with several potential beneficiaries such as: power utilities, industry directly involved (inverters, photovoltaic panels, batteries, electric vehicles), industries and businesses in general, residential condominiums, remote communities, military bases, hospitals, data centers, university campi, marine power grids, electric plane networks, oil & gas offshore platforms, among others.

The MG market in Brazil is on trend due to Brazilian Law No. 14.300 - 2022 [44], which establishes that utilities can remunerate distributed generation owners to provide ancillary services; and regulates the connection of batteries at the electricity grid. It is also feasible for the Brazilian Federal Government to use MGs in a new stage of the "*Luz para Todos*" program [45] to improve power quality in rural areas and to bring energy to isolated communities on seaside/riverside communities or indigenous islands. In this scenario, it would save fossil fuel, cabling structure and the use of costly underwater cables. Lastly, it is noteworthy the advantage of using MGs in environments threatened by environmental disasters, where small unaffected systems may continue to operate independently.

1.2 Microgrid Structure and Problem Statement

In this PhD dissertation, it is proposed the study and development of a hierarchical MG control, in which loads, generators and storage systems are allocated in a distributed way along an ac bus. An example of a MG with such architecture is shown in Fig. 1.1–a. The energy sources are connected to the MG bus through their respective converters. The loads are represented as any consumer of electricity. Further, the PCC is where the entire MG is connected or disconnected to the main power grid.

This MG topology represents a typical three-phase distribution system that includes both three-phase and single-phase converters. In addition, the converters are split into voltage or current controlled modes. Besides, for the MG smooth transition between its operating modes, there must be a control strategy that manages the operation of the converters. This heterogeneous situation, and closer to practical reality, is still rarely explored in literature, which mostly presents tests and solutions for cases that are little applicable, as discussed in detail in Section 2.3.

The coordination of DERs considered herein occurs through a Central Controller (CC) usually installed at the PCC. The CC is responsible for processing the Power-Based Control (PBC) algorithm, in which scaling coefficients are defined for the power contribution of each generator. Thus, converters are coordinated to perform active/reactive power sharing, and offering unbalance power compensation as ancillary services [11]. Consequently, a low data narrowband communication link is required to exchange information between CC and the DERs. The content of the data transmitted from the DERs to the CC comprises the current status of output powers and rated and generation capacities; the reverse path is basically constituted by the scaling coefficients that are detailed in

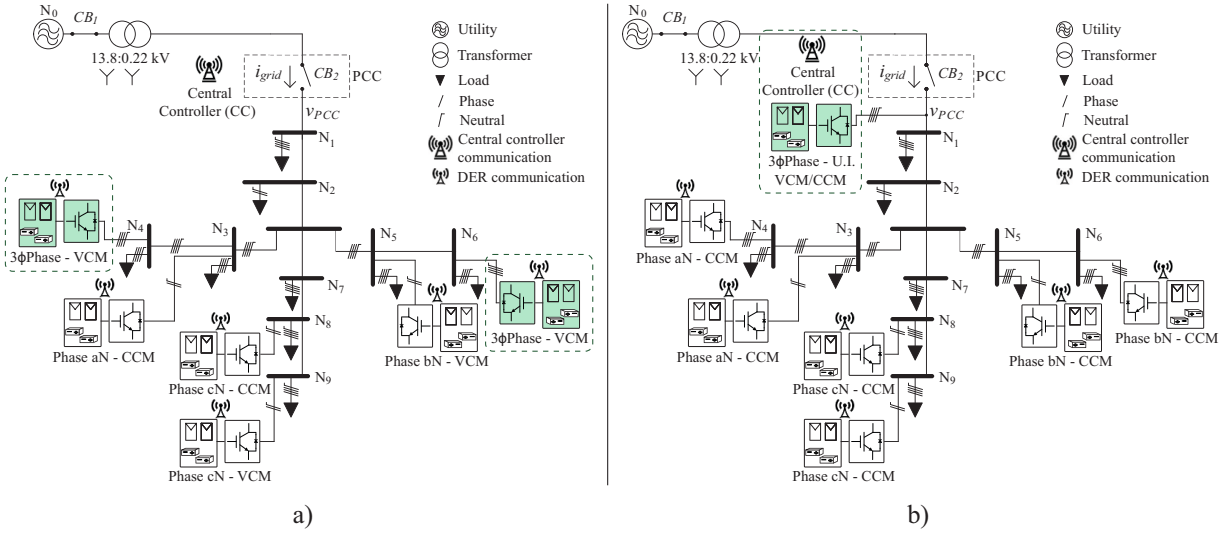

Figure 1.1: Three-phase microgrid structures with a) single- and three-phase distributed units, considering CCM and VCM DERs; b) U.I. and CCM DERs.

Chapter 4.

A hierarchical control divided in three main layers is considered. The primary layer is dedicated to the local control of each DER, with its basic functions. The PBC is implemented in the secondary layer. And the tertiary layer is controlled by the distribution system operator defining the references of grid power flow. The hierarchical control is fully detailed in Section 4.2.

Most works on the adoption of hierarchical centralized architecture usually comprises two classes of active components: a centralized utility-interactive converter and DERs, as shown in Fig. 1.1–b). The former operates in CCM as a grid-supporting converter during MG grid–connected mode, and it operates in VCM as grid–forming converter when the MG is islanded. Such converter, named Utility Interface (UI), is sited at the PCC and also guarantees smooth transition between MG operation modes [46]. The latter components can be further classified as grid-connected inverters usually operating in CCM. Such devices consist of DERs equipped with any sort of primary energy source.

The necessity of a central converter (i.e., UI) to form the islanded MG, as shown in Fig. 1.1–b), is considered a critical disadvantage of this approach. First, because it is difficult to design a converter to assume all the load transients when the MG is in islanded mode. Second, because it is a single point of failure, and it is critical during islanded operation. Third, because it reduces the capability of the MG expansion. And forth, because it is an expensive element for the MG. Besides, critical islanding detection is required, once the UI switches its operating mode, that is, switches from CCM to VCM, when the MG is islanded.

This gap is identified and the precursor goal of this work is to remove the central converter, but still maintain the centralized control, as shown in Fig. 1.1–a). Notably, the central controller is also a single-point of failure, however such an element is quite cheap

in a MG implementation, and its redundancy is feasible. For this, it is necessary that one or more converters assume the role of grid-forming converter in islanded operation. Thus, a new converter control structure is proposed to achieve smooth transition between grid-connected and islanded modes and correct parallelism between other converters. Also, an improved PBC, considering a new MG structure, is proposed and the same advantages of using the PBC with the UI are achieved. The new MG structure is more heterogeneous in terms of converters control and topology, and a central converter is no longer needed, which is a limitation of the previous proposals.

1.3 Objectives

1.3.1 Main objective

Considering the discussions presented and the benefits that may come from the spread of advanced MGs, the main objective of this work is to:

Develop a MG control strategy in which the central converter is replaced by distributed VCM converters (i.e., distributed grid-forming converters), being able to fulfill the three main targets for advanced MGs:

i) operate in grid-connected mode and regulate the power flow with the main grid;

ii) operate in islanded mode and control voltage and frequency;

iii) coordinate DERs through a power sharing method in both operating modes.

1.3.2 Secondary objectives

As secondary objectives arising from the primary one, this work aims to:

- Develop a self-adaptive control for grid-forming converter, i.e., VCM converter, capable of:
  - *i*) providing precise active/reactive power in grid-connected (GC) mode;
  - *ii*) performing seamless transitioning from GC to islanded (IS) mode;
  - *iii*) achieving proportional power sharing among other VCM converters;
  - *iv*) accomplishing smooth and automatic reconnection to the main grid.
- Integrate different sorts of converters in a MG control strategy, characterizing it as a heterogeneous MG.
- Compensate harmonic current circulation when a VCM converter is connected to a distorted grid.

1.4 Contributions

This dissertation main contributions are highlighted according to each topic related to the developed objectives:

1. **Self-adaptive control for grid-forming converter (Ch. 3)**

   A droop-based power-control loop is proposed capable of achieving the four main objectives required for grid-forming converters. The main novelty of this solution is the no need of high-speed communication between the converter and the CC, but rather a flag signaling is employed. Therefore, this solution can be deployed in large MG sites with several grid-forming converters. Additionally, this method is tolerant to grid voltage variation, and no critical islanding detection is required. This chapter also contributes with the development of a methodological procedure for properly designing power-loop controllers, limits values of saturators, and guidelines for practical applications.

2. **MG coordinated control for heterogeneous converters (Ch. 4)**

   The proposed MG control improves the so-called PBC and uses it together with the self-adaptive control for VCM converters. The main contribution of this new method is the absence of a central converter. Besides, it is proposed a complete centralized/hierarchical control for MGs capable of performing the following features, such complete MG control is not previously found in literature:

   - accurate grid power flow control;
   - proportional power sharing between all DERs;
   - unbalance compensation;
   - participation of single- and three-phase DERs;
   - participation of CCM and VCM converters;
   - participation of DERs with self-imposed constraints;
   - voltage and frequency restoration;
   - operation in both grid-connected and islanded modes;
   - smooth transitioning between operating modes;
   - no need for critical islanding detection.

3. **Compensation of harmonic current when VCM converters are connected to distorted grids (Ch. 5)**

   It is proposed a novel strategy that aims to synthesize, at the output of the VCM converter, the same harmonic voltage detected at the PCC. The harmonic voltage

reference for the VCM converter is synchronized with the PCC harmonic voltage using GPS modules; and its phase synchronization information and amplitude are broadcast by communication. The main contribution of this method is the voltage synchronization in grid-connected mode using low-bandwidth communication.

1.5 Publications

The results presented in this dissertation are a collection from research published in scientific journals and national and international conferences, as listed below:

1.5.1 Journal Papers

1. **L. S. Araujo**, D. I. Brandao, and B. J. Cardoso Filho, "Power-based Droop Control for Heterogeneous Converters connected in Microgrids," *Applied Energy*, 2022 – *under review.*

2. **L. S. Araujo**, T. Caldognetto, D. I. Brandao, and P. Mattavelli,"Harmonic Voltage Synchronization Using GPS Modules for Grid-Connected Power Converters," *IEEE Open Journal of Power Electronics*, 2022 – *under review.*

3. A. J. Masi, **L. S. Araujo**, T. Oliveira, D. I. Brandao, B. Cardoso Filho, T. A. C. Maia, "Advanced Microgrid: Active Power Flow Control and Communication Constraints," *Applied Energy*, 2022 – *under review.*

4. G. Reis, D. I. Brandao, J. Oliveira, **L. S. Araujo**, and B. J. Cardoso Filho, "Case Study of Single-Controllable Microgrid: A Practical Implementation,' *Energies*, vol. 15, no. 17:6400, 2022.

5. **L. S. Araujo** and D. I. Brandao,"Self-adaptive control for grid-forming converter with smooth transition between microgrid operating modes," *International Journal of Electrical Power & Energy Systems*, vol. 135, p. 107479, 2022.

6. **L. S. Araujo**, A. M. S. Alonso, D. I. Brandao, "Decentralized control of voltage-and current-controlled converters based on ac bus signaling for autonomous microgrids," *IEEE Access*, vol. 8, p. 202075-202089, 2020.

7. D. I. Brandao, **L. S. Araujo**, A. M. S. Alonso, G. L. dos Reis, E. V. Liberado, and F. P. Marafao, "Coordinated control of distributed three- and single-phase inverters connected to three-phase three-wire microgrids," *IEEE Journal of Emerging and Selected Topics in Power Electronics*, vol. 8, no. 4, pp. 3861-3877, 2020.

8. D. I. Brandao, **L. S. Araujo**, T. Caldognetto, J. A. Pomilio, "Coordinated control of three- and single-phase inverters coexisting in low-voltage microgrids," *Applied Energy*, vol. 228, p. 2050-2060, 2018.

1.5.2 Conference Papers

1. **L. S. Araujo**, T. Caldognetto, D. I. Brandao, and P. Mattavelli, "Circulating Harmonic Current Reduction in Distorted Voltage Conditions using GPS-based Synchronization," in *2022 IEEE 13th International Symposium on Power Electronics for Distributed Generation Systems (PEDG 2022)*, 2022, Kiel, Germany.

2. **L. S. Araujo**, N. T. D. Fernandes, D. I. Brandao, B. J. Cardoso Filho, "Smart-Battery: An Active-Battery Solution for Energy Storage System," in *2019 IEEE 15th Brazilian Power Electronics Conference (COBEP) and 5th Southern Power Electronics Conference (SPEC)*, 2019, Santos, SP, Brazil.

3. **L. S. Araujo**, D. I. Brandao, S. M. Silva, B. J. Cardoso Filho, "Reactive Power Support in Medium Voltage Networks by Coordinated Control of Distributed Generators in Dispatchable Low-Voltage Microgrid," in: *2019 IEEE 28th International Symposium on Industrial Electronics (ISIE)*, 2019, Vancouver, Canada.

4. **L. S. Araujo**, A. M. S. Alonso, W. M. Ferreira, H. P. Couto, D. I. Brandao, F. P. Marafao, J. A. Pomilio, "Estrategia De Controle Para Coordenacao De Conversores Monofasicos E Trifasicos Distribuidos Em Microrredes," in: *XXII Congresso Brasileiro de Automatica*, 2018, Joao Pessoa, PB, Brasil.

1.6 Dissertation Outline

This dissertation is outlined into six chapters, organized according to the development of the objectives of this work. The first chapter, Ch. 1, introduces the research topic, pointing out the problem statement, as well as the objectives and contributions of this work. Ch. 2 shows the literature review covering the main research studies that addressed the related objectives of this dissertation in order to highlight the literature gaps. To eliminate the necessity of a central converter, in Ch. 3, a control structure for dispersed VCM converters is proposed and developed. The proposed control enables multiple grid-forming converters to provide precise active/reactive power in GC mode, to achieve proportional power sharing, and to perform seamless transitioning between operating modes. In Ch. 4, the control of VCM converters developed in Ch. 3 is used in a MG with heterogeneous converters. A centralized control strategy, that is, a modified power-based control, is proposed to allow the MG to operate in grid-connected mode regulating

the PCC power flow, operate in islanded mode controlling voltage and frequency, and coordinate DERs through a power sharing method in both operating modes. Next, in Ch. 5, it is considered the scenario where a distorted grid is present. Thus, a control strategy for grid-connected VCM converters is proposed to limit unnecessary circulation of harmonic current. The research presented in Ch. 5 was developed during a short mobility exchange at the Power Electronics Group of University of Padova - Italy, under supervision of Prof. Tommaso Caldognetto and Prof. Paolo Mattavelli. For better organization and clarity, each development chapter presents experimental hardware-in-the-loop results to validate the effectiveness of the proposed solution. Finally, Ch. 6 discusses the general conclusions drawn from the dissertation and the research perspectives.

This work has been developed under the Research and Technological Development Program of the Electric Energy Sector regulated by ANEEL under the title "Technical and commercial arrangements for the insertion of energy storage systems in the Brazilian electric sector", project id ANEEL PD-00553-0046/2016, with Petrobras as the project proponent. As part of this project, it was implemented a real test-bench of a single-controllable microgrid in the Engineering School of the Federal University of Minas Gerais (UFMG) using commercial devices. Appendix A shows the most important aspects and details of this implementation, which uses the PBC as coordinated control for the inverters and for provision of ancillary services.

Chapter 2

Literature Review

2.1 Introduction

This chapter explores a literature review of the most recent papers related to the topics of the development of this dissertation, separated into:

1. Grid-forming converter control for smooth transition between MG operating modes;
2. Secondary control for advanced MGs; and
3. Harmonics compensation for VCM converters.

2.2 On Grid-forming Converter Control

In recent years, the research community has pursued the concept of grid–forming converter. This class of converter is capable of supporting the operation of an ac power system under normal, disturbed, and emergency conditions without relying on services from synchronous generators or synchronous condensers [47]. The grid–forming converter is a VCM converter with specific functionalities to operate in MGs:

i) precise output active/reactive power control in GC mode;

ii) seamless transitioning from GC to IS mode;

iii) proportional power sharing among VCM converters;

iv) smooth and automatic reconnection to the main grid.

Several types of control for VCM converters are proposed in literature to achieve these objectives, e.g., hybrid current and voltage mode (HCVM) control, virtual synchronous generator (VSG) and self–adaptive control. In the HCVM control, the inverter operates in CCM during the GC state, and in VCM during the IS state [48–50]. In this

method, it is necessary to switch between control modes depending on the MG operating mode, which requires extremely fast islanding detection to prevent high inrush currents and triggering electrical protection. In [51], a HCVM control is proposed and tested on a real MG with high-speed communication for islanding detection and grid synchronization. In VSGs, the converter is controlled to mimic the synchronous generators under grid and load disturbances. However, few works consider the transition between operating modes and, when examined [52], implementation is complex and requires measurements of grid quantities in real-time. Thus, this approach hinders the use of multiple grid-forming converters.

The most recent and adherent works that consider seamless or smooth transition of grid-forming converters are presented as follows [49, 50, 52–74]. Centralized solutions for seamless mode transition are proposed in [53] and [54], which are communication independent approaches, but do not support multiple grid-forming converters and require critical islanding detection. Also in [55], a converter that interfaces with the main grid is adopted to achieve MG resynchronization without communication. However, it represents a single point of failure, reduces the capability of the MG expansion and it is an expensive element for the MG. In [56], seamless disconnection is achieved using a droop based self–adaptive control method in which, during GC operation, the power controller tracks active and reactive power references; and during IS mode the power controller saturates and the converter operates as conventional droop control. In [57], three cascade control loops are used, but the external loop controls the grid current instead of the output power in GC mode (grid current – ac voltage – inductor current); also using limiters. When islanding occurs the VCM converter changes from grid current control to a version of droop control. However, it requires islanding detection and switching of control mode that may cause voltage and current overshoot. Also, real-time signals that are constantly changing (e.g., voltage angle or frequency) are used into the control loop to achieve re-synchronization. Thus, the control performance and stability are highly affected by communication delays. An interesting approach is presented in [58], in which two cascade control loops are implemented with a phase-locked-loop (PLL) that generates the reference of voltage loop. Thus, in GC mode the voltage controller takes no action and the converter operates in CCM; when islanding occurs it automatically runs in VCM. However, in IS mode, the converter operates as an isochronous generator. Therefore, it does not perform parallelism with other grid-forming converters. In [59] and [60], proportional-derivative (PD) controllers are used in droop equations to enhance the transition response. But, in [59], a secondary control that sends frequency and voltage values to DERs is used to resynchronization; and in [60] the resynchronization is performed by means of slip frequency. The authors of [61] present a hierarchical control structure that enables seamless transfer from one MG operating mode to the other and improves voltage/frequency regulation and resynchronization. However, it is a communication-based approach that needs to send quantities

to be used in the control loop. Besides, the DERs are not able to control their individual active and reactive power. In [62] and [63] a hierarchical structure with a disturbance observer (DOB) based feed-forward scheme is proposed to attenuate disturbance effects. In [64], communication is used in a control method that takes into account the circulating current to eliminate power sharing mismatching. A distributed control based on consensus protocol is used in [65] and [66] to perform power sharing in IS mode and resynchronization to GC mode. Some works [68, 70] present different solutions of seamless transition to IS mode, but they do not consider the reconnection process. Other works focus only on the smooth transition from IS to GC mode [67]; or focus on the reconnection when the grid and/or MG voltages are slightly distorted [69, 73]. The authors of [71] propose a controller that permits PV plants to operate seamlessly in GC and in IS mode; but only one grid-forming DER is considered and grid-voltage measurement is used for the reconnection method, same as presented in [72]. In [74], a controller formulated through an optimization problem is used to ensure seamless transition between GC and IS modes.

The most relevant works that consider seamless GC to IS transition and smooth reconnection are summarized and compared in Table 2.1. Some works consider only one

Table 2.1: Summary of literature review on grid-forming converters.

Ref.	**Control approach**	P & Q control in GC	Tolerance to grid voltage variation	Seamless GC to IS transition	Mult. grid-forming converters	Smooth reconnection	Critical islanding detection	High speed communication
[49],2019	Hybrid curr. and volt. mode	Only P	✗	✓	✗	✓	Required	Required
[50],2020	Modified HCVM	✓	✗	✓	✗	✗	Required	Required
[54],2015	Centralized utility–interface converter	✓	✗	✓	✗	✓	Required	Not req.
[57],2020	Self-adaptive control method with grid current control.	✓	Only f_{grid}	✓	✓	✓	Not req.	Required
[58],2020	Self-adaptive control method with voltage reference generated by a PLL	✓	✓	✓	✗	✓	Not req.	Required
[52],2020	VSG based control	✓	✓	✓	✗	✓	Not req.	Required
[61],2011	Communication-based hierarchical control	✗	✗	✓	✓	✓	Not req.	Required
[62],2018	Hierarchical structure with DOB based feed-forward	✗	✗	✓	✓	✓	Required	Required
[64],2020	Mechanism to eliminate the circulating–current	Only P	✗	✓	✓	✓	Required	Required
[65],2018	Distributed control with consensus protocol	✓	✗	✓	✓	✓	Required	Required
[60],2019	PD power controllers with slip frequency resync.	Only P	✗	✓	✗	✓	Not req.	Not req.
Herein	Self–adaptive control with automatic reconnection	✓	✓	✓	✓	✓	Not req.	Not req.

grid–forming converter, i.e., the parallelism between converters in IS mode is not considered; other works do not perform proportional active and reactive power sharing; or only the transition from GC to IS mode is considered. Still, some approaches need critical islanding detection to perform mode transition properly. Above all, the main issue in the reconnection process considered in the literature is the need of sending signals such as grid voltage phase angle, frequency or amplitude, which may require high-speed communications, as shown in Table 2.1. In MGs with large geographical size, with many DERs, fast communication could be unpractical.

2.3 On Secondary Control for Advanced MGs

Three main targets are mandatory for advanced MGs: *i*) operate in grid-connected mode and steer the power flow with the upstream grid; *ii*) operate in islanded mode and regulate voltage and frequency; and *iii*) coordinate DERs through power sharing methods avoiding undesirable current circulation in both grid-connected and islanded modes.

Several sorts of MG control strategies were developed along the last decades in order to achieve the three main objectives [75, 76]. However, most of the papers focus on only one or two objectives, such as: voltage and frequency restoration and power sharing in islanded mode, or grid power flow control in grid-connected mode. Therefore, a gap is identified in literature of a strategy capable of fulfilling concomitantly all three objectives and also considering different sorts of DERs in its control.

Initially, most of the control strategies of DERs applied to MG were based on the well-established concept of droop and reverse droop control, and the MGs were proposed without information and communication technology (ICT) infrastructure, only locally adjusting the droop gains [77,78]. However, conventional droop controllers suffer from drawbacks such as poor frequency and voltage regulation due to their constant deviation from nominal condition, inaccuracy of power sharing among DERs, low stability margin, power line impedance dependence, and slow dynamic response. These disadvantages are accentuated under weak networks like off-grid MG operation [77, 79, 80]. To overcome these problems, decentralized modified droop with stability and adaptive restriction are proposed in [79]. Then, with the emerging of low-bandwidth communication infrastructure, the MG structures based on central controller, and neighboring-communication (i.e., multi-agent system) have become more attractive [81–83], because they achieve more accurate power sharing, lower values of voltage and frequency deviation, and flexible energy management and operation of MG. However, centralized architectures have some inherent drawbacks compared to the decentralized ones. Typical examples are lower reliability and more expensive cost because of ICT.

Considering the aforementioned aspects, the more adherent and cutting-edge works are summarized and analyzed. A strategy that does not rely on communication

is shown in [84]. It improves the islanded MG voltage regulation and reactive power sharing among DERs using state estimators and optimal control. Nevertheless, due to the current development of low-bandwidth communication infrastructure, MG secondary control based on central controller or neighboring-communication (i.e., multi-agent system or consensus protocol) have become more common. Communication-based strategies achieve more accurate power sharing, lower values of voltage and frequency deviation, and better management and operation of MG. In [85], a distributed secondary control is developed to improve reactive power sharing, and restore voltage and frequency in an islanded MG. Each DER has its own secondary layer, so voltage, frequency and power offset information are transmitted from one DER to another.

Regarding distributed virtual impedance methods, in [86], VCM converters are coordinated to perform reactive power sharing and voltage regulation. A similar approach is used in [87], but considering also CCM units and performing harmonic compensation at the expense of precise proportional sharing. Further, imbalance compensation is also performed in [88]. In [89], online estimation of feeder impedance is used for optimal tuning of the complex virtual impedance to improve reactive power sharing. More recently, an iterative virtual impedance regulation strategy is proposed for improving balanced, unbalanced and harmonic current sharing [90].

Neighboring communication is used in [91, 92] to perform active/reactive power sharing and voltage/frequency regulation in an islanded MG. In [93,94], proportional active power sharing is performed in an islanded MG using a distributed approach with reduced communication, that is, event-triggered strategy. However, reactive power sharing is not taken into account. A decentralized power sharing approach for islanded MG that restricts thermal damage of converter components to avoid over-stressing is proposed in [95]. All the papers mentioned above are applied only in islanded MG, therefore, the power flow at the PCC is not controlled and power sharing in grid-connected mode is not performed.

In [96], the PCC power flow is controlled using a cooperative method, but, only grid-connected mode is considered. A complete work is found in [65], in which consensus protocol is used to control DERs in both grid-connected and islanded mode. The PCC power flow is controlled, the power-sharing is achieved, frequency and voltage are restored in islanded mode, and it performs smooth reconnection. However, only three-phase VCM converters are considered and critical islanding detection is required to perform mode transitioning. In [97], a distributed control method is developed to achieve energy level balancing, active/reactive power sharing, and voltage/frequency synchronization of heterogeneous battery storage devices. The batteries are considered heterogeneous in terms of energy level and power, although the difference in the converter control structure and self-constraints are not taken into account. Moreover, smooth transition between operating modes is not considered.

Regarding the adoption of hierarchical centralized architecture, the well-known

PBC is a complete strategy capable of performing proportional power sharing in grid-connected and islanded modes [98]. The PBC has undergone improvements over time in order to enhance its benefits. It can be chronologically divided in three generations. The first generation of PBC (PBC-I) [98] was originally developed for controlling dispersed inverters in a single-phase MG. It is achieved proportional sharing of active and reactive power among DERs by defining two scalar coefficients (α_P, α_Q) that are broadcast to the DERs. It can be easily extended to three-phase networks, but it does not provide unbalance compensation. Also, all DERs are considered in CCM.

The second generation of PBC (PBC-II) described in [99] defines six scalar phase coefficients (α_{Pm} and α_{Qm}), where m stands for phases a, b, and c, applied to a three-phase four-wire MG. It shares proportionally the active and reactive power among the DERs that are connected at the same m-th phase and provides load unbalance compensation at the PCC. However, it drives also the three-phase inverters for unbalanced operation, which may be undesirable due to the high ac power component absorbed at the dc-side of the inverter. Moreover, all DERs are considered in CCM.

Then, the third generation of PBC (PBC-III) is proposed in [100]. All the features of PBC-II are contemplated, but otherwise the three-phase DERs may operate balanced by defining eight scalar coefficients (α_{Pm}, α_{Qm}, $\alpha_{P3\phi}$ and $\alpha_{Q3\phi}$). Again, all DERs are still considered as CCM. Table 2.2 shows the main PBC evolutions over recent years.

Table 2.2: Evolution of PBC Strategy for MG Application

PBC Gen.	**Features**	**Ref**
PBC-I	Proposed to single-phase MG. Proportional power sharing of active and reactive power among DERs by two scalar coefficients (α_P, α_Q). If extended for three-phase networks, it does not compensate current unbalance. All DERs are considered CCM.	[98]
PBC-II	Proposed to three-phase four-wire MG. It proportionally shares active and reactive power among DERs that are connected at the same m-phase and provides current unbalance compensation at the PCC by six scalar phase coefficients (α_{Pm}, α_{Qm}), where m represents phases a, b and c. Three-phase DERs operate unbalanced. All DERs are considered CCM.	[99]
PBC-III	Proposed to three-phase four-wire MG. It proportionally shares active and reactive power among DERs that are connected at the same m-phase and provides current unbalance compensation at the PCC by eight scalar phase coefficients (α_{Pm}, α_{Qm}, $\alpha_{P3\phi}$, $\alpha_{Q3\phi}$). The three-phase DERs may operate balanced. All DERs are considered CCM.	[100]

To verify the PBC applicability, a three-phase three-wire MG with three- and single-phase inverters in both VCM or CCM is considered in [11]. This strategy enables to arrange a flexible MG control method in which the DERs may operate in different ways: 1) three-phase DERs that must operate balanced, proportionally contributing to active and reactive power sharing; 2) single or three-phase DERs operating in both VCM or CCM; 3) explore the fact that with only two single-phase DERs, connected in different

phases, it is possible to compensate three-phase three-wire load unbalance, in accordance with Steinmetz principle [101] [102].

The PBC has been improved over the years, and the most recent advance performs grid power flow control, proportional power sharing, and considers single- and three-phase DERs working in CCM and VCM [11]. In [103], the benefits of PBC is combined with consensus protocol to decrease communication implementation costs, while flexibility and reliability are enhanced. A serious disadvantage of these MG structures using the PBC approach is the necessity of a central converter, named Utility Interface (UI), to form the islanded MG. Central converter is a single point of failure and critical during islanded operation, which reduces the capability of the MG expansion, it is difficult to design one single converter to assume all transients due to the arbitrariness of the loads, and it is an expensive element for the MG.

2.4 On Harmonics Compensation for VCM Converters

In low-voltage grids, the widespread use of power converters for DERs, like photovoltaic and batteries, allows a number of advantageous functionalities for electrical power systems, but some challenges still exist toward optimal operation [104]. A relevant power quality issue is the unwanted harmonic current circulation between the converters and the mains when grid voltages are distorted, which is actually a common condition.

Regarding the zero-level control of grid-connected power converters, two main approaches are employed, that is, *i)* current-controlled mode (CCM) or *ii)* voltage-controlled inverter (VCI). The VCI approach is very popular, despite of a higher complexity, mainly because it allows grid-forming functionality in islanded conditions and smooth transitions between grid-connected and islanded modes [56, 105].

In grid-connected mode, VCIs typically use droop loops (e.g., P-f & Q-V laws) to provide to the inner voltage-control loop a sinusoidal voltage reference that is synchronized with the main grid voltage. Additional outer control loops may also be included to achieve active and reactive output power reference tracking [105, 106]. Notably, the converter voltage references are typically purely sinusoidal.

However, the grid voltage in low-voltage power systems may present significant harmonic components [107]. The IEEE Std. 519-2022 [108], for example, recommends a limit of 8% to the voltage total harmonic distortion (THD) for low-voltage grids. Consequently, when a VCI with purely sinusoidal voltage is connected to a grid with distorted voltage, there is an harmonic current flowing between the two sources, due to the different harmonic content. This exchange of harmonic current among the two sources is referred to as harmonic circulation currents herein, analogously to what is done in [109] considering

fundamental quantities. Harmonic circulation currents are unnecessary and impair distribution efficiency, effectiveness of protection devices, and further deteriorates the quality of the currents fed at the PCC.

The distortion of low-voltage grids is usually due to a voltage drop in line impedances caused by non-linear loads. Thus, some works propose the use power converters to directly compensate the related harmonic currents [110–112]. In this type of approach, the non-linear load current, or the grid current, is sensed and used to generate the current compensation reference. Regarding harmonic voltage compensation, the converter control commonly uses the point-of-common-coupling (PCC) voltage and a virtual impedance in the control loop to generate a voltage reference and try to compensate the distortion [113–115]. The main drawback of these approaches is that measuring the PCC voltage or current as quantities used for control is not practical, due to the distance of the PCC from distributed converters. Also, the performance of this type of strategy often depends on the specific values of the line impedances. Some works contemplate approximating the PCC voltage with the voltage at the point-of-connection (PoC) [116], but this is not always acceptable, due to the differences in voltage amplitude and phase related to the circulation of fundamental active and reactive power through the distribution lines. Notably, this issue is particularly relevant for the reduction of harmonic circulation currents aimed herein. The PCC/PoC approximation for harmonic circulation current reduction is used in [117], where, instead of measuring the PCC voltage and use it directly in the control loop, low-bandwidth communication is applied for sending PCC voltage harmonic amplitude to the converters. The PCC voltage harmonic components are extracted in synchronous reference frame and then transmitted to each converter controller, then the transmitted data consist of mainly dc signals. In such kind of approaches, the angle used in the Park transformations performed in the converter control and in the PCC measurement block may differ, due to phase-shifts related to power circulation along the distribution lines and the fact that the two systems are not synchronized. This impairs the quality of the performed compensation.

Recently, the use of global positioning system (GPS) technology has attracted interest as one of the several options to achieve the synchronization of converters in low-voltage MGs. In [118], the GPS signal is used to directly synchronize the microprocessors clock of droop-based grid-forming inverters in order to maintain the parallelism of the converters. In [119] and [120], the GPS is used together with advanced phase-locked-loops (PLLs) to improve the synchronization of dispersed converters and the main grid. However, these proposals rely on fast communication, because the rotating angle of the grid voltage needs to be transmitted to the converters.

GPS synchronization is also employed in converters control to perform harmonic current sharing between the converters [121], or to overcome frequency and phase deviations during islanded operation of a MG [122–125]. Thus, the converters may operate as

isochronous generators, keeping the frequency fixed [126]. However, these approaches are applied only to islanded MGs, and do not consider the grid-connected mode. Furthermore, real GPS modules are not always used to test the control.

Therefore, harmonic voltage compensation for VCM converters is still in development. Also, the use of synchronization means like GPS signals to improve the performance of grid-connected power converters connected to low-voltage grids is currently relatively new and only partially explored in the literature.

2.5 Conclusions

This chapter presented and compared the most cutting-edge research papers related to the specific topics of development of this dissertation. A critical analysis was carried out in order to identify the literature gaps. In summary, the literature papers that address grid-forming converter control for smooth transition between MG modes require critical islanding detection due to control mode switch, or require high-speed communication to perform reconnection. The papers regarding secondary control for advanced MGs normally focus on only one or two objectives, which means that a complete strategy is lacking, especially one that considers different sorts of DERs in its control. On the harmonics compensation for VCM converters, most of the papers do not take into account the phase shift caused by distribution lines, thus, proper synchronization is not performed. Some papers contemplate the use of GPS modules for synchronizing VCM converters, but only islanded operation is considered. Thus, the contributions of the control methods proposed in the following chapters were endeavored to fill the identified gaps.

Chapter 3

Self–adaptive Control for Grid-forming Converter

3.1 Introduction

The self–adaptive control is a control approach for grid-forming converters, which normally consists of three cascade control loops (output power – ac voltage – inductor current) with the addition of saturators [56]. The self-adaptive control approach is based on the well-known droop control equations, and no switching from CCM to VCM, and vice-versa, is needed. In addition, seamless transitioning from GC to IS is accomplished through the introduction of limiters in the control scheme to saturate or de-saturate the output of the power regulator under occurrence of islanding. Therefore, critical islanding detection is not required.

This chapter proposes an innovative solution to the self–adaptive control with a new method to achieve the four main objectives required for multiple grid-forming converters. The main novelty of this solution is the no need of high-speed communication between the DERs and the CC, but rather a flag signaling. Therefore, this solution can be deployed in large MG sites with several grid-forming converters. Additionally, this method is tolerant to grid voltage variation and no critical islanding detection is required.

The well-known three cascade control loops are implemented with saturators at the power controller to guarantee the first three objectives (i.e., precise power control, seamless islanding and autonomous power sharing). This chapter also contributes with the development of a methodological procedure for properly designing power-loop controllers, limits values of saturators, and guidelines for practical applications.

The smooth reconnection from IS to GC (i.e., the forth objective) is driven through a CC, which broadcasts a signal ("flag") informing the DERs that the MG is in the reconnection procedure. This signal can be interpreted as a Boolean information that just informs that the MG will soon reconnect. Thereby, the grid–forming DER changes its

operating frequency, so that the MG and the main grid temporally run with a slight frequency difference. Thus, occasionally, there is a time interval in which the angle difference between the two voltages is small enough to perform the reconnection (i.e., slip frequency technique), and a synchrocheck relay governs the switch that reconnects the MG to the mains.

The flag signal is not considered a real-time communication, but rather only signaling, because there is no byte data exchange. The flag signaling does not transfer voltage phase information, and it is not used in the DER control loop. Besides, the reconnection procedure is not affected by packet loss or latency. Also, this signal can be redundant and sent more than once to increase reliability. Besides, the requirements and complexity for its implementation are minimal; a latency of $167ms$ is shown in Section 3.4 without loss of performance.

3.2 Proposed Control for Self–adaptive Grid–forming Converter

The grid–forming converter considered herein is shown in Fig. 3.1. It is composed of a conventional three-phase half-bridge inverter with a LCL output filter and a local circuit breaker, CB_0. The inductor current (i_{L1}), capacitor voltage (v_{CF}), output current (i_{out}), and the point-of-connection (POC) voltage (v_{POC}) are measured and used in the control loops. Switch S_1 is controlled by the CC together with a synchrocheck relay [127], which is responsible for reconnecting the MG, detailed in Section 3.2.3.3. The circuit breaker CB_2 is driven by the distribution system operator (DSO). The converter topology is not the goal of this chapter, which restricts its focus on the development of the control. The MG can also include grid–following converters without jeopardizing the overall system operation, they would only be part of the equivalent load.

Two possible configurations for switch S_1 are proposed, as shown in Fig. 3.2. In Fig. 3.2-a), it is proposed to include a contactor in series with the circuit breaker CB_1; thus the synchrocheck relay governs the contactor for reconnection, and the CB_1 acts only in case of faults. In Fig.2-b), another possible configuration is shown with a solid-state relay (SSR) [128] of lower rated current in parallel with the contactor. In this second approach, the synchrocheck relay governs both the contactor and the SSR simultaneously. The solid-state relay closing time delay is about $1ms$ [129], which allows the closing procedure to be almost instantaneous and with very low deviation from both voltages. Thus, the SSR closes first assuming the grid transient current; and the contactor closes right-after with an average delay of $40ms$. At steady-state, the SSR opens up, and the contactor assumes the operation. The use of only a SSR is discouraged due to the lack of galvanic isolation and high losses.

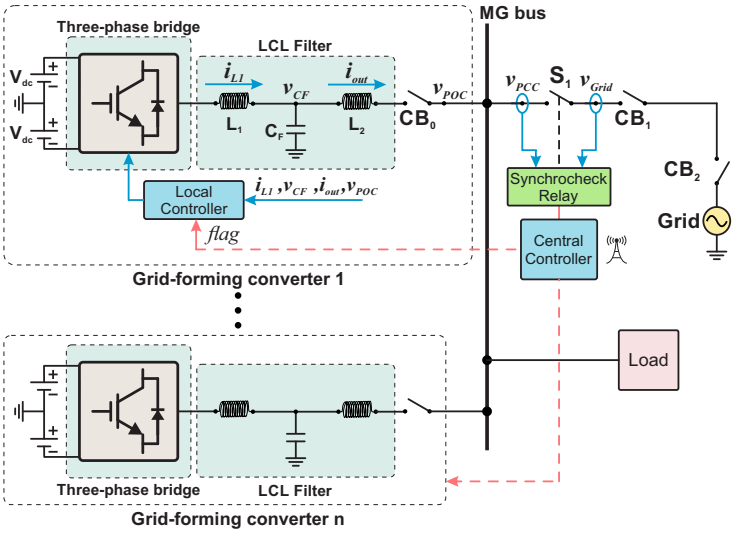

Figure 3.1: MG structure and grid–forming converter electric diagram.

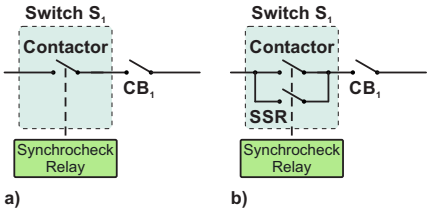

Figure 3.2: Possible switch S_1 configuration: a) Three-phase contactor; b) Three-phase contactor in parallel with a three-phase solid-state relay (SSR).

The converter control scheme is split into three loops: *i*) external power–loop responsible for controlling the output power during grid–connected operating mode, and for smooth transition to islanded mode; *ii*) voltage–control loop that regulates the voltage across C_F capacitor; and *iii*) inner current–loop that controls the current through the L_1 inductor and guarantees overcurrent protection.

3.2.1 External power–loop

Fig. 3.3 shows the block diagram of the proposed external power control loop. This loop is split into active and reactive power loops. The power control is based on droop equations relating active power with frequency and reactive power with voltage. Despite considering low voltage grids (predominantly resistive), droop equations were developed for grids with inductive characteristics, since the output inductance of the converters LCL filters are much higher when compared to line resistance. Nevertheless, the formulation proposed herein differs from the conventional droop in two main points: 1) an outer loop with an integrator is used, and 2) the integrator is limited at certain values. When the MG operates at GC mode in steady–state, the *frequency switch* is in position "2", thus,

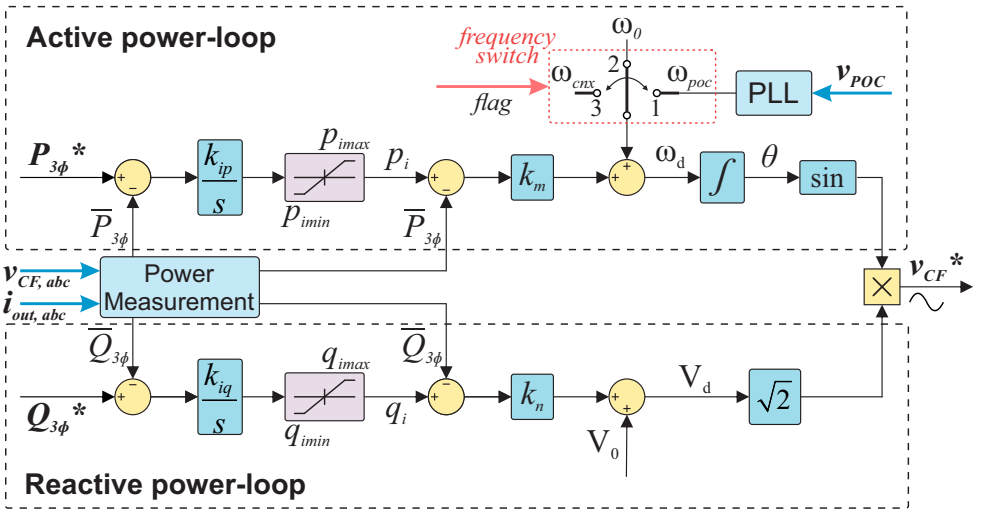

Figure 3.3: Power control loop of the grid–forming converter.

the control equations are shown in (3.1) and (3.2):

$$\omega_d = \omega_0 + k_m \cdot (p_i - \overline{P}_{3\phi}) \tag{3.1}$$

$$V_d = V_0 + k_n \cdot (q_i - \overline{Q}_{3\phi}) \tag{3.2}$$

where ω_d and V_d are the angular frequency and the voltage magnitude that generate the converter voltage reference (v^*_{CF}); ω_0 and V_0 are the rated grid frequency and voltage magnitude; k_m and k_n are the droop coefficients for active and reactive power; $\overline{P}_{3\phi}$ and $\overline{Q}_{3\phi}$ are the calculated average active and reactive power at the converter output; and p_i and q_i equations are shown in (3.3) and (3.4):

$$p_i = \frac{k_{ip}}{s} \cdot (P^*_{3\phi} - \overline{P}_{3\phi}) \tag{3.3}$$

$$q_i = \frac{k_{iq}}{s} \cdot (Q^*_{3\phi} - \overline{Q}_{3\phi}) \tag{3.4}$$

where k_{ip} and k_{iq} are the integral gains; and $P^*_{3\phi}$ and $Q^*_{3\phi}$ are the references of active and reactive power.

The external power–loop implemented with the extra integrator enables accurate active and reactive power control during GC mode. However, in IS mode, the extra integrator takes the system out of its nominal limits of frequency and voltage whether the converter output power differs from its power references. To overcome this issue, a limiter is included at the output of the integrator. Such operation is discussed in Section 3.2.3.2.

3.2.2 Inner voltage and current control loops

The inner control loops are composed of a voltage–loop and a current-loop in cascade, as shown in Fig. 3.4. The voltage–loop controls the v_{CF} voltage to track the

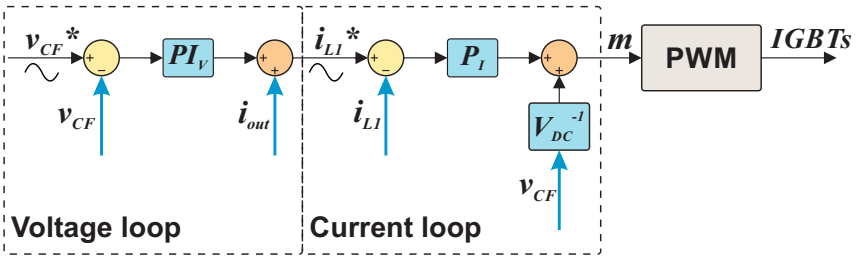

Figure 3.4: Current and voltage control loops of the grid–forming converter.

voltage reference imposed by the power–loop. A PI controller is adopted and an output current (i_{out}) feedback is used to compensate the disturbance. The current–loop controls the i_{L1} current to track its reference provided by the voltage loop. A proportional controller (P_I) is used and the capacitor voltage measurement (v_{CF}) decouples the disturbance, where V_{DC} is dc-link voltage rated value. The zero-level control implementation is not the focus herein. Thus, the PI controller with disturbance compensation signals (i_{out} and v_{CF}) is chosen because it achieves satisfactory results and its implementation is simple. Other more advanced controllers could be used with AC signals, e.g., proportional-resonant controller [130].

3.2.3 System Operation

Considering the black–start of such a converter to connect to an energized grid, before turning on CB_0, it is necessary to synchronize the converter output voltage (v_{CF}) to the POC voltage (v_{POC}). Thus, *frequency switch* starts in position "1" to phase-lock the voltage angle. Also, for a smoother connection, the power references ($P^*_{3\phi}$, $Q^*_{3\phi}$) are set to zero at the black-start to avoid inrush currents at the converter connection. After voltage synchronization, CB_0 is turned on, and *frequency switch* is turned to position "2".

In summary, the frequency switch takes on three different positions depending on the converter operation:

1: (ω_{POC}) - Converter synchronization at black-start;

2: (ω_0) - Normal operation at both GC or IS modes;

3: (ω_{cnx}) - Transitory operation at the MG reconnection process – where "*cnx*" stands for connection – explained in detail in Section 3.2.3.3.

3.2.3.1 Accurate power control in grid-connected mode

In GC mode the voltage and frequency values are set by the main grid. Thus, the external power–loop steers the converter to exchange accurate active and reactive power to the grid, characterizing a power dispatchable converter.

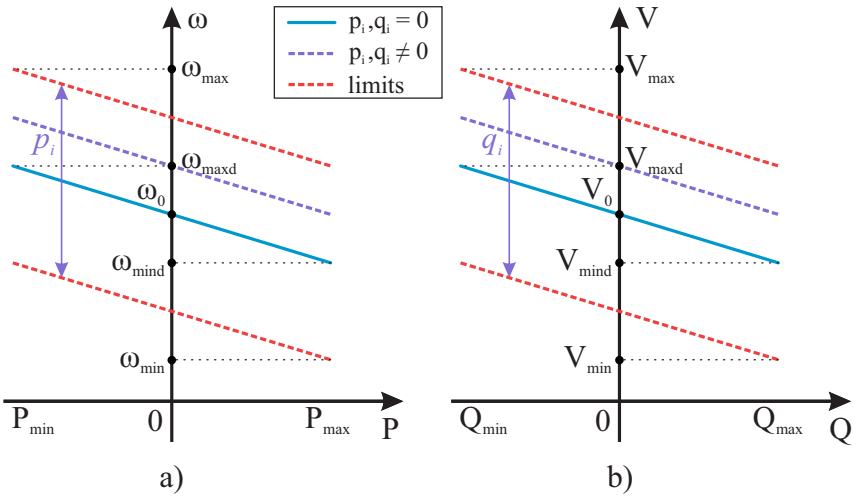

Figure 3.5: Droop curve with external power–loop: a) $P-\omega$; b) $Q-V$.

The extra integrator output (i.e., p_i, q_i) changes the *y-intercept* coefficient of the droop curves, as shown in Fig. 3.5. The curve displacement allows the converter to provide non–zero power at grid voltage rated values, as ω_0 and V_0. Therefore, this implementation zeros the output power error even under grid voltage variation, and allows to control the dynamics of the output power when proper controller design is adopted. The curve boundaries are explained in Section 3.3.

3.2.3.2 Seamless transition to islanded mode

When the main grid is absent, CB_2 opens and the grid–forming converter forms the MG voltage. However, under power balance mismatching the external power loops may overflow and the islanded MG voltage and frequency may exceed the normal operational limits. Hence, a saturator is implemented after the integrator to keep voltage magnitude and frequency within their maximum and minimum values.

In fact, when p_i and q_i saturate, the converter operates temporarily as a shifted conventional droop–control, as one of the red dashed curves in Fig. 3.5. For example, if the power errors are positive values, p_i and q_i saturate in their maximum value and the converter operates automatically in conventional droop equation, as shown in (3.5) and (3.6). This implementation guarantees smooth transition to IS mode without fast islanding detection, no switching control mode from CCM to VCM, and no large voltage and current transients.

$$\omega_d = \omega_0 + k_m \cdot (p_{imax} - \overline{P_{3\phi}}) \tag{3.5}$$

$$V_d = V_0 + k_n \cdot (q_{imax} - \overline{Q_{3\phi}}) \tag{3.6}$$

The CC detects whether the MG is islanded or if the mains is reestablished; and then drives S_1 according to the occasion. When islanding is detected, the CC opens S_1.

Islanding detection is required for security reasons and can be performed using, e.g., a remote islanding detection method [131].

In steady-state of IS mode, the external power controller saturates, due to the mismatching of power reference ($P^*_{3\phi}$) and power output ($\bar{P}_{3\phi}$), so both converters operate as conventional droop-control with the power reference (pi) saturated at p_{imax} or p_{imin} (see Fig. 3.3). The saturators are designed to maintain the power sharing when operating as conventional droop control, detailed in Section 3.3.5. Therefore, only reactive power sharing would be impaired due to different voltage profiles, which is adjusted by the secondary control.

When islanding is detected by the CC, the power references ($P^*_{3\phi}$ and $Q^*_{3\phi}$) may be updated by the MG secondary control aiming to restore the MG voltage magnitudes to rated values, and to improve the power sharing. Thereby, the power–loop integrators desaturate and, once the output power and power reference match, the voltage and frequency return to their nominal operating values. Note that the islanded detection is not critical to the operation, but only enhances power quality by eliminating voltage and frequency deviations in steady-state. The development and implementation of the secondary control layer is shown in Ch. 4.

3.2.3.3 Smooth reconnection

When the mains is reestablished and detected by the CC, the reconnection process starts. The CC broadcasts a signal flag to the grid–forming converter indicating that the mains is stable. Then, the DER turns the *frequency switch* to position "3" to prepare to operate GC again.

Since in the steady-state of the IS mode the secondary control drives the converter power references to restore the MG frequency and voltage to their rated values, the converter power error is null when the frequency switch is turned to position "3". Thus, the converter changes its operating frequency to ω_{cnx}, and the islanded MG operates at ω_{cnx} frequency in the reconnection interim. The ω_{cnx} value is slightly different from the rated frequency (i.e., $2\pi 60.1\ rad/s$); it is explained in detail in Section 3.3.6.

In the reconnection interim, the operating frequency of the islanded MG must be different from the main grid frequency. This small frequency deviation is the key to the automatic reconnection. As the islanded MG operates in a different frequency of the main grid, occasionally, there is a time interval in which the angle difference between the two voltages is small enough to perform the reconnection. The CC monitors both voltage angles (v_{PCC} and v_{grid}); and at the instant that they are in–phase, the synchrocheck relay automatically closes S_1 and the MG operates in GC mode again. Besides the phase, the synchrocheck relay must verify that the MG complies with the frequency, voltage level and phase-sequence [132].

As the power controllers of the grid–forming converter are already desaturated,

they can track their power references in the reconnected operation, even with different droop frequency (ω_{cnx}). After ensuring that the MG is grid–connected and stable, the CC turns the reconnection flag off, and then the converter changes the *frequency switch* to position "2" returning to ω_0 again.

The reconnection process is automatic and allows smooth transition with reduced transient currents and voltages. The grid–reconnection does not require fast communication with multiple grid–forming converters, i.e., the CC does not transmit the v_{grid} angle to grid–forming converter synchronization or other time–variant signals, which would be a critical issue in large MGs. Moreover, during IS state, if the secondary layer control communication fails, the grid–forming converter would still operate stable, but in a slightly inferior condition in terms of voltage and frequency deviation values. Finally, if the main grid reconnects before the island is detected – as it is used to happen with distribution automatic reclosers – the MG would still be operating at GC mode properly, so no switching of control mode is required.

3.3 Design of Control Parameters

This section details the design of the parameters of the proposed grid–forming converter control, from inner loops to external power controllers and limiters.

3.3.1 Inner loops controllers

The controllers used for the capacitor voltage (v_{CF}) and inductor current (i_{L1}) are developed. The plant model is shown in Fig. 3.6, in which the open loop transfer function can be obtained. The controllers are tuned based on any desired technique [133], one used the frequency response analysis.

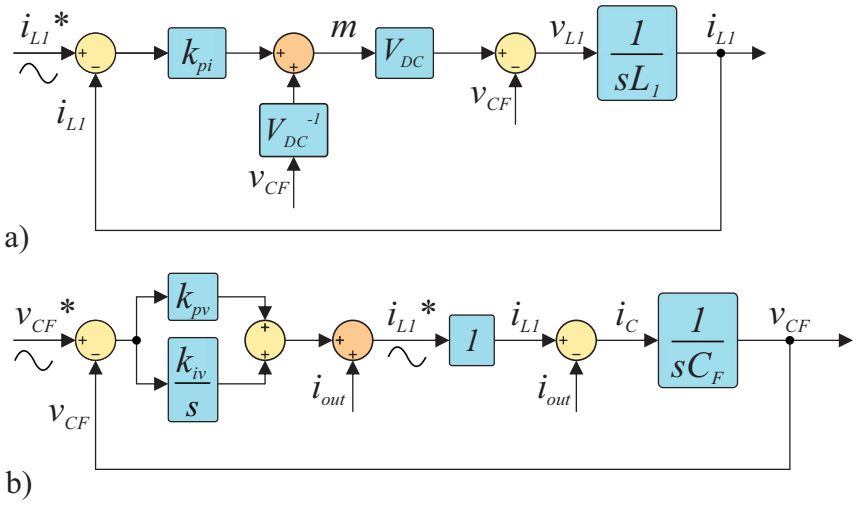

Figure 3.6: Model for the inner a) current– and b) voltage–loop controller design.

It is recommended to design the cutoff frequency of the current controller a decade below from the switching frequency. For the voltage controller, a cutoff frequency at most half the cutoff frequency of the current loop is recommended. Thus, the control design for each loop is considered independent and can be analyzed individually. In this case study, for the current loop the cutoff frequency is $1200Hz$; and for the voltage loop, the cutoff frequency is $600Hz$ and the phase margin of 60° is considered.

3.3.2 Droop control parameters

To define the droop coefficients k_m and k_n, which are based on the IS operating mode, one can use the conventional approach of maximum allowed voltage and frequency deviation such as:

$$k_m = \frac{\omega_{maxd} - \omega_{mind}}{P_{max} - P_{min}} \tag{3.7}$$

$$k_n = \frac{V_{maxd} - V_{mind}}{Q_{max} - Q_{min}} \tag{3.8}$$

where ω_{maxd} and ω_{mind} are the maximum and minimum angular frequency values allowed variation (herein considered $(2 \cdot \pi \cdot 60.5)\ rad/s$ and $(2 \cdot \pi \cdot 59.5)\ rad/s$, respectively); P_{max} and P_{min} are the maximum and minimum converter active power; V_{maxd} and V_{mind} are the maximum and minimum phase voltage values allowed in normal grid operation (herein considered 131 V_{rms} and 123 V_{rms}, respectively); and Q_{max} and Q_{min} are the maximum and minimum converter reactive power. The frequency and voltage limits are determined based on the *normal* operation limits of low–voltage grids of the Brazilian Grid Code PRODIST–8 [134].

3.3.3 External power–loop controllers

The design of the power–loop controllers k_{ip} and k_{iq} considers the simplified system model shown in Fig. 3.7. The line impedance is neglected as the inverter output impedance is usually much higher than the line impedance value [135].

The power flow equations of the system of Fig. 3.7 are:

$$P = 3 \cdot \frac{V_{CF} \cdot V_g \cdot sin\theta}{X_2} \tag{3.9}$$

$$Q = 3 \cdot \frac{V_{CF}^2 - V_{CF} \cdot V_g \cdot cos\theta}{X_2} \tag{3.10}$$

where X_2 is the L_2 inductor reactance of the converter.

Considering that the grid voltage and the inductor reactance are constant, the small–signal linearization of the power flow equations around the equilibrium points "θ_{eq}"

and "$V_{CF_{eq}}$" are:

$$\widetilde{P} = \frac{3 \cdot V_g}{X_2} \left(V_{CF_{eq}} \cdot cos\theta_{eq} \cdot \tilde{\theta} + sin\theta_{eq} \cdot \widetilde{V_{CF}} \right) \tag{3.11}$$

$$\widetilde{Q} = \frac{3}{X_2} \left[V_g \cdot V_{CF_{eq}} \cdot sin\theta_{eq} \cdot \tilde{\theta} + (2 \cdot V_{CF_{eq}} - V_g \cdot cos\theta_{eq}) \cdot \widetilde{V_{CF}} \right] \tag{3.12}$$

where the tilde ($\tilde{}$) refers to the small-signal variation around the operating point.

The angle equilibrium point is set to $\theta_{eq} = 0$ and the voltage equilibrium point is set to the nominal grid voltage $V_{CF_{eq}} = V_g$ then, the linearized power flow equations are reduced to:

$$\widetilde{P} = \frac{3 \cdot V_g^2}{X_2} \cdot \tilde{\theta} \tag{3.13}$$

$$\widetilde{Q} = \frac{3 \cdot V_g}{X_2} \cdot \widetilde{V_{CF}} \tag{3.14}$$

Based on Fig. 3.3, and considering constant grid quantities, the small–signal linearized control equations are:

$$\tilde{\theta} = \frac{1}{s} \cdot \widetilde{\omega}_d \tag{3.15}$$

$$\widetilde{\omega}_d = k_m \cdot \left[\frac{k_{ip}}{s} \cdot (\widetilde{P}^*_{3\phi} - \widetilde{\overline{P}}_{3\phi}) - \widetilde{\overline{P}}_{3\phi} \right] \tag{3.16}$$

$$\widetilde{V}_d = k_n \cdot \left[\frac{k_{iq}}{s} \cdot (\widetilde{Q}^*_{3\phi} - \widetilde{\overline{Q}}_{3\phi}) - \widetilde{\overline{Q}}_{3\phi} \right] \tag{3.17}$$

The average active and reactive power output are obtained through a Moving Average Filter (MAF). When tuned at 60 Hz, the MAF frequency dynamic is similar to a first order low-pass filter (LPF) tuned in 15 Hz, analyzing the spectrum up to 10 Hz [136]. Thus, the MAF transfer function at 60 Hz is approximated to a LPF transfer function at $\omega_c = 2\pi 15$ rad/s:

$$MAF(s) = \frac{\omega_c}{s + \omega_c} \tag{3.18}$$

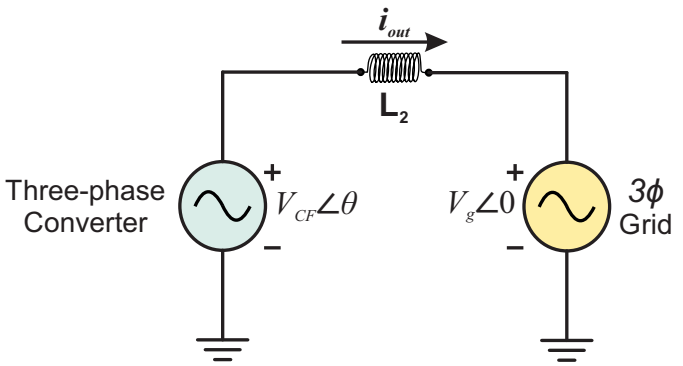

Figure 3.7: Simplified grid–connected converter model.

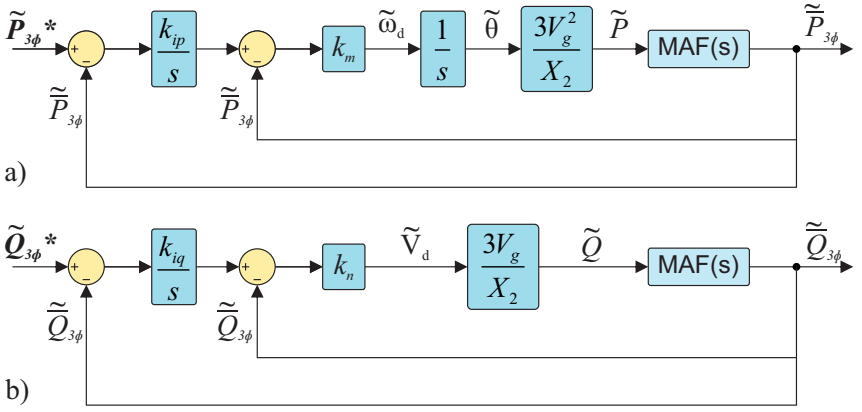

Figure 3.8: Small-signal model for the external a) active power– and b) reactive power–loop controller design.

Therefore, (3.13)–(3.18) can be represented as a block diagram of the small-signal model for the external power–loops controller design, as shown in Fig. 3.8. The open-loop transfer function is then obtained, and the controllers can be tuned based on any desired technique [133]. A cutoff frequency of at least a decade below the cutoff frequency of the voltage loop is recommended. In this case study, the cutoff frequency and the phase margin for the active and reactive power loop are $1.92Hz$ and 85°, and, $1.24Hz$ and 87°, respectively.

3.3.4 Sizing the Coupling Inductor

To guarantee the regulated power flow when the VCM converter operates grid-connected, it is important to size the coupling inductor, L_2, correctly [137]. The desirable inductor size can be seen as the minimum size that the inductor can have, and still being able to satisfy the delivery requirements. First, it is important to define the maximum value of the capacitor voltage of the inverter, V_{CF}^{max}, which is usually related to the dc-link voltage, V_{DC}. Herein, one considers $V_{CF}^{max} = V_{DC}$. Second, one sets the maximum active, P_{max}, and reactive, Q_{max}, power that the converter is able provide. Third, one limits the maximum power angle, θ_{max}. Apart from θ_{max}, the other values must be already defined in pre-design stages, that are not demonstrated in this work. Regarding θ_{max} definition, the following guidelines are highlighted.

At zero active power, θ is ideally zero, that is, both v_{CF} and v_g are in-phase. On the other hand, θ_{max} is the power angle at maximum active power. Thus, θ_{max} should not be chosen too small, because it is actually the range that the voltage controller can have to synthesize a voltage to provide that given active power. For example, if θ_{max} is chosen as one degree, the voltage controller would have only a one degree margin to go through all P_{max} of the converter, which implies in a very precise or even impractical control. However, θ_{max} cannot be chosen too big either, considering that it is desired to operate in the linear portion of the $P(\theta)$ characteristic. A reasonable choice for the maximum value for θ to

operate in the linear portion is 30°. Other important aspects in defining the maximum power angle, θ_{max}, must be analyzed:

i) the smaller the power angle, the smaller is the inductor to transfer power, thus, the more precise the controller and instrumentation resolution must be to guarantee the power synthesis due to small angle range. The range of the power angle cannot be allowed to get too small, e.g., as one degree, to avoid errors in the power to become unacceptable;

ii) the smaller the V_{CF} voltage, the smaller the inductor must be to transfer power, and thus, the smaller is the power angle;

iii) the smaller the inductor, the cheaper and less bulky.

Thus, (3.19) and (3.20) are derived from (3.9) and (3.10), for one leg of the converter, to establish a starting point for inductor sizing. Two values of the maximum inductor reactance, X_2, are calculated, one chooses the smallest among them.

$$X_2^{max1} = \frac{V_{CF}^{max} \cdot V_g \cdot \sin(\theta_{max})}{P_{max}} \tag{3.19}$$

$$X_2^{max2} = \frac{V_{CF}^{max2} - V_{CF}^{max} \cdot V_g \cdot \cos(\theta_{max})}{Q_{max}} \tag{3.20}$$

where V_g is the rated value of the grid voltage.

3.3.5 External power–loop saturators limits

The saturators limits are defined to keep the IS operation in the allowable *temporary* range of frequency and voltage deviation, according to standards and grid codes. First, the maximum (ω_{max}) and minimum (ω_{min}) frequency values that the MG can reach in *extreme* operation are defined; as well as the maximum (V_{max}) and minimum (V_{min}) voltage values. Thus, the saturators limits are calculated in (3.21)–(3.24):

$$p_{imax} = \frac{(\omega_{max} - \omega_0)}{k_m} + P_{min} \tag{3.21}$$

$$p_{imin} = \frac{(\omega_{min} - \omega_0)}{k_m} + P_{max} \tag{3.22}$$

$$q_{imax} = \frac{(V_{max} - V_0)}{k_n} + Q_{min} \tag{3.23}$$

$$q_{imin} = \frac{(V_{min} - V_0)}{k_n} + Q_{max} \tag{3.24}$$

The maximum considered frequency and voltage values are shown in Table 3.1. The limits are determined based on the *temporary* operation limits of low–voltage grids of

the Brazilian Grid Code PRODIST–8 [134].

This approach ensures that the maximum and minimum limits of voltage and frequency are maintained in IS operation. In GC mode, the saturators limits allow to exploit full active power, even when the grid frequency deviates in normal operation. The reactive power, otherwise, is affected by the voltage drop of line impedance in GC mode, thus, the limits of the reactive power saturators can be relaxed to exchange more reactive power with the main grid. However this would cause larger voltage deviation in IS mode. Therefore, there exists a trade–off between reactive power exchange capability during GC mode and voltage deviation during IS mode.

Table 3.1: Maximum and minimum frequency and voltage values in temporary operation

ω_{max}	ω_{min}	V_{max}	V_{min}
$(2 \cdot \pi \cdot 61)\ rad/s$	$(2 \cdot \pi \cdot 59)\ rad/s$	$135\ V_{rms}$	$119\ V_{rms}$

3.3.6 Reconnection frequency definition

The reconnection frequency (ω_{cnx}) is a value slightly different from the rated grid frequency, as explained in Section 3.2.3.3. According to [134], in normal grid operation, the frequency may vary between 59.9 Hz and 60.1 Hz, thus, it is chosen a value outside this range. As in the most common operation the grid–forming converter feeds the MG loads, i.e., its output power is positive, then one chooses ω_{cnx} at the upper limit to maintain the positive power flow when grid–connection is established and to reduce transient currents. Therefore, ω_{cnx} value is chosen as $2 \cdot \pi \cdot 60.1 rad/s$. This frequency difference is in accordance to the IEEE Standard 1547-2018 – Synchronization parameter limits for synchronous interconnection to an energized local electric power system to an energized area electric power system [132].

3.4 Real-time Hardware-in-the-loop Results

The proposed control for grid-forming converter in MG applications is tested in this section under different case studies in order to verify and validate its effectiveness. It is used the *Typhoon HIL 604* real–time emulator to run all the power stage. The control stage is implemented onto industrial TI TMS320F28335 control cards which send back the PWM gate control signals to all six switches of each converter modeled on the HIL system, as shown in Fig. 3.9. Two identical DERs with the proposed control are implemented, and a CC which detects the grid absence/presence and governs the switch S_1 is considered. The quantities are measured using two Keysight DSOX2014A oscilloscope that are triggered simultaneously. The hardware-in-the-loop test presents results widely recognized for the

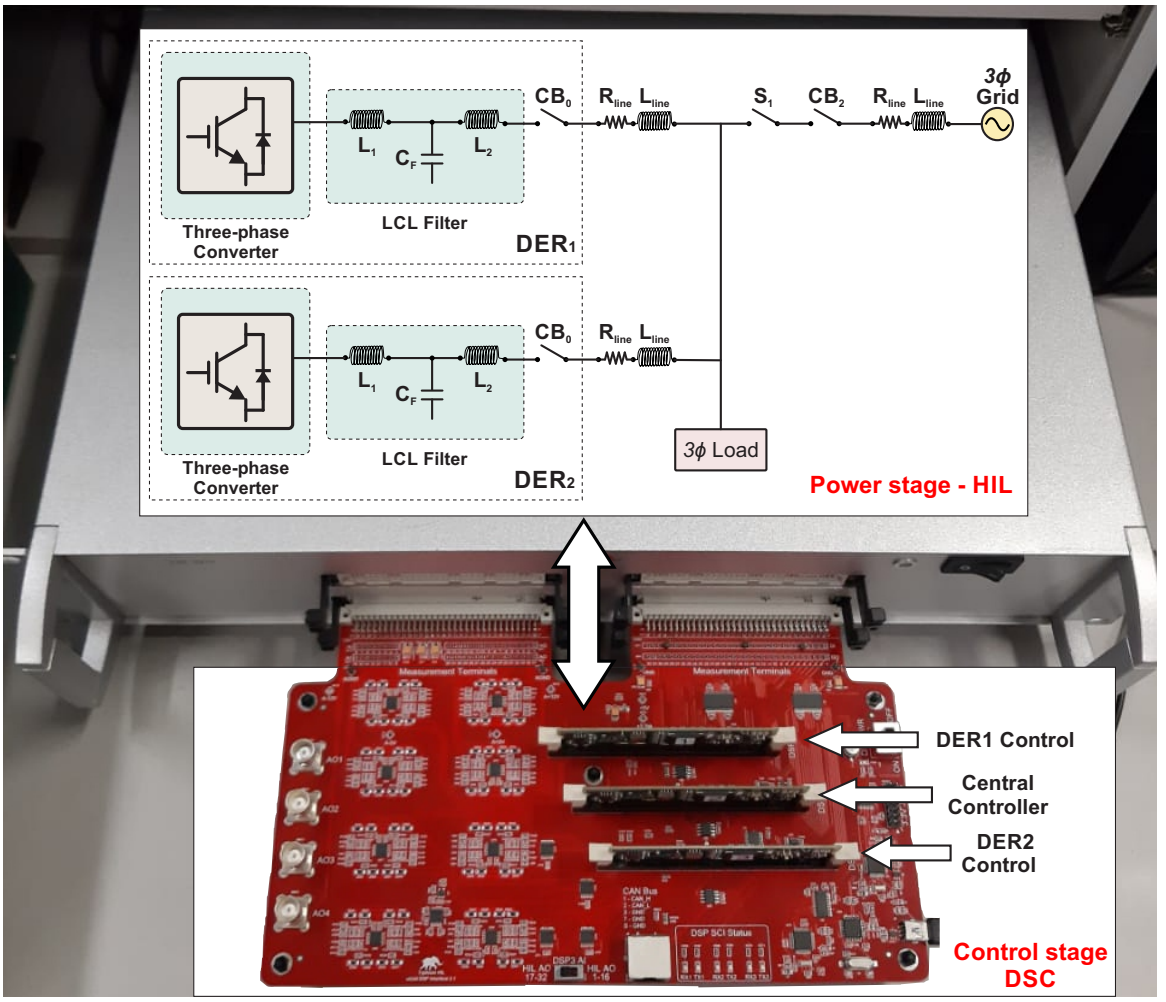

Figure 3.9: Hardware-in-the-loop setup for control validation.

reliability and representativeness of the real plant. Table 3.2 summarizes the system parameters and the controller gains that are used throughout the following tests. The system line impedances (R_{line} and L_{line}) represent a distance of 30 meters between each node, that is, 60 meters from DER_1 to the grid, and 60 meters from DER_2 to the grid.

3.4.1 Power-loop controller model verification

To validate the power–loop model developed in Section 3.3.3, Fig. 3.10 shows the step response of the small-signal model represented in Fig. 3.8 together with Matlab/Simulink simulation and HIL results of an active (Fig. 3.10-a) and a reactive (Fig. 3.10-b) power step during GC operation. The controllers k_{ip} and k_{iq} are tuned to perform a settling time of a step response of about $0.3s$. It is noted that the simulation and model curves are overlapped and the HIL curve is slightly nonidentical, which validates the model of Fig. 3.8.

Table 3.2: System and Control Parameters

System Parameter	**Value**	**Control Parameter**	**Value**
dc-link voltage (V_{DC})	408 V	Gain (k_{pi})	4.27
DER rated power (Sn)	10 kVA	Gain (k_{pv})	1.79
Filter inductor (L_1)	3.85 mH	Gain (k_{iv})	3895
Filter capacitor (C_F)	164.46 μF	Gain (k_{ip})	12
Filter inductor (L_2)	250 μH	Gain (k_{iq})	17.8
Line resistance (R_{line})	0.12 Ω	Gain (k_m)	$3.141e^{-4}$
Line inductance (L_{line})	7.96 μH	Gain (k_n)	$4e^{-4}$
Switching frequency	12 kHz	Sat. (p_{imax})	$10e^3$
Rated grid frequency	60 Hz	Sat. (p_{imin})	$-10e^3$
Rated grid phase-voltage	127 V	Sat. (q_{imax})	$10e^3$
per-phase star-load	$2.42\Omega + 3.21mH$	Sat. (q_{imin})	$-10e^3$
$P_{load3\phi}$ and $Q_{load3\phi}$ at rated conditions	16 kW, 8 $kvar$	θ_{max} @ $V_{CF}^{max} = 127V$	1.12°

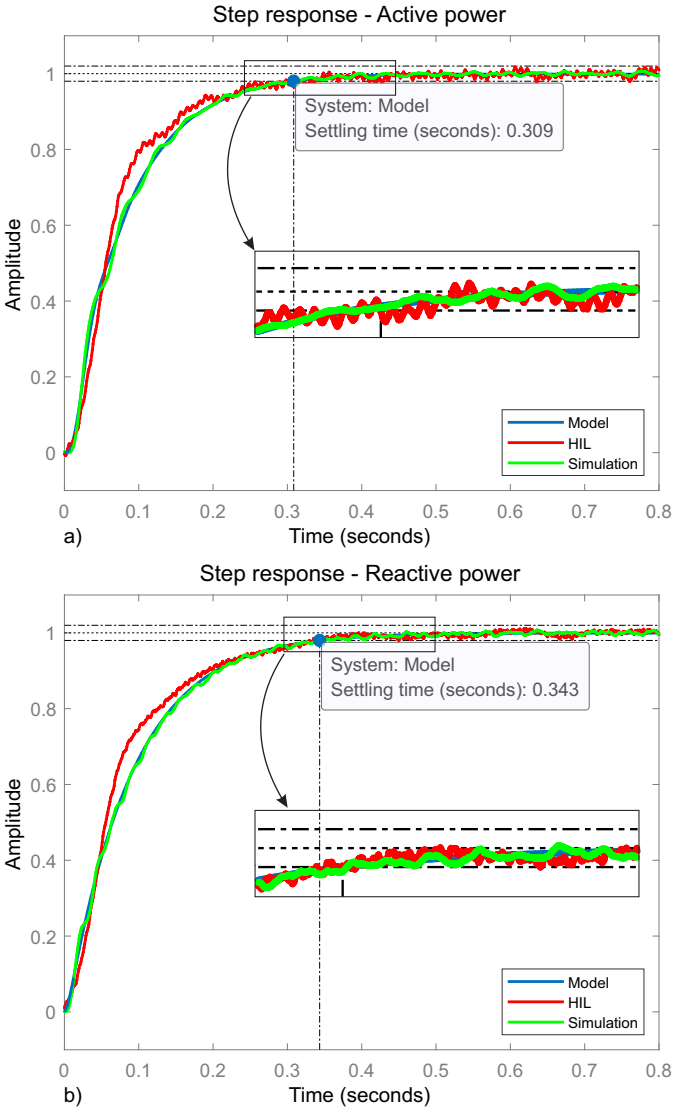

Figure 3.10: a) Step response of active power; b) Step response of reactive power.

3.4.2 Seamless grid-connected to islanded operation transition

This case study verifies the accuracy of P & Q control of the DERs in GC mode; and the seamless transition of parallel DERs without PCC voltage transient during the state passage. Fig. 3.11 shows: the phase-a PCC voltage, frequency, and phase-a DERs currents. At the first instant the MG is in GC mode, and DER_1 and DER_2 provide controlled power ($P_{3\phi} = 6kW$, $Q_{3\phi} = 3kvar$) each, with currents of same amplitude and phase. The DER_1 and DER_2 currents show THD [1] of 1.58% and 2.2%, respectively. When the mains is suddenly disconnected (CB_2 opens), the PCC voltage quality is guaranteed without disturbance, and both DERs instantly share the load current supplied by the main grid. In IS mode, the DER_1 and DER_2 currents show THD of 3.06% and 3.28%, respectively. The THD of the PCC voltage in GC mode is 0.39%, and in IS state is 2.35%. Since the power references for each converter ($P^*_{3\phi} = 6kW$, $Q^*_{3\phi} = 3kvar$) are smaller than the load power that each converter provides ($P_{load3\phi}/2 = 8kW$, $Q_{load3\phi}/2 = 4kvar$), the amplitude and the frequency of the MG voltage saturate at a value lower than the rated ones, according to (3.5) and (3.6). The frequency is saturated above 59 Hz, and the thresholds defined in Table 3.1 are guaranteed. It is worth highlighting that no island detection is needed for continuous operation.

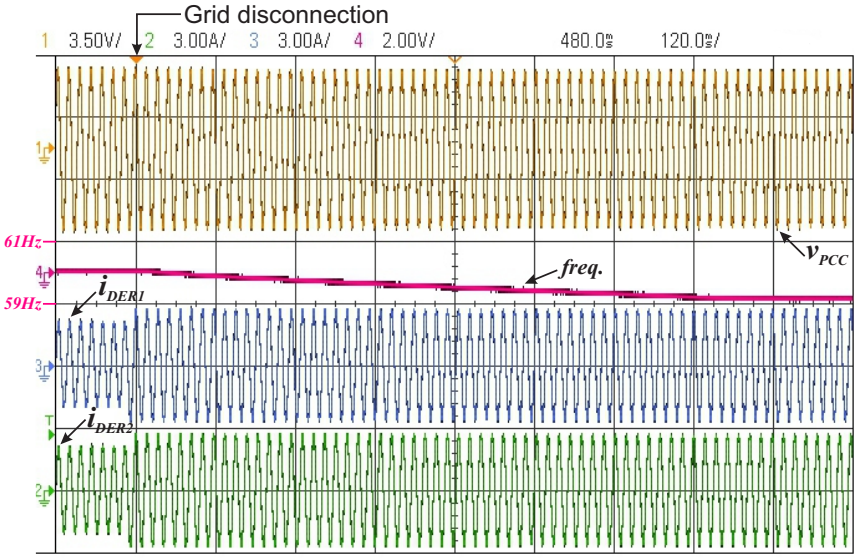

Figure 3.11: Results of the transition from grid–connected to islanded operation. (Ch1:40V/V; Ch2:12A/A; Ch3:12A/A; Ch4:1Hz/V – 60Hz offset.)

3.4.3 Secondary control in islanded mode

For security reasons and to improve the IS operation in steady-state, a MG island detection is used in the CC. When the CC detects that the MG is in IS mode, it turns

[1] The THD is defined as the ratio of the RMS amplitude of harmonic current to the RMS amplitude of the fundamental current [138].

S_1 off and the MG secondary control acts to restore the voltage and frequency to their rated values, improving the quality of the PCC bus voltage. Fig. 3.12-a) shows the instant that the secondary control updates the power references from $P^*_{3\phi} = 6kW$, $Q^*_{3\phi} = 3kvar$ to $P^*_{3\phi} = 8.2kW$, $Q^*_{3\phi} = 4.1kvar$ for each DER, and the voltage amplitude and frequency automatically desaturate and return to their rated values. The power sharing is also improved in terms of proportional contribution as shown in Fig. 3.12-b). After the secondary control acts, during IS mode, the DER_1 and DER_2 currents show THD of 0.47% and 0.71%, respectively; and the THD of the PCC voltage is 0.35%. Note that there is no disturbance at the PCC voltage and on the load current because no switching of control mode is required.

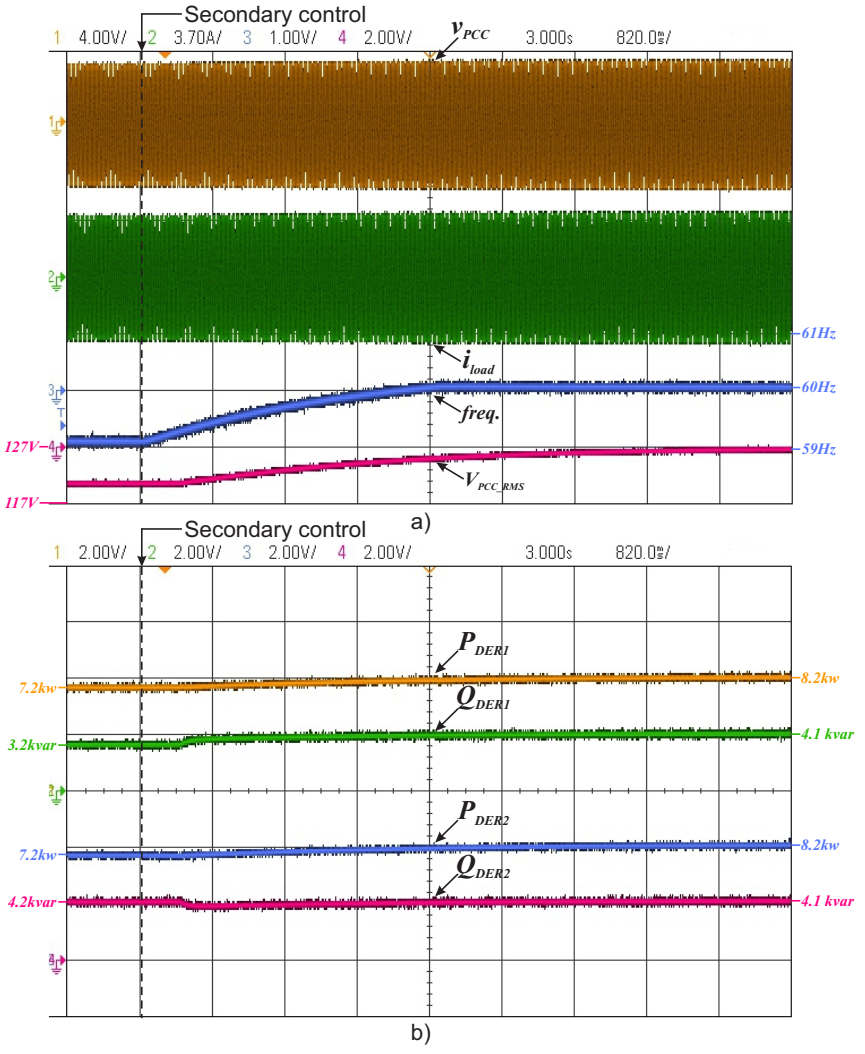

Figure 3.12: Results of the secondary control in islanded mode. a) Ch1:40V/V; Ch2:16A/A; Ch3: 1Hz/V – 60Hz offset; Ch4: 5V/V – 127V offset. b) Ch1: 2000W/V; Ch2:2000var/V; Ch3:2000W/V; Ch4:2000var/V.

3.4.4 Islanded operation to grid-connected transition

When the main grid is reestablished (i.e., CB_2 turns on), the CC broadcasts a flag to the DERs informing that the reconnection process will start. Hence, each DER changes its *frequency switch* to position '3'. Since the secondary control updates the power references to match the load power, the power errors are null, and the converters can

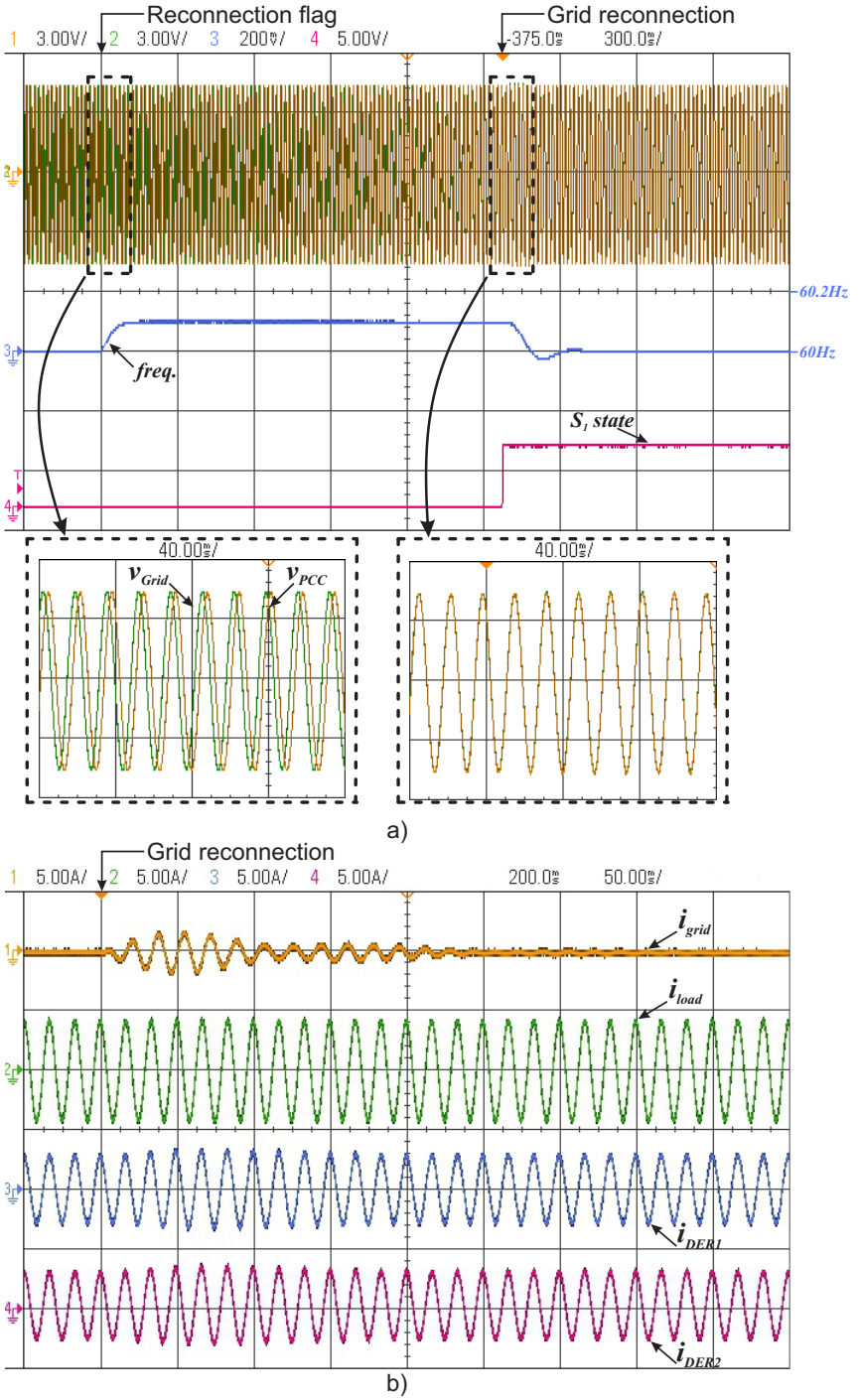

Figure 3.13: Results of the transition from islanded operation to grid–connected. a) Ch1:40V/V; Ch2:40V/V; Ch3:1Hz/V – 60Hz offset; Ch4:1V/V. b) Ch1:12A/A; Ch2:16A/A; Ch3:12A/A; Ch4:12A/A.

change the MG frequency momentarily different than 60 Hz, as shown in Fig. 3.13-a). Thus, the PCC voltage synchronizes to the grid voltage in approximately 1.65s. When the phase difference is minimal, the synchrocheck relay closes S_1, returning to the GC mode. Fig. 3.13-b) shows the currents at the grid, load and DERs at the reconnection instant. No apparent inrush current or voltage transient are shown during the reconnection process; only a small grid current transient ($i_{gridmax} = 19\ A$) is noted due to the frequency mismatching. Since the secondary control had already updated the DERs references to supply the load and operate at rated frequency/voltage in IS state, the main grid do not contribute to the load power at reconnection. The grid current during grid-reconnection is not controlled and is not eliminated. The proposed method based on slip frequency technique is to minimize the grid current at reconnection ensuring a small phase difference between the MG and mains voltages at the time of switch closure. When the reconnection process is finished and the grid is stable, the CC turns the flag off and the DERs operate at *frequency switch* position '2' again. This method does not influence at the system stability as no extra controller is inserted in the DER control levels.

3.4.5 Power control under grid voltage variation

This test is performed to verify that the proposed control can regulate the output power even under grid voltage and frequency variation during GC mode, as shown in Fig. 3.14. Initially, the grid is operating with its rated values, and DER_1 provides $P_{3\phi} = 6kW$ and $Q_{3\phi} = 3kvar$. In Fig. 3.14-a) there is a grid frequency step from $60Hz$ to $59.9Hz$, and in Fig. 3.14-b) there is a grid voltage step from $127V$ to $124V$. When the frequency varies from $60Hz$ to $59.9Hz$ the active power shows a 40% variation in relation to its power reference ($6kW$), but there is no large current or reactive power transient. When the voltage varies from $127V$ to $124V$, the reactive power varies 2.5 times the reference ($3kvar$), and the current presents a peak value of $38A$, which represents 52% of overshoot regarding the reference value. Nevertheless, the current and power values return to their set-points in less than 0.5s. The power loop is designed to be slow (settling time of a step response of about 0.3s), and the effective power tracking is achieved in steady state. The transient dynamics can also be adjusted considering the perturbations in the design of the power loop controllers.

3.4.6 Different load conditions in mode transition

Fig. 3.15 shows a case study that considers three system transitions: first, two VCM converters provide $6kW$ and $3kvar$ to the grid, and a load consumes $16kW$ and $8kvar$. At t_1, there is a large load step to $8kW$ and $4kvar$, the VCM converters are disturbed, but the control properly rejects such disturbance in less than 0.1s as shown in the zoom clip of Fig. 3.15. At t_2, there is an unintentional islanding and, at t_3, another

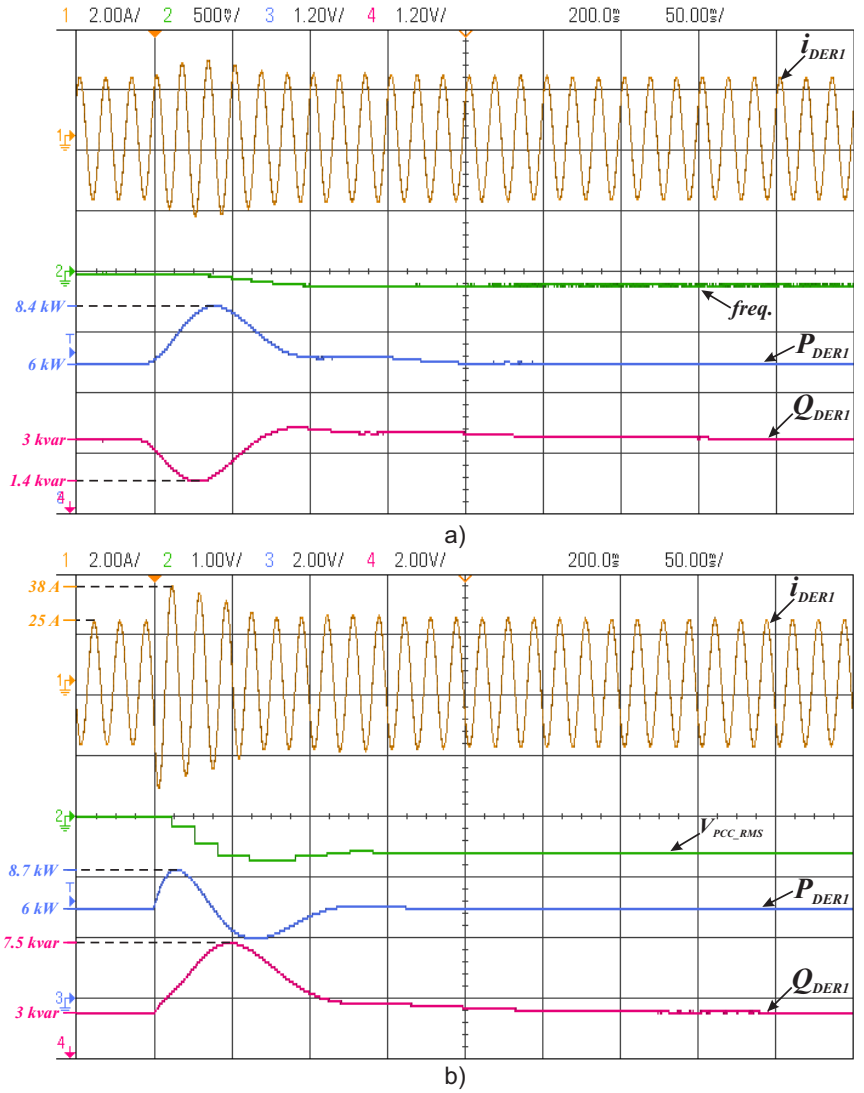

Figure 3.14: Results of the power control with a) Grid frequency variation (Ch1:12A/A; Ch2:1Hz/V – 60Hz offset; Ch3:2000W/V; Ch4:2000var/V.); and b) Grid voltage variation (Ch1:12A/A; Ch2:5V/V – 127V offset; Ch3:2000W/V; Ch4:2000var/V.).

load step to $16kW$ and $8kvar$. The zoom clips show that the system does not present voltage or current overshoots during the islanding and load step variations. In Fig. 3.15, the behavior of DER_2 is omitted due to its similarity with DER_1. Besides, it is worth underlining that a similar result of [57] (Fig. 24) shows a response of 0.25s despite using external grid current control.

Before the islanding, the power references ($P^*_{3\Phi} = 6kW$, $Q^*_{3\Phi} = 3kvar$) of the VCM converters are superior to the load power ($8kW$ and $4kvar$) – considering that the load power is divided by both converter. Then, when islanding occurs, the frequency and amplitude of the voltage saturate above the rated value ($60.26Hz$ and $130.75V$), as shown in Fig. 3.15. This situation is contrary to that shown in Fig. 3.11. When the load step occurs in the islanded operation (t_3), and the load assumes the previous values of $16kW$ and $8kvar$, the frequency and amplitude of the voltage saturate in the lower values

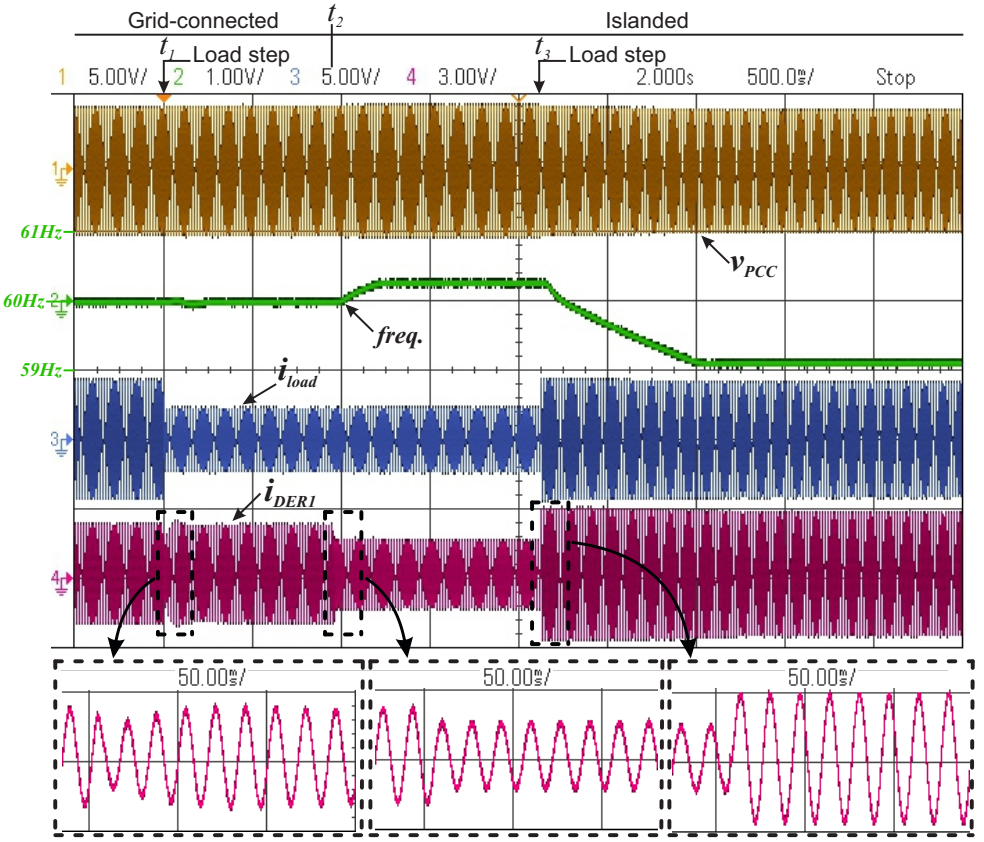

Figure 3.15: Results of mode transition from grid–connected to islanded operation with different load conditions. (Ch1:40V/V; Ch2:1Hz/V – 60Hz offset; Ch3:16A/V ; Ch4:12A/V.)

(59.1Hz and 120.6V), the same as in Fig. 3.11. The voltage amplitude behaves akin to the frequency, so, due to the limited channels on the oscilloscope, it is omitted.

3.4.7 Evaluation of delays in the reconnection process

3.4.7.1 Reconnection process with S1 closing time delay

The deployment of only a contactor (Fig. 3.2-a) for switch S_1 requires a case study considering the closing time delay developed in this section. In contactor manufacturers catalog [139], a minimum and a maximum closing time is guaranteed. For contactors AC-3 of rated currents from 115A to 1000A, the operating closing time varies from 20ms (minimum) to 80ms (maximum) in the worst cases. Two cases are considered: a closing time of 40ms (average) and 80ms (critical), shown in Fig. 3.16-a) and -b), respectively. In Fig. 3.16-a), there is a peak in the grid current (i_{grid}) of 24A, which is barely noticed in the DERs currents. In Fig. 3.16-b), a transient peak in the grid current of 48A arises, but it is not sufficient to cause any substantial disturbance to the system. In both cases the DERs maximum currents are not exceeded. Nevertheless, to reduce the closing time delay, the average delay specified at manufacture's catalog can be compensated in the synchrocheck relay command. For example, for a contactor with a closing time delay of

$40 - 80ms$, the synchrocheck relay may operate $60ms$ before the phase difference reaches its set-point; thus, the actual delay would be a maximum of $\pm 20ms$.

Anyhow, considering the worst-case scenario of an $80ms$ closing time delay (Δt_{delay}), and a frequency difference (Δf) of $0.1Hz$, this would impact in a phase difference ($\Delta\theta$) of 2.88°, as shown in (3.25). This phase difference is in accordance to the IEEE Standard 1547-2018, which requires a maximum phase difference of 20°. Considering a phase difference of 20° and a frequency difference of $0.1Hz$, the closing time delay can be approximately $0.5s$, which is much greater than the closing time of the commonly used contactors.

$$\Delta\theta = 360 \cdot \Delta f \cdot \Delta t_{delay} \tag{3.25}$$

3.4.7.2 Reconnection process with flag signaling delay

The results in this section show that even the DERs receiving the reconnection flag at different time frames, the MG still reconnects smoothly to the main grid. The MG is initially in IS state, and the CC informs the DERs with a flag that the reconnection process will soon begin. DER_2 receives the flag approximately 10 cycles after DER_1, i.e., 167 ms delay, and a small transitory is noted at DERs current when the flag is received, as shown in Fig. 3.17-a). Nevertheless, the reconnection is still smooth with a grid current transient of $15A$, as shown in Fig. 3.17-b).

3.4.8 Islanded operation under adverse conditions

3.4.8.1 Uneven line impedances

In this section, the line impedance of DER_2 is twice the line impedance of DER_1. Fig. 3.18 shows the DERs output power initially in GC mode, in which both DERs provide the same active and reactive power, independent of the line impedance. After the grid disconnection, it is noted that DER_1 contributes with a larger amount of reactive power than DER_2 ($Q_{DER1} = 4460var$; $Q_{DER2} = 3000var$). However, the power sharing is reestablished with the secondary control. The active power, on the other hand, is shared all over the process. In fact, line impedance only influences the reactive power sharing in IS mode, as expected for conventional droop.

3.4.8.2 DERs with different power ratings

This case study considers DER_2 with half of the power rating of DER_1. Fig. 3.19 shows the DERs output power initially in GC mode, in which DER_2 provides half of the active and reactive power of DER_1. After the grid disconnection, it is noted that the active power is still shared proportionally ($P_{DER1} = 7360W$; $P_{DER2} = 3700W$), but the

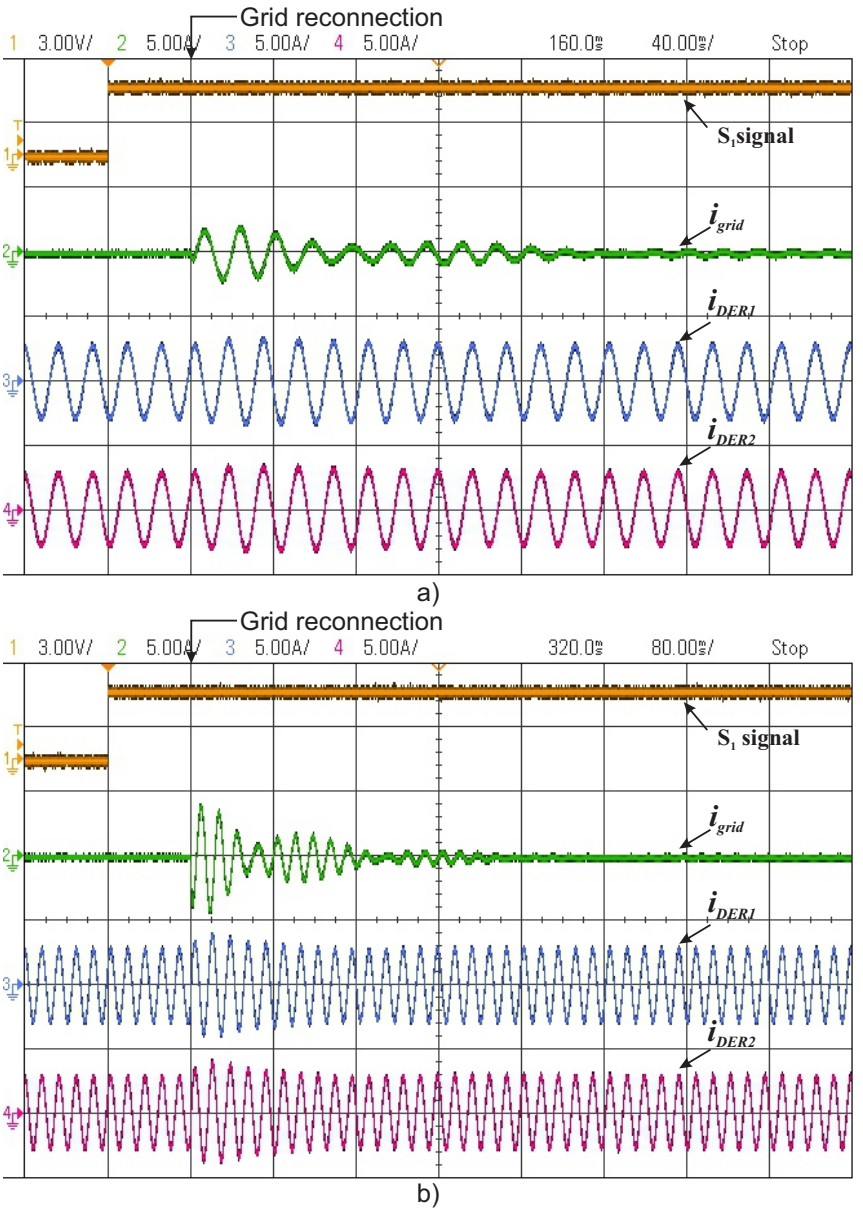

Figure 3.16: Results of different switch S_1 closing time in the reconnection process. a) Switch S_1 closing time delay of $40ms$. b) Switch S_1 closing time delay of $80ms$. (Ch1: 1V/V; Ch2:12A/A; Ch3:12A/A; Ch4:12A/A).

reactive power sharing is impaired ($Q_{DER1} = 2920var$; $Q_{DER2} = 2720var$). However, the control structure implemented in the converters (Fig. 3.3) allows the power sharing to be reestablished with the secondary control, as shown in Fig. 3.19.

3.5 Conclusions

This chapter proposed a control method for grid–forming voltage-controlled mode converters to proper microgrid operation in both islanded and grid–connected modes with smooth transition between them. The main novelty of this method is that it does not rely on high–speed communication for resynchronization, and no critical islanding de-

tection is required, which would be an issue in large microgrids with many distributed generators. The results performed in hardware-in-the-loop have shown that the proposed method achieves precise output active and reactive power control in grid-connected mode even under frequency/voltage variation; seamless transitioning from grid–connected mode to islanded mode; autonomous power sharing between other voltage-controlled mode converters; and smooth reconnection to the main grid after islanding. Thus, the proposed control structure would be suitable for implementation in distributed VCM converters in order to replace the central converter approach.

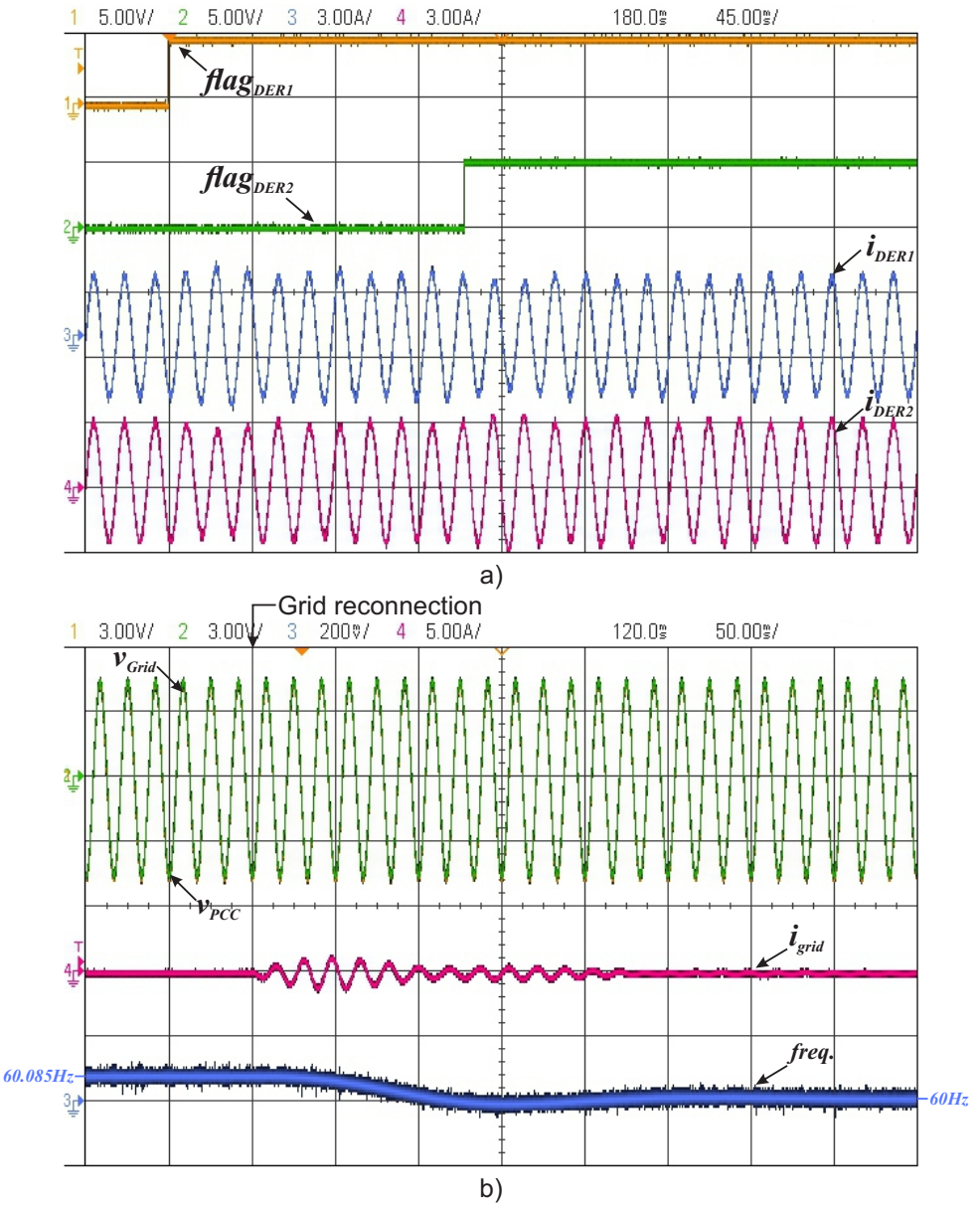

Figure 3.17: Results of different signal flag receiving time in the reconnection process. a) DERs currents and flag receiving time. (Ch1: 1V/V; Ch2:1V/V; Ch3:12A/A; Ch4:12A/A) b) Grid and PCC voltages, grid current and MG frequency at reconnection time. (Ch1: 40V/V; Ch2:40V/V; Ch3:1Hz/V; Ch4:12A/A).

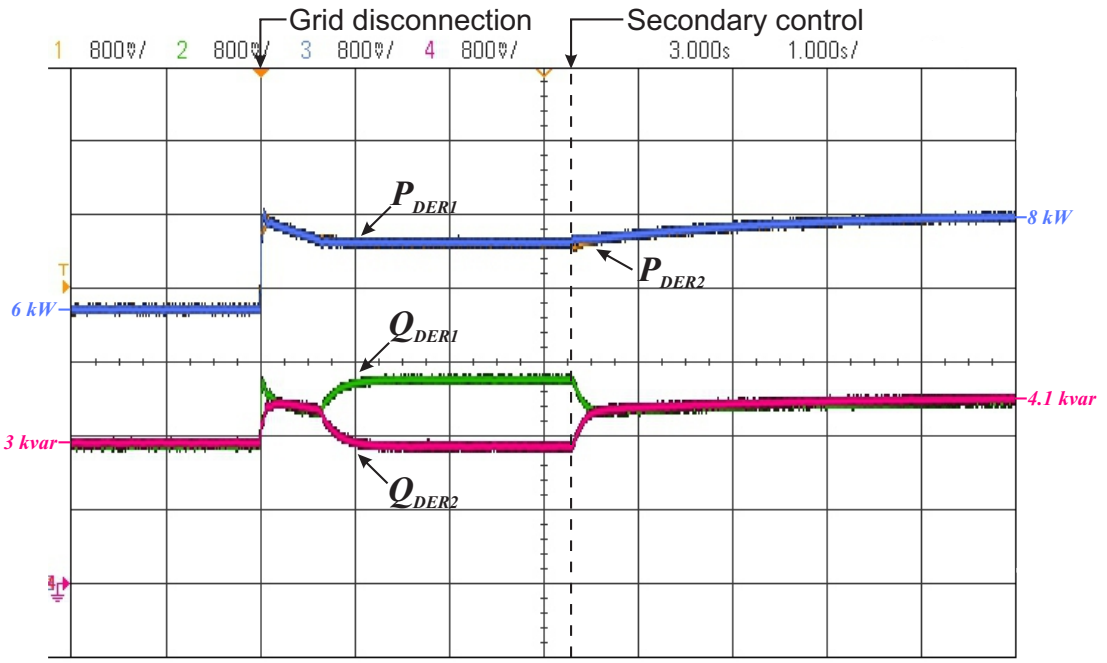

Figure 3.18: Results of mode transition from grid–connected to islanded operation with different line impedance between converters. (Ch1:2000W/V; Ch2:2000var/V; Ch3:2000W/V ; Ch4:2000var/V.)

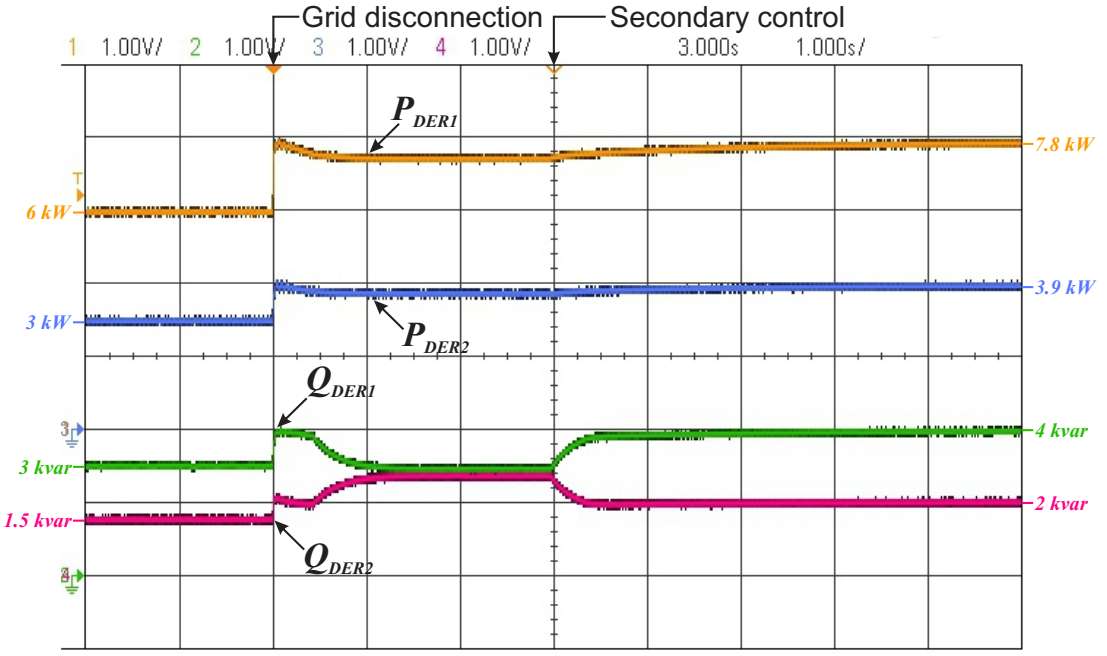

Figure 3.19: Results of mode transition from grid–connected to islanded operation for converters with different power ratings. (Ch1:2000W/V; Ch2:2000var/V; Ch3:2000W/V ; Ch4:2000var/V.).

Chapter 4

Centralized Control for Heterogeneous Converters

4.1 Introduction

Considering the literature review presented in Section 2.3, a gap is identified regarding a strategy capable of fulfilling concomitantly the advanced MGs objectives and also considering different sorts of DERs in its control. Thus, this chapter proposes a complete hierarchical control for MGs able to perform the following features:

- precise grid power flow control;
- proportional power sharing among all DERs;
- power unbalance compensation at PCC;
- participation of single- and three-phase DERs;
- participation of CCM and VCM converters;
- participation of DERs with self-imposed constraints;
- voltage and frequency restoration;
- operation in both grid-connected and islanded modes;
- smooth transitioning between operating modes;
- no need for critical islanding detection and previous knowledge of MG parameters.

The proposed MG control modifies the so-called PBC and uses it together with the droop-based power-loop for VCM converters developed in Ch. 3. One fundamental particularity of this new method is the absence of the central converter in comparison to previous works [11,103]. Herein, multiple distributed VCM converters are able to form the

MG in islanded mode and still perform power-sharing with other heterogeneous DERs. Thus, a new MG structure is introduced to achieve all these features. Besides, only scaling coefficients are communicated to DERs power loop, that is, no other information is transmitted from the CC to DERs, so there is no switching operation in DERs environment.

4.2 Hierarchical Control

The PBC is a MG control strategy implemented in MG applications based on a hierarchical centralized architecture for low–voltage distribution networks in urban areas. Its main premise is to provide active/reactive power sharing among DERs in proportion to their available capability. Also, when running in connected mode and depending on the energy resources availability, to provide accurate controlled active/reactive power to the upstream grid.

This strategy features coordinate regulation of DERs by a central unit located at the PCC, as shown in Fig. 4.1(a). The possibility of providing controlled active and reactive power to the grid makes the MG model to become dispatchable in active and reactive power. Also, the PBC inherits as main advantages low implementation complexity, minimum requirements in terms of ICT (i.e., narrowband and low data rate communication), not requiring previous knowledge of the network parameters, and it supports the plug-and-play integration of new DERs. The information exchanged between the CC and DERs consists only on average values.

The adopted hierarchical MG control approach is basically split into three layers as shown in Fig. 4.1b). This division is done according to the updated frequency rate

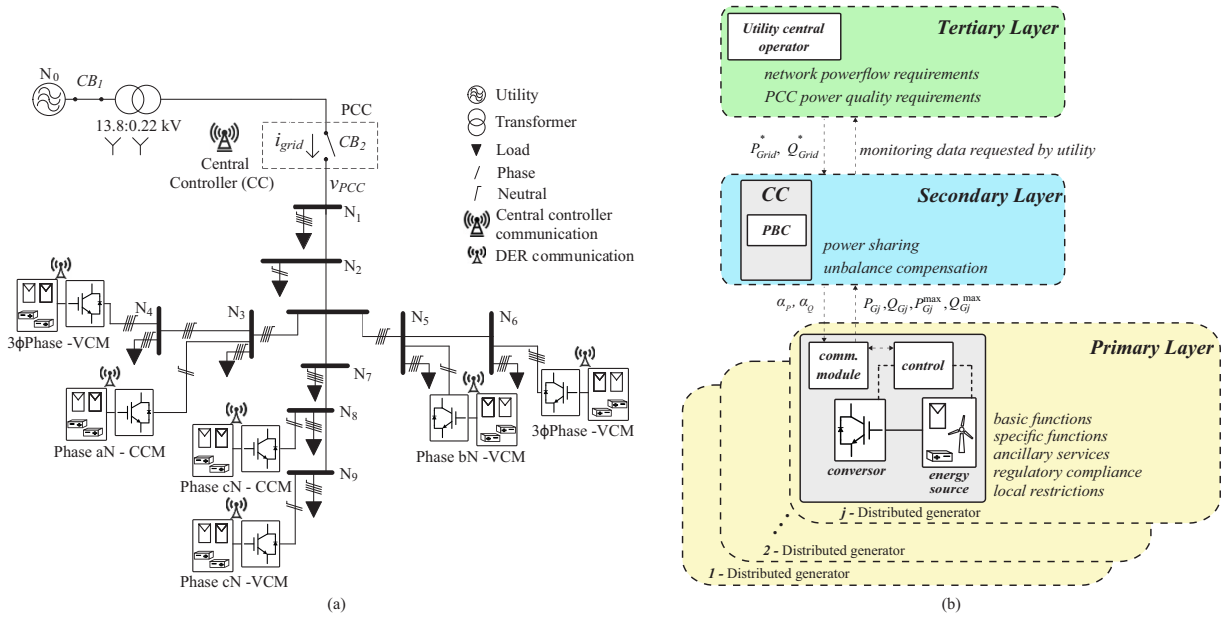

Figure 4.1: a) Low-voltage three-phase microgrid. b) MG hierarchical control architecture.

of the handled variables, also upon the imperativeness of the layer for the system overall adequate operation.

The primary layer is the fastest one, working on the kHz scale, and it is responsible for the local operation of DERs. This layer includes the basic and specific functions, which are the elementary operational functions of the converter to work according to standardized requirements, such as the current and voltage control, dc–link control, and grid synchronization. Depending on the PES and local grid codes, there are some specific functions for each of them [140]. Ancillary services are complementary offered, being not vital for the converter operation. It is worth underlining that local controllers guarantee compliance with grid codes, and do not rely on the communication link.

The secondary layer comprises the PBC algorithm and it is executed based on a fundamental frequency rate ($\approx 20\ ms$) or slower. This layer works toward the proportional power sharing, where the power quantities of each DER are sent to the CC. Thereupon, the CC broadcasts the new portion of power that each DER shall provide, according to their capability. Hence, the secondary layer is dependent on communication. However, if the communication is lost, the MG still operates assuming the functionalities of the primary layer.

The tertiary layer is the slowest, being updated few times per day. It is responsible for defining the references for the active or reactive power flow between the MG and the main grid, therefore it only works under interconnected mode. This layer allows the interaction with the utility's distribution system operator (DSO), in terms of active and reactive power flow. Note that there is no control loop in this layer; it just generates the active and reactive power references based on technical or economic interests within the mutual agreed contract.

4.3 Microgrid Structure and Converters Control

A MG structure that comprises all sorts of DERs described in Section 4.1 is shown in Fig. 4.2. The MG is connected to the main grid at its PCC through switch S_1. The CC is installed at the PCC to measure PCC voltage, v_{PCC}, and grid current, i_{grid}, and thus, to calculate PCC power quantities. The CC is equipped with a communication device to receive power quantities from the DERs and to broadcast the scaling coefficients back to them. Both the proposed PBC and the *Restoration Control* are implemented in the CC, which is responsible to calculate the appropriate values of the coefficients. Also, a synchrocheck relay is used to reconnect the MG from islanded to grid-connected mode. It measures the voltages at the main grid and PCC and detects when both voltages are in-phase, then it closes switch S_1 so the MG reoperates grid-connected.

The loads and DERs are spread out over the MG with different values of line impedance between them. Notably, there is not a central converter for grid-forming role in

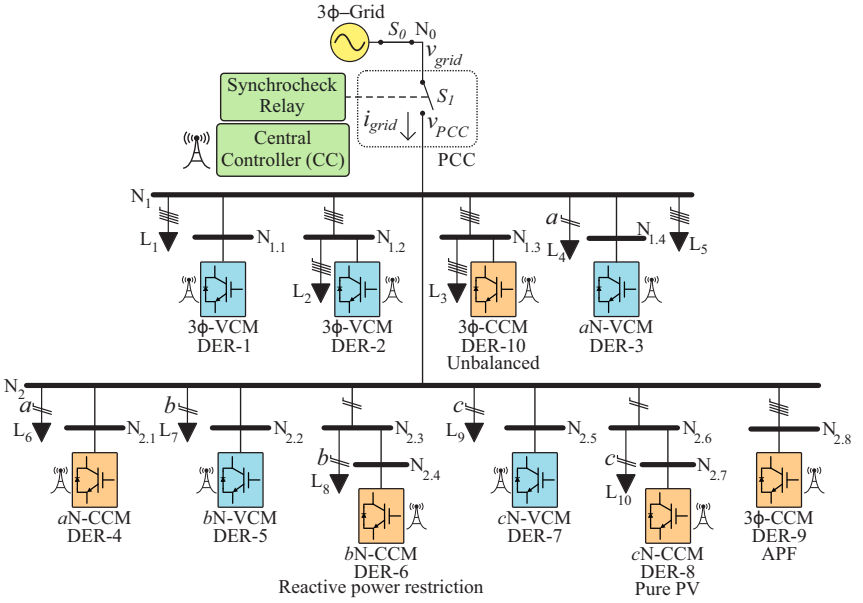

Figure 4.2: Three-phase Microgrid structure with heterogeneous converters.

this MG structure. Thus, the distributed 3Φ-VCM DERs are responsible for grid-forming in islanded operation. The DERs are also equipped with communication for participating in the coordinated control. Single- and three-phase VCM DERs, single- and three-phase CCM DERs, and DERs with self-imposed limits are considered, thus, characterizing a heterogeneous MG.

The control scheme of the single- and three-phase DERs, under both CCM and VCM, are devised in abc-frame as shown in Fig. 4.3. The control scheme of a CCM DER, highlighted in orange, comprises an inner inductor-current control and an outer power control loop. Then, the inverter tracks a precise instantaneous current reference, which is given by the power loop. The VCM DER control scheme, highlighted in blue, is split into three loops: *i*) external power-loop responsible for controlling the output power during grid-connected operating mode, and for smooth transition to islanded mode; *ii*) voltage-control loop that regulates the voltage across C_F capacitor; and *iii*) inner current-loop that controls the current through the L_1 inductor and guarantees over-current protection. The power-loop for VCM converters is shown in Fig. 4.4. It is adapted from Ch. 3, which is a droop-based control that allows accurate output active and reactive power control in grid-connected mode and seamless transitioning from grid-connected to islanded mode. In Ch. 3, the power loop also contains a frequency switch for smooth reconnection of multiple grid-forming converters to the main grid, which is moved in this proposal to the CC, as explained in Section 4.4.2. The use of this power-loop at VCM converters allows a MG structure that operates in both modes without a central converter and critical islanding detection.

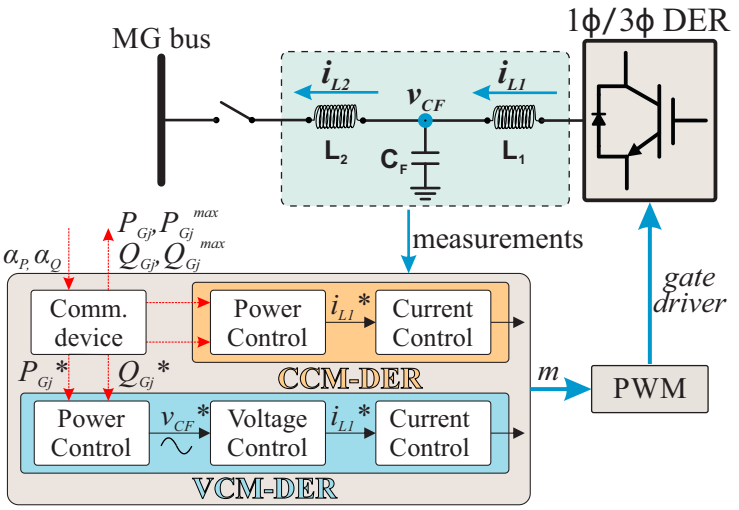

Figure 4.3: Primary control of CCM and VCM DERs.

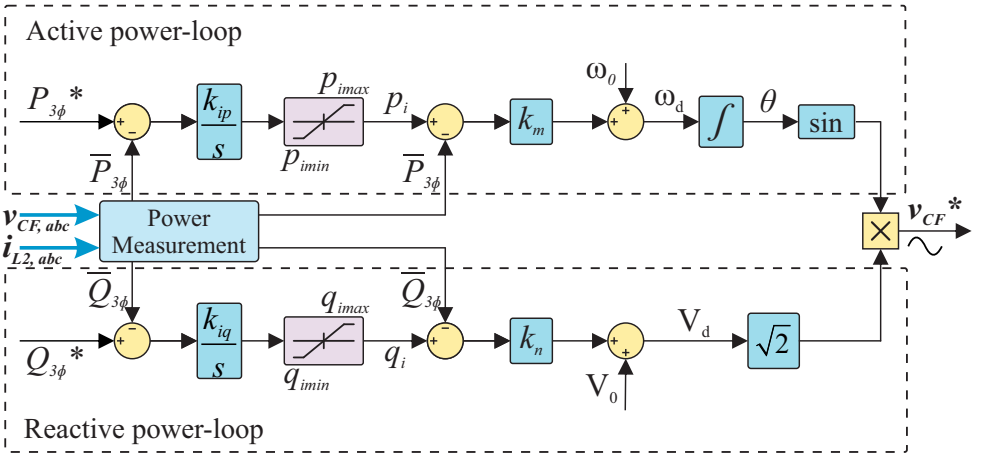

Figure 4.4: Power control loop of VCM DERs.

4.3.1 DERs self-imposed limits

Most of the DERs installed at distribution level are not designed to participate in a coordinated control for MGs. Thus, due to manufacturing and application reasons, some DERs may present self-imposed limits. Nevertheless, in this chapter is proposed a coordinated control that allows the DERs already installed to be engaged in the provision of ancillary services, without the need of retrofitting. Four types of self-imposed limits are considered, as follows:

4.3.1.1 Three-phase DERs that must operate balanced

These converters are considered fed by hybrid PV and batteries sources or only by batteries (or other type of dispatchable source, e.g., fuel cell). The necessity of the converter to always operate balanced is mainly related due to the small dc-link capacitor that is usually specified in commercial three-phase PV inverters. Thus the dc-link oscillation, caused by unbalanced currents, would impair the converter operation [141].

4.3.1.2 DERs with reactive power processing constraint

Generally, the diodes thermal resistance of commercial inverters power modules are higher than those of the IGBTs – in ABB Hi Pack IGBTs, for example, the difference is almost double [142]. In [143] and [144] it is shown that the diode temperature exceeds the IGBT temperature. When reactive power is synthesized, the peak current and the maximum synthesized voltage are not in-phase, which causes current circulation through the diodes bridge. These manufacturing and operating aspects lead the converter to have a maximum rated reactive power, that is, nameplate reactive power, different from its maximum active power. Thus, these constraints are taken into account in the proposed coordinated control strategy.

4.3.1.3 Pure PV DERs

This type of DER represents single or three-phase inverters fed by PV sources that do not hold storage systems. The DER active power reference is provided by its implemented maximum power point tracking (MPPT) algorithm, so it always delivers the maximum power available at that instant. This way, one obtains maximum use of the PV source, but active power sharing is not performed. If the inverter does not provide its maximum rated power, due to irradiation conditions, the remaining available inverter power can be exploited for reactive power processing and the DER can contribute to reactive power sharing and unbalance compensation.

4.3.1.4 Active power filter

An active power filter (APF) is a converter that only holds a dc capacitor in its dc–link. Thus, it is considered to only process non–active terms, e.g., reactive power or unbalanced power when a three-phase converter is considered. This way, its active power reference is null, but the APF contributes to reactive and unbalanced power sharing.

4.4 Centralized Control for Heterogeneous Distributed Converters

This section develops the centralized coordinated control used for achieving tight grid power flow control, proportional power sharing, and unbalance compensation in both grid-connected and islanded modes. An improvement in the MG structure using the PBC strategy is proposed herein, in which a central converter is not required, so distributed three-phase VCM DERs act as grid-forming converters in islanded mode. Thus, the PBC is modified to consider the distributed VCM converters and the converters with self-imposed limits. In islanded operation, a *Restoration Control* is proposed to be applied together

with the PBC, so voltage and frequency deviations are restored, and VCM converters keep sharing power with other DERs regardless their power electronic topology and limits.

4.4.1 Modified Power-based Control

For the sake of understanding, the PBC is split into three main cyclical steps: 1) each DER sends its power quantities that characterizes its status to CC; 2) PBC algorithm is processed in CC and the scaling coefficients are calculated and broadcast to DERs; and 3) the local controller of each DER sets its active and reactive power references based on the scaling coefficients received. The latter step is explained in detail to each sort of DER.

4.4.1.1 Data Packet from DERs to Central Controller

The control is performed on the basis of the status of distributed units, which is collected by the CC at the beginning of each control cycle (k). The status of a j-th DER (j = 1, 2, ..., J) is a set of power quantities representing the availability of generating power of the DER, which includes: the measured output active, $P_{Gj}(k)$, and reactive, $Q_{Gj}(k)$, power; and the maximum capacity of providing active, $P_{Gj}^{max}(k)$, and reactive, $Q_{Gj}^{max}(k)$, power, given by (4.1); where A_{Gj} is the rated apparent power of DER$_j$; and, if local storage is present, the minimum active power, $P_{Gj}^{min}(k)$, that can be absorbed. Both VCM and CCM DERs are included on these quantities.

$$Q_{Gj}^{max}(k) = \sqrt{A_{Gj}^2 - P_{Gj}^2(k)} \tag{4.1}$$

4.4.1.2 PBC Algorithm Processed in Central Controller

Once the CC has gathered all the required information, the status of the whole MG is computed in terms of the power quantities introduced in the following steps. Let us indicate with m a generic phase of a three-phase system, and with 3ϕ any three-phase quantities for three-phase balanced devices. Active and reactive power calculations are analogous, so only active power quantities are demonstrated. The mentioned steps and computed quantities are:

i) Total active power delivered by three-phase, $P_{G3\Phi t}(k)$, and single-phase, $P_{Gmt}(k)$, DERs at cycle k:

$$P_{G3\Phi t}(k) = \sum_{j=1}^{J} P_{G3\Phi j}(k) \tag{4.2}$$

$$P_{Gmt}(k) = \sum_{j=1}^{J} P_{Gmj}(k) \tag{4.3}$$

Similarly, it is calculated the total minimum, $P^{min}_{G3\Phi t}(k)$, $P^{min}_{Gmt}(k)$, and maximum, $P^{max}_{G3\Phi t}(k)$, $P^{max}_{Gmt}(k)$, balanced and *per-phase* capacity of providing active power.

Three-phase converters that allow unbalanced operation are treated here as three single-phase converters connected on the same node. Their reported quantities must be properly addressed to the phases they represent.

ii) Total capacity of active power available by DERs for contributing to the whole MG power needs:

$$P^{max}_{Gt}(k) = P^{max}_{G3\Phi t}(k) + \sum_{m=1}^{M} P^{max}_{Gmt}(k) \tag{4.4}$$

iii) Total active power, $P_{MGmt}(k)$, demanded by the MG *per phase* during cycle k:

$$P_{MGmt}(k) = P_{gridm}(k) + P_{Gmt}(k) + \sum_{j=1}^{J} P_{VCM3\Phi mj}(k) \tag{4.5}$$

where $P_{gridm}(k)$ is *per phase* active power measured at the grid side of PCC; and $P_{VCM3\Phi mj}(k)$ is *per phase* active power delivered by j-th 3Φ-VCM DERs.

iv) Total three-phase active power, $P_{MGt}(k)$, processed within the MG at cycle k:

$$P_{MGt}(k) = P_{G3\Phi t}(k) + \sum_{m=1}^{M} P_{MGmt}(k) \tag{4.6}$$

Note that $P_{G3\Phi t}(k)$ comprises the power provided by balanced 3Φ-VCM and 3Φ-CCM DERs, so both types of converters share power in grid-connected and during islanded mode. The distribution power losses through line impedance are automatically considered in this calculation, likewise any other distributed inverter not participating in the PBC.

v) In possession of the total power absorbed and generated in the MG, the CC calculates the references for the total three-phase active power, $P^{*}_{G3\Phi t}(k+1)$, to be delivered by three-phase balanced DERs in the next control cycle, *k+1*; and the references for the total *per phase* active power, $P^{*}_{Gmt}(k+1)$, to be provided by single-phase DERs and for each phase of three-phase unbalanced DERs:

$$P^{*}_{G3\Phi t}(k+1) = P_{MGt}(k) - [\sum_{m=1}^{M} P^{*}_{gridm}(k+1) + P^{*}_{VCM3\Phi t}(k)] \tag{4.7}$$

$$P^{*}_{Gmt}(k+1) = P_{MGmt}(k) - [P^{*}_{gridm}(k+1) + \frac{P^{*}_{VCM3\Phi t}(k)}{3}] \tag{4.8}$$

These DERs related references are computed by the CC to regulate the power flow

at MG's PCC among the different phases, according to the energy state of the DERs. Note that they are estimated for a next control cycle, based on the quantities measured during the actual cycle k.

$P^*_{gridm}(k+1)$ is *per phase* active reference of the grid power flow determined by a tertiary control layer, and guarantee the balanced condition at the grid side. They may be set based on energy management strategies [13, 14], or on optimization algorithms [145], or zero in islanded mode.

$P^*_{VCM3\Phi t}(k)$ is the sum of all j-th 3Φ-VCM DERs active power references at cycle k, $P^*_{VCM3\Phi j}(k)$, i.e., $P^*_{VCM3\Phi t}(k) = \sum_{j=1}^{J} P^*_{VCM3\Phi j}(k)$. The active power reference of each j-th 3Φ-VCM DER is set by multiplying the scaling coefficient $\alpha_{P3\phi}$ (4.9) by its maximum active power capacity (4.13), i.e., $P^*_{VCM3\Phi j}(k) = \alpha_{P3\phi} \cdot P^{max}_{VCM3\Phi j}$.

Note that the computation explained so far is developed in the CC. In this modified version of PBC, $P^*_{VCM3\Phi t}(k)$ is added so distributed 3Φ-VCM DERs share power with other DERs even in islanded mode, as detailed in Section 4.4.2.

vi) Finally, the 3ϕ scaling coefficients $\alpha_{P3\phi}$ and $\alpha_{Q3\phi}$, and the phase scaling coefficients α_{Pm} and α_{Qm} (all ranging in the interval [-1, 1]) are computed and broadcast to all DERs. $\alpha_{P3\phi}$ and $\alpha_{Q3\phi}$ are sent to three-phase balanced devices only, while α_{Pm} and α_{Qm} are broadcast to single-phase units connected to the corresponding m-phase, and for three-phase unbalanced DERs. Active power is controlled by variable α_P, while reactive power is controlled by variable α_Q. Negative and positive signals of α_P and α_Q represents, respectively, storage and delivery of active power, and capacitive and inductive reactive power.

$$\alpha_{P3\Phi} = \frac{P^*_{G3\Phi t}(k+1)}{P^{max}_{Gt}(k)} \ , \ \alpha_{Q3\Phi} = \frac{Q^*_{G3\Phi t}(k+1)}{Q^{max}_{Gt}(k)} \tag{4.9}$$

$$\alpha_{Pm} = \frac{P^*_{Gmt}(k+1)}{P^{max}_{Gmt}(k)} \ , \ \alpha_{Qm} = \frac{Q^*_{Gmt}(k+1)}{Q^{max}_{Gmt}(k)} \tag{4.10}$$

It is worth underlying that in steady-state, the coefficients are summarized in (4.11) and (4.12), which verifies that the DERs actually perform power sharing with each other.

$$\alpha_{P3\Phi} = \frac{\sum_{m=1}^{M} P_{Gmt}(k) + P_{G3\Phi t}(k)}{P^{max}_{Gt}(k)}, \textit{ in steady-state} \tag{4.11}$$

$$\alpha_{Pm} = \frac{P_{Gmt}(k)}{P^{max}_{Gmt}(k)}, \textit{ in steady-state} \tag{4.12}$$

4.4.1.3 Power Reference Generator of DERs local controller

Once the DERs have received the scaling coefficients, they establish their local active and reactive power references. It is emphasized that any type of overload in steady–state is avoided, since the saturation of the scalar coefficients are taken into account by the CC itself. Also, the active power injection takes precedence over reactive power contribution, which is assigned sequentially, (4.1). Although, for transient protection it is still required the proper limiter in DER's local control loops. The power references are separated according to different types of DERs, as follows:

i) Single-phase and/or balanced three-phase DERs

Both DER topologies single-phase and balanced three-phase generate their power references similarly, but using their correspondent coefficients α_{Pm}, α_{Qm} or $\alpha_{P3\phi}$, $\alpha_{Q3\phi}$, here generalized as α_P and α_Q. Given α_P and α_Q, the DER local control sets its active and reactive power injection according to (4.13) and (4.14). Where, $P^*_{Gj}(k)$ and $Q^*_{Gj}(k)$ are respectively the active and reactive power references for j-th DER at the current control cycle.

$$P^*_{Gj}(k) = \alpha_P \cdot P^{max}_{Gj} \tag{4.13}$$

$$Q^*_{Gj}(k) = \alpha_Q \cdot Q^{max}_{Gj}(k) \tag{4.14}$$

ii) Unbalanced three-phase DERs

The three-phase converter that allows unbalanced operation receives all the six phase scaling coefficients (α_{Pm} and α_{Qm}), and sets different power references for each phase, proportional to the coefficients. For this, the three–phase DER power is equally divided into each phase, and the maximum available phase capacity for reactive power compensation, $Q^{max}_{G3\phi mj}(k)$, is calculated:

$$A_{G3\phi mj} = \frac{A_{G3\phi j}}{3} \tag{4.15}$$

$$P^{max}_{G3\phi mj} = \frac{P^{max}_{G3\phi j}}{3} \tag{4.16}$$

$$Q^{max}_{G3\phi mj}(k) = \sqrt{A^2_{G3\phi mj} - P^2_{G3\phi mj}(k)} \tag{4.17}$$

Thus, the power references for each phase are calculated:

$$P^*_{G3\phi mj}(k) = \alpha_{Pm} \cdot P^{max}_{G3\phi mj} \tag{4.18}$$

$$Q^*_{G3\phi mj}(k) = \alpha_{Qm} \cdot Q^{max}_{G3\phi mj}(k) \tag{4.19}$$

In this type of converter, it is expected greater dc-link voltage oscillation than in balanced converters, so dc capacitors should be properly designed.

iii) DERs with reactive power processing constraint

DERs that have limits in reactive power processing, due to manufacturing reasons, must establish the maximum reactive power according to their current condition of power supply. For exemplification, consider a single-phase converter that can process only 44% of reactive power, as in [132]. The rated (i.e., nameplate) reactive power, $Q^{max}_{Gjrated}$, is calculated in (4.20), yet the maximum capacity of providing reactive power in cycle k, $Q^{max}_{Gj}(k)$, is calculated in (4.21). If $Q^{max}_{Gj}(k)$ value is greater than $Q^{max}_{Gjrated}$, then $Q^{max}_{Gjrated}$ is sent to CC and it is used to receive the coefficients, otherwise $Q^{max}_{Gj}(k)$ is used, as shown in Fig. 4.5. Then, the active and reactive power references are set as in (4.13) and (4.14).

$$Q^{max}_{Gjrated} = 0.44 \cdot A_{Gmj} \tag{4.20}$$

$$Q^{max}_{Gj}(k) = \sqrt{A^2_{Gj} - P^2_{Gj}(k)} \tag{4.21}$$

iv) Pure PV DERs

Pure PV DER must exploit its active power to maximize the use of its renewable source. Thus, the active power reference is its maximum available active power, (4.22), and it does not participate in active power sharing. In case of no restriction in processing reactive power, its reactive power reference is provided as in (4.14), ensuring three-phase DERs to operate balanced (typical commercial inverter). If the DER has reactive power restriction, its reference is calculated as in Section 4.4.1.3*iii*). Otherwise, if the DER should operate with unity power factor, its reactive power

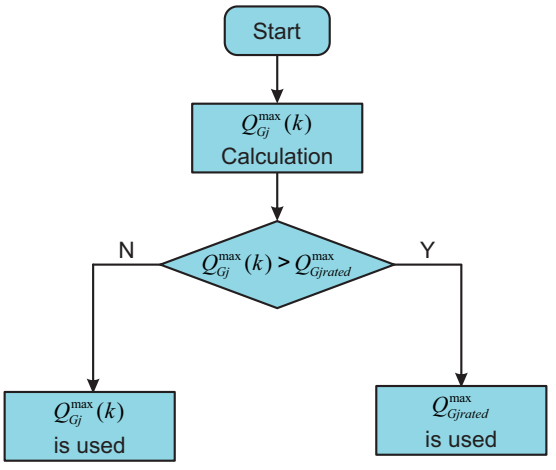

Figure 4.5: Flowchart of maximum reactive power evaluation.

reference is simply null.

$$P^{*}_{GPV}(k) = P^{max}_{GPV}(k) \tag{4.22}$$

v) Active power filter

An APF is a converter without active power supply, so its active power reference is null. Usually, this kind of converter is able to operate unbalanced, thus, its reactive power reference is defined as in (4.19). Thus, APFs contribute to reactive power and imbalance compensation.

4.4.2 3-phase VCM DERs References and Restoration Control

In the proposed MG structure, 3Φ-VCM DERs provide controlled active and reactive power in grid-connected mode, participating in the PBC and sharing power with other DERs. Thus, they receive the same coefficients as other balanced 3Φ-CCM DERs, $\alpha_{P3\Phi}$ and $\alpha_{Q3\Phi}$, and set their power references as in (4.13) and (4.14).

When islanding occurs, the power controllers (Fig. 4.4) saturate and 3Φ-VCM DERs operate droop-controlled. Thus, the MG runs with a natural voltage and frequency deviation. Thereby, the control scheme of Fig. 4.6 is proposed. When islanding is detected by the CC, the *islanding switch* is turned to position 2, and the coefficients, $\alpha_{P3\Phi-\mathrm{VCM}}$ and $\alpha_{Q3\Phi-\mathrm{VCM}}$, change to a frequency and voltage restoration control. The *Restoration Control* detects the PCC frequency and voltage deviation and updates the coefficients of 3Φ-VCM DERs through the output of a *PI*. The *PI* of both loops must be designed to obtain slower dynamics than the power-loop embedded in DERs. The complete procedure of this design is out of scope of this work. In this way, the power controllers desaturate and the islanded MG operates at rated condition. When 3Φ-VCM DERs are desaturated, they automatically share active and reactive power with each other and among other DERs that participate in PBC. Notably, in islanded mode, the power reference $P^{*}_{VCM3\Phi t}(k)$ of (4.7) is not sent to 3Φ-VCM DERs by their coefficients. Nevertheless, 3Φ-VCM DERs provide that same amount of power indirectly, as power balance, due to the lack of power in the equation.

For reconnecting the islanded MG to the main grid, the *reconnection switch* is turned to position 2. Thus, frequency reference value is slightly different from the rated frequency (i.e., 60.1 Hz), and 3Φ-VCM DERs form the MG voltage at that frequency. As the islanded MG operates in a different frequency of the main grid, occasionally, there is a time interval in which the angle difference between the two voltages is small enough (lower than 20° [132]) to perform the reconnection. The CC monitors both voltage angles (v_{PCC} and v_{grid}); at the instant that they are in-phase, the synchrocheck relay automatically closes S_1 and the MG operates in GC mode again. Then, CC turns the islanding switch

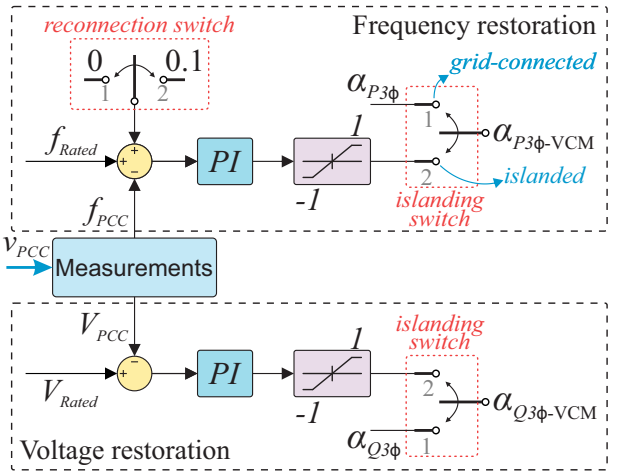

Figure 4.6: Restoration Control diagram at Central Controller.

to position *1*, and 3Φ-VCM DERs receive $\alpha_{P3\Phi}$ and $\alpha_{Q3\Phi}$. As their power controllers are already desaturated, they can track their power references and keep sharing power according to the PBC.

4.5 Real-time Hardware-in-the-loop Results

The proposed strategy is deployed and verified under different case studies in a real-time hardware-in-the-loop (HIL) setup using external controllers, as shown in Fig. 4.7. Hardware-in-the-loop simulation shows results widely recognized for the reliability and representativeness of the real plant. Two *Typhoon HIL 604* real-time emulator are connected in parallel to be able to implement the MG electric circuit of Fig. 4.2, the converters circuits shown in Section 4.3.1 and the *Central Controller*. The converters control signals are acquired by industrial TI TMS320F28335 control cards, in which the converters control are implemented. Seven control cards are used: the control of three-phase converters are implemented in one controller for each, and the control of one single-phase VCM and one CCM converters share the same control card. The controllers send back the PWM gate signals to switch each converter deployed on the HIL system.

The rated grid phase-voltage and frequency are $127V$ and $60Hz$, respectively. Uneven line impedances are modeled according to a real low-voltage distribution grid. Table 4.1 shows DERs rated maximum active and reactive power, and their respective constraints, and Table 4.2 shows the line impedance parameters. The sample and switching frequency of all DERs are $12kHz$. The CC sample frequency is $10kHz$, for the sake of grid power calculation, but the scaling coefficients are transmitted to DERs once per second. Thus, the CC updates the coefficients before the DERs update the output power. This ensures that the control can be implemented by low-bandwidth communication and is not impaired by communication delays [11].

Table 4.1: DERs rated power

DERs	$P_{max}[kW]$	$Q_{max}[kvar]$	Constraints
3ϕ-VCM DER-1	24	18	balanced operation
3ϕ-VCM DER-2	24	18	balanced operation
aN-VCM DER-3	6	6	–
aN-CCM DER-4	3	3	–
bN-VCM DER-5	6	6	–
bN-CCM DER-6	5	3.5	limited reactive power
cN-VCM DER-7	6	6	–
cN-CCM DER-8	6	*proportional*	pure-PV
3ϕ-CCM DER-9	–	6 / phase	unbalanced APF
3ϕ-CCM DER-10	10 / phase	10 / phase	unbalanced operation

Table 4.2: Line impedances parameters.

Branch	Length [m]	R [Ω]	L [μH]
N_0–N_1	30	0.026	8.753
N_1–$N_{1.1}$	30	0.026	8.753
N_1–$N_{1.2}$	30	0.026	8.753
N_1–$N_{1.3}$	30	0.0189	8.753
N_1–$N_{1.4}$	15	0.0131	4.376
N_1–N_2	15	0.0131	4.376
N_2–$N_{2.1}$	10	0.0369	3.714
N_2–$N_{2.2}$	15	0.0131	4.376
N_2–$N_{2.3}$	15	0.0131	4.376
$N_{2.3}$–$N_{2.4}$	10	0.0219	3.713
N_2–$N_{2.5}$	15	0.0131	4.376
N_2–$N_{2.6}$	15	0.0131	4.376
$N_{2.6}$–$N_{2.7}$	10	0.0219	3.713
N_2–$N_{2.8}$	10	0.0219	3.713

4.5.1 Grid-connected operation

The following case studies consider the MG at grid-connected operation, i.e., switch S_1 is closed. The proposed control strategy is analyzed under four transient conditions:

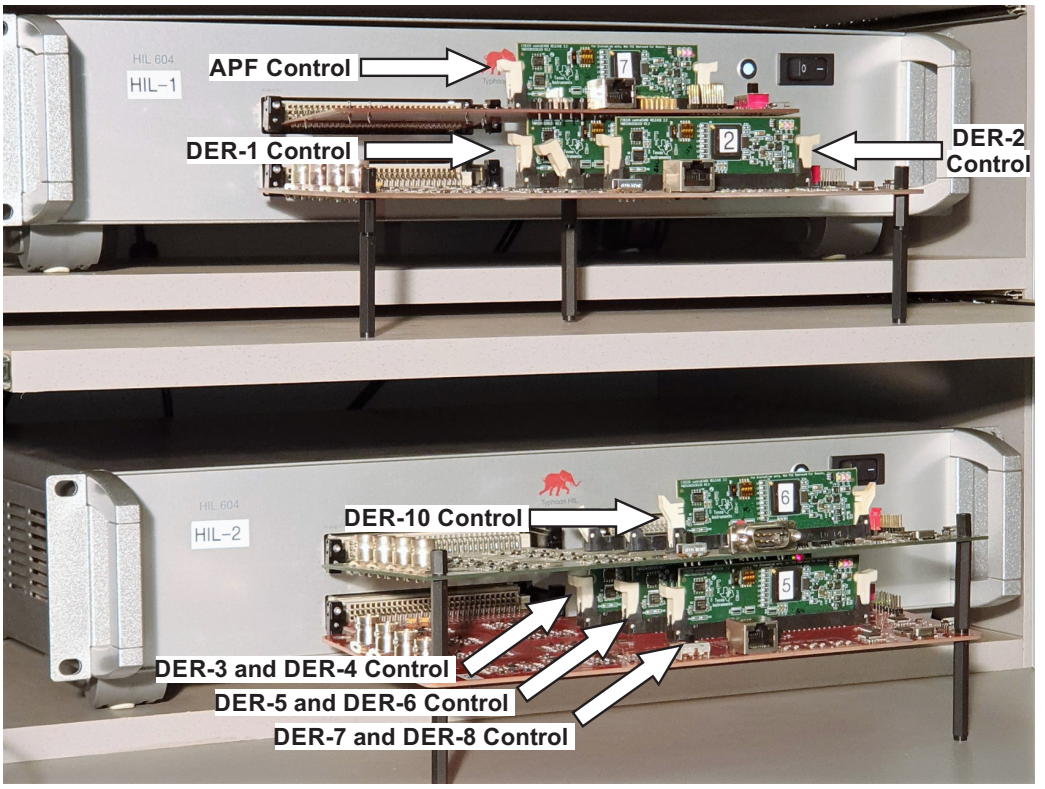

Figure 4.7: Hardware-in-the-loop setup for control validation.

4.5.1.1 Centralized control activation

Fig. 4.8 shows the transient results of the PCC quantities when the PBC is activated. At the first moment, all DERs are connected to the MG bus but without providing power (PBC is off). It can be noted that the PCC current and power are unbalanced, and there is a neutral current, $i0_{grid}$, of 25.5 $Arms$. When the PBC is turned on, the DERs provide power to the MG according to their references sent by the CC. In this case, the grid power flow is set to zero, i.e., $P^*_{grid}, Q^*_{grid} = 0$. PCC current and power quantities decrease to about zero, and $i0_{grid}$ decreases to 5.5 $Arms$, as the PBC does not contain an integral controller and due to measurement inaccuracies – each DER control contains an intrinsic error that is multiplied in a MG with many DERs – the quantities do not reach zero. At the first period of Fig. 4.9 is shown the steady-state of PCC and DERs power for this condition.

4.5.1.2 Grid power step

Fig. 4.9-a) shows the transient results when the grid power references change from zero to $P^*_{grid} = -10kW$ and $Q^*_{grid} = -1kvar$. The PCC power flow is accurately-controlled, and the unbalanced load is compensated by the DERs. As the active and reactive power step are done at the same time, one can note that the active power dynamics takes precedence over the reactive power, and the reactive power dynamics are influenced by the

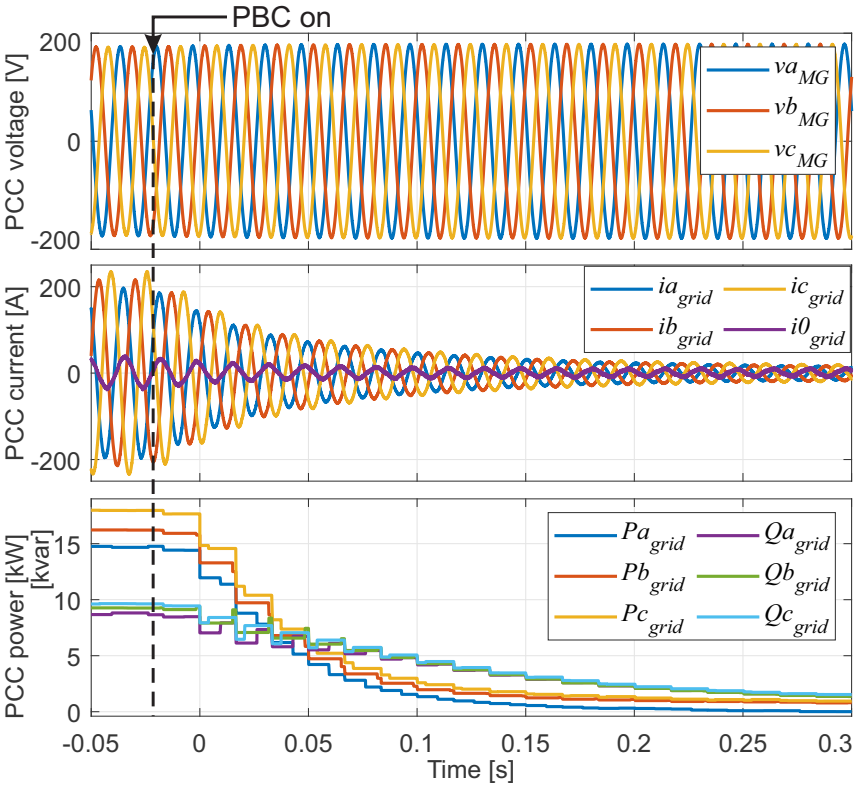

Figure 4.8: HIL Results: Grid-connected mode - PBC activation.

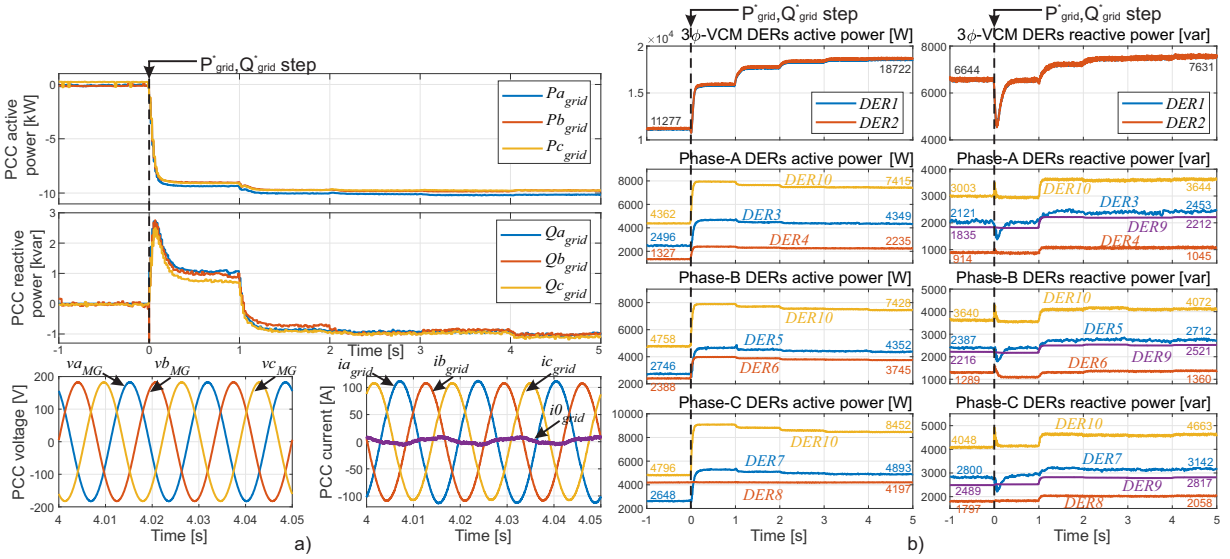

Figure 4.9: HIL Results: Grid-connected mode - performance under grid power step; a) PCC quantities; b) DERs quantities.

active power, specially in VCM converters, as shown in Fig. 4.9-b). CCM converters are more accurate in power control, and active and reactive power loops are more decoupled, thus performing better power sharing.

Fig. 4.9-b) shows that all heterogeneous DERs, including the ones with constraints, operate properly coordinated:

i) 3ϕ-VCM DERs share the same power and operate balanced, as shown in Fig. 4.10;

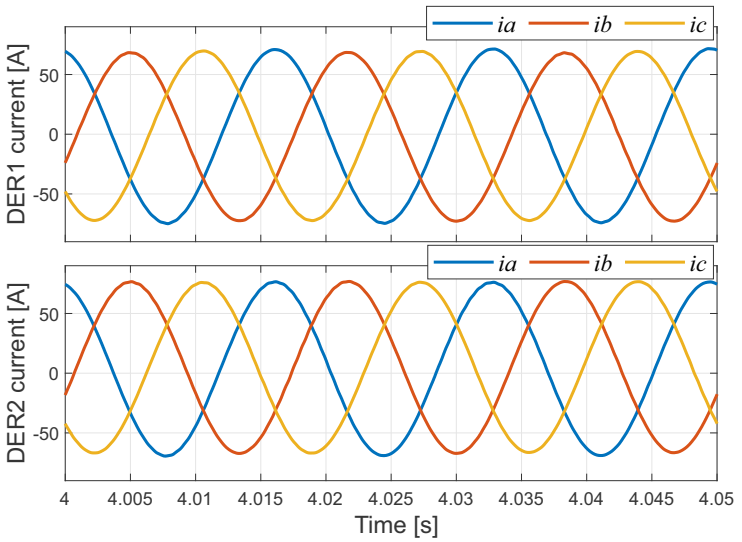

Figure 4.10: HIL Results: Grid-connected 3ϕ-VCM converter operating balanced.

ii) 1ϕ-phase DERs connected at the same m-phase, regardless of whether they are VCM or CCM, share the same proportional power with the m-phase of the 3ϕ-DERs and APF that are able to operate unbalanced. For instance, after the power step, phase-a DERs provide about 74% of their maximum active power and 36% of maximum reactive power; ***iii)*** pure-PV DER-8 provides its maximum active power (at this case study it is considered $4kW$) and shares its remaining reactive power, according to (4.1), i.e., it provides $2058var$, which is 46% of its maximum capacity of $4472var$ for that active power condition;
iv) DER-6 operates properly according to Fig. 4.5. Before the grid power step, DER-6 uses $Q^{max}_{G6rated} = 3500\ var$ for reactive power contribution, because $Q^{max}_{G6} > Q^{max}_{G6rated}$, i.e., $Q^{max}_{G6} = \sqrt{5000^2 - 2388^2} = 4392\ var$. After grid power step, DER-6 provides more active power, then, $Q^{max}_{G6} = \sqrt{5000^2 - 3745^2} = 3312\ var$, which is lower than $Q^{max}_{G6rated}$. Thus, DER-6 uses Q^{max}_{G6} for reactive power contribution, i.e., it provides 41% of its current maximum reactive power ($Q_{G6} = 0.41 \cdot 3312 \approx 1360\ var$).

4.5.1.3 Grid disturbances

In Fig. 4.11, grid power references are $P^*_{grid} = -4kW$ and $Q^*_{grid} = 0$, and it is shown the system behavior when the grid voltage sags from $127V$ to $122V$. In Fig. 4.12, the grid frequency fluctuates from $60Hz$ to $59.9Hz$ when grid power references are set to zero, $P^*_{grid}, Q^*_{grid} = 0$. In both cases, the PCC power is restored after the transient when the PBC is updated, showing resilience to grid disturbances.

4.5.1.4 Load Step

In Fig. 4.13, it is shown the transient of a load step when the MG is in grid-connected mode and the grid power references are set to zero, $P^*_{grid}, Q^*_{grid} = 0$. When the load step occurs, the grid momentary supplies the new load, until the next updated cycle

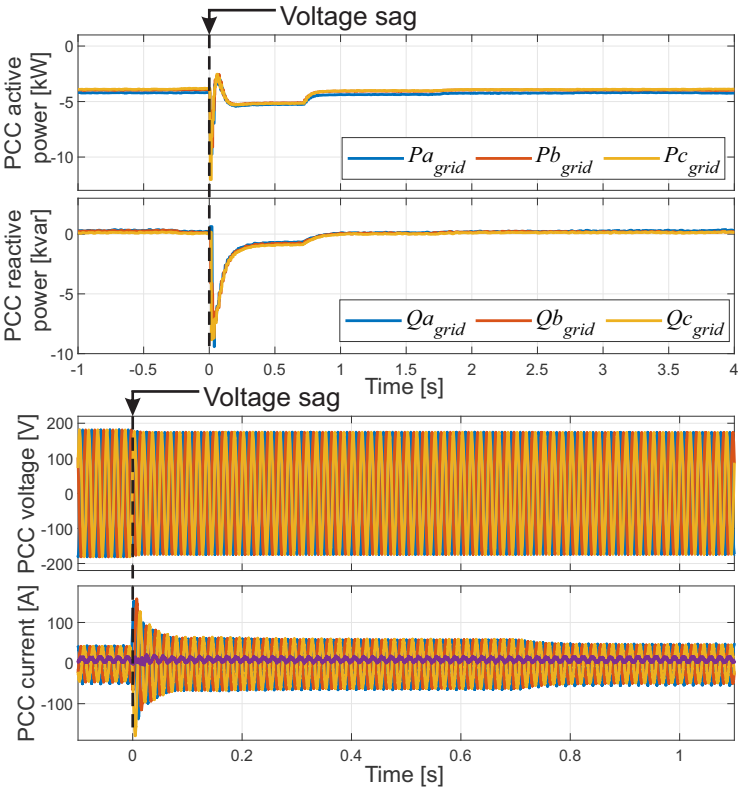

Figure 4.11: HIL Results: Performance under grid voltage sag.

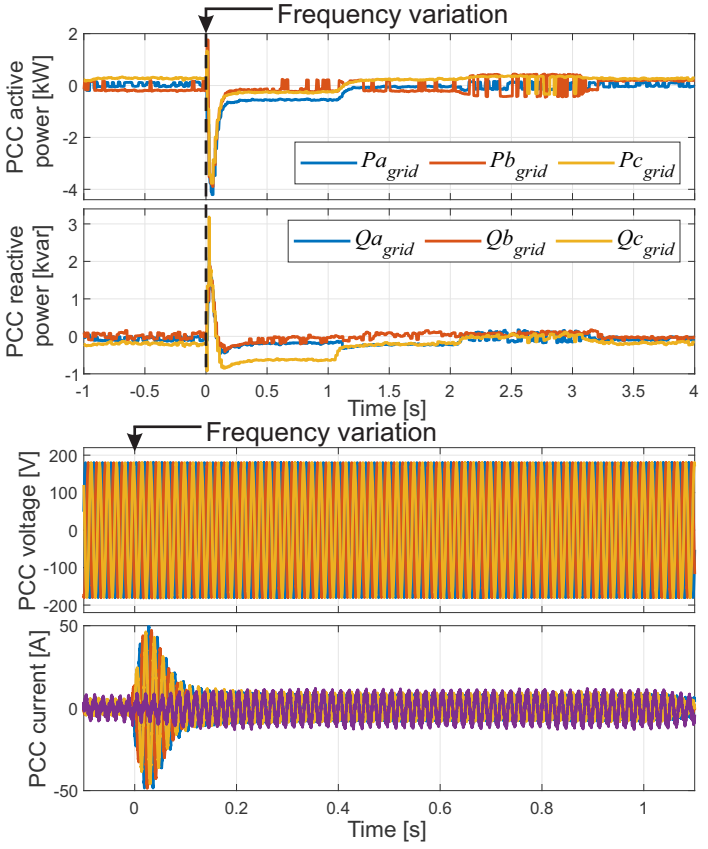

Figure 4.12: HIL Results: Performance under grid frequency variation.

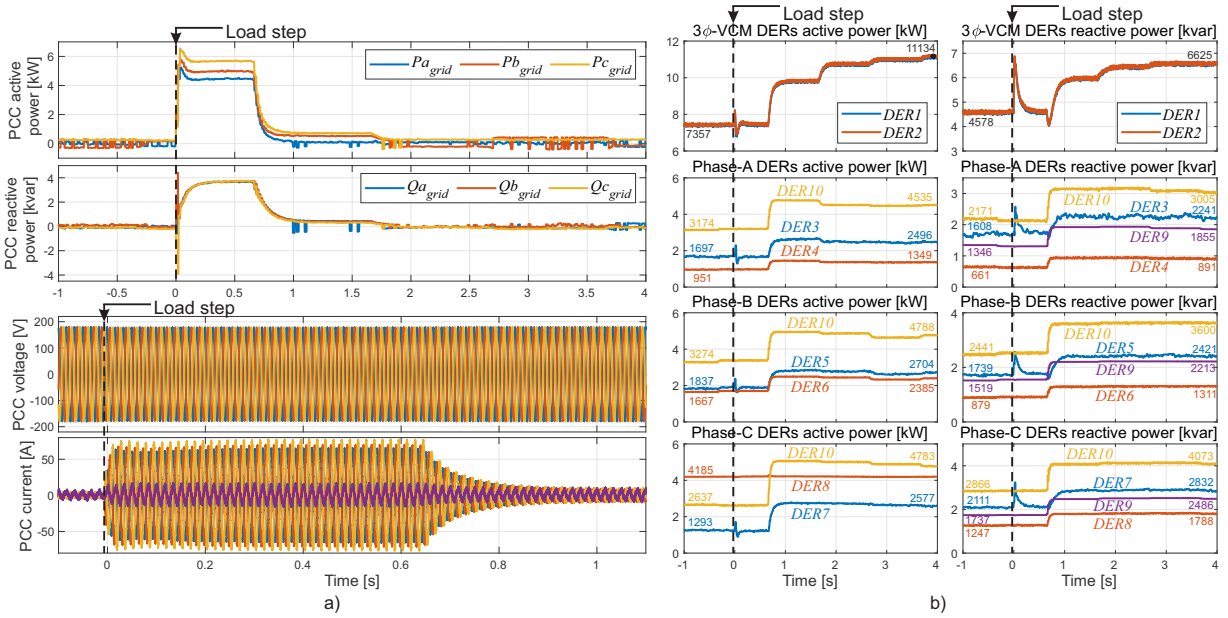

Figure 4.13: HIL Results: Grid-connected mode - performance under load step; a) PCC quantities; b) DERs quantities.

of the PBC. When the DERs receive the updated coefficients, the PCC power is controlled again and the load power is shared between the DERs.

4.5.2 Transition from grid-connected to islanded operation

The proposed control strategy allows smooth transition from grid-connected to islanded operation, as shown in Fig. 4.14. Islanding occurs suddenly, while the grid power references are $P^*_{grid} = -5kW$ and $Q^*_{grid} = -2kvar$. The smooth transition is achieved without a central converter and without fast islanding detection, because VCM converters are implemented with the control proposed in [105]. As grid power references are non-zero when islanding occurs, there is a transient current which is shared between the VCM converters. However, right after islanding, 3ϕ-VCM converters do not participate in power sharing, as they are working for power balancing in this transitory interim, as shown in the first period of Fig. 4.15. Also, one can note that the system shows a voltage and frequency deviation which is momentary until the islanding is detected. Despite that, the system is in equilibrium, there is no disturbances at the PCC voltage and the CCM converters keep providing the same active and reactive power values.

4.5.3 Islanded operation mode

When islanding is detected by the CC, it opens S_1, and grid power references are set to zero, $P^*_{grid}, Q^*_{grid} = 0$. Thus, the scaling coefficients change, and power sharing is performed between the converters, as shown in Fig. 4.15. However, 3ϕ-VCM converters are saturated and do not participate in power sharing, which keeps causing voltage and

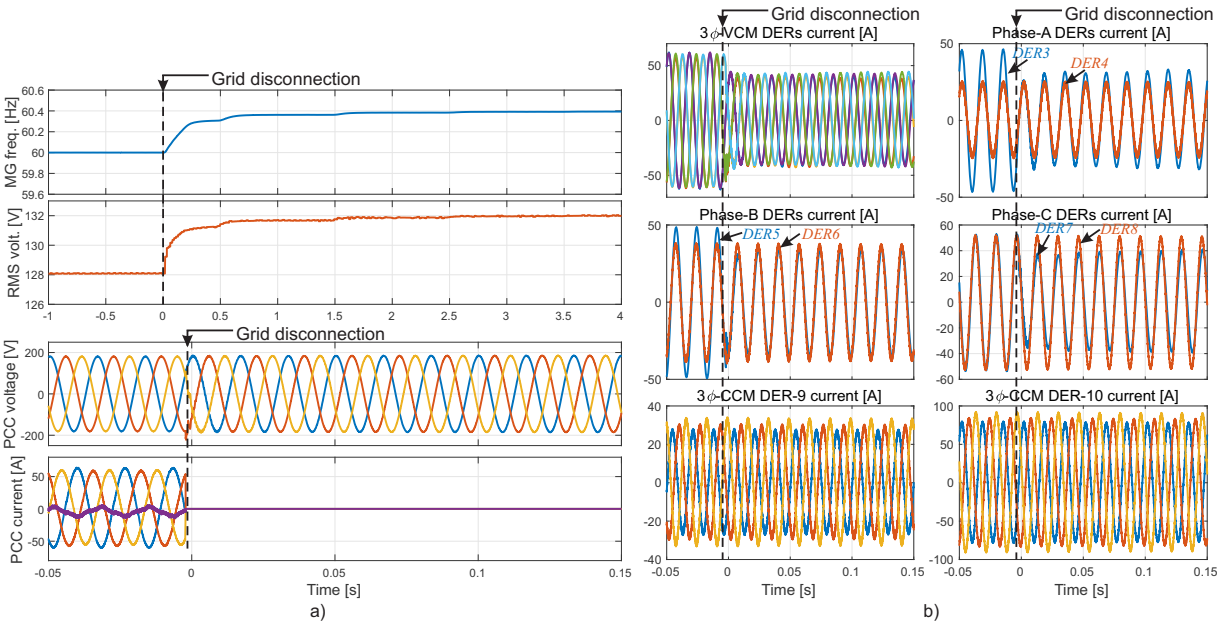

Figure 4.14: HIL Results: Transition from grid-connected to islanded mode; a) PCC quantities; b) DERs quantities.

frequency deviation. Therefore, the proposed *Restoration Control* is turned on, that is, *islanding switch* is turned to position 2 in Fig. 4.6, at 40s and 57s for voltage and frequency, respectively. The *Restoration Control* changes 3ϕ-VCM converters coefficients to restore the islanded MG voltage and frequency to their rated values. Also, the usage of such control automatically achieves power sharing between several grid-forming converters and other DERs, i.e., 3ϕ-VCM converters provide the proportional average power between the three phases.

4.5.3.1 PV withdraw

Fig. 4.16 shows the transitory condition when pure-PV DER-8 promptly stops providing power, i.e., an emulation of a sudden PV power variation. Right after the transitory, at t=0s, VCM converters instantly supply the active power lack, but CCM converters keep providing the same power amount. 3ϕ-VCM converters increase phase-C power, but decrease the other phases contribution, that is, they operate momentarily unbalanced, which brings 1ϕ-VCM converters to provide more power. The zoom clips of the frame "3Φ-VCM DERs active p." of Fig. 4.16 show the currents of DER-1 before and after the PV withdraw, evidencing the unbalanced operation that causes the transient 3Φ-VCM DERs active and reactive power oscillation. When PBC is updated, at $t = 0.75s$, the power sharing is re-arranged, thus, 3ϕ-VCM converters return to balanced operation and the power oscillation disappears. One can note that DER-8 increases its reactive power contribution, as in (4.14), due to the capacity of using all its rated power for reactive power provision.

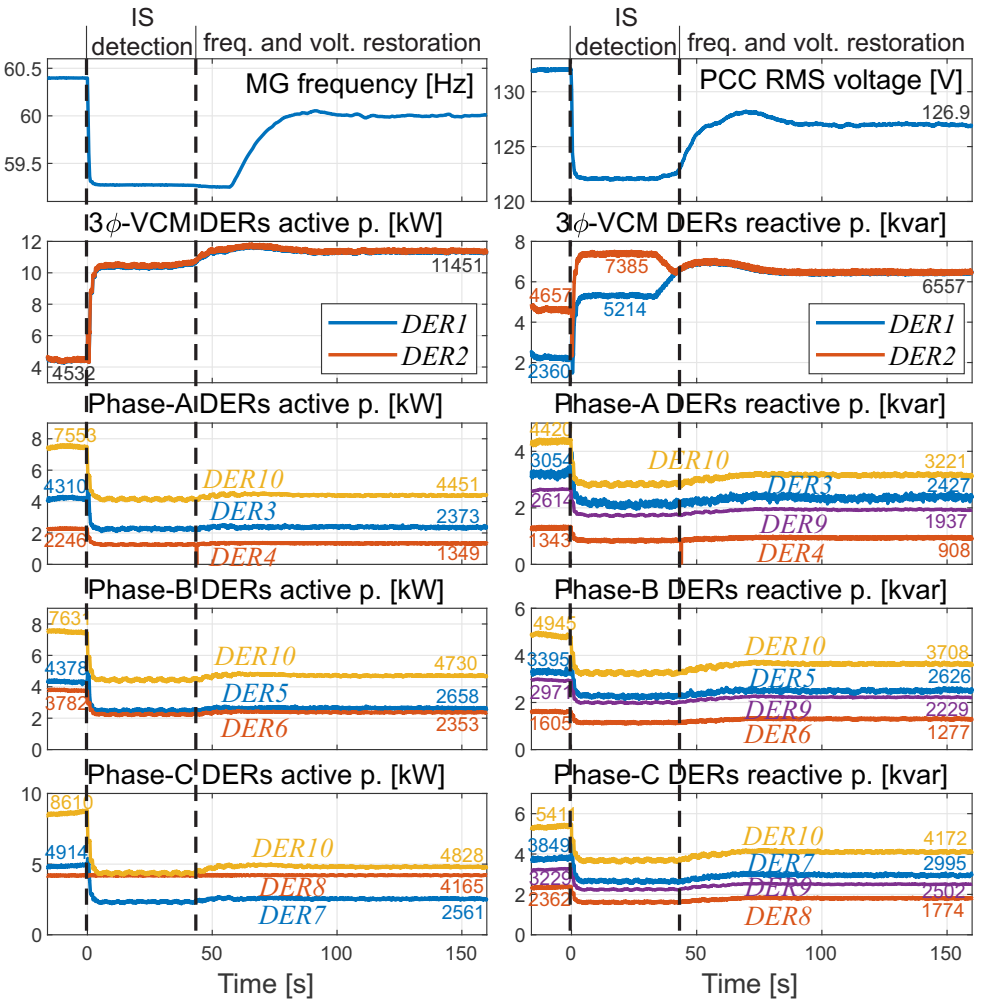

Figure 4.15: HIL Results: Islanded operation mode.

4.5.4 Reconnection transition

The reconnection transition is shown in Fig. 4.17. Once the main grid and the MG are prepared to reconnect, the *reconnection switch* is turned to position 2 in Fig. 4.6. Thus, α_P coefficients of 3ϕ-VCM converters are adjusted, therefore the MG operating frequency changes to $60.1Hz$. As mains voltage and the MG voltage are on different frequencies, there is a period when the phase difference between the two voltages is minimal (i.e., slip frequency synchronizing). Then, the synchrocheck relay detects it and closes S_1, returning the MG to grid-connected mode. When S_1 is closed, the *Restoration Control* is disabled, that is, *islanding switch* turns to position 1 in Fig. 4.6. Thus, the coefficients for the 3ϕ-VCM converters are defined by PBC again, in order to control the PCC power flow. At grid reconnection, the PCC voltage does not present any disturbances, and inrush current peak is $50A$, which corresponds to approximately 10% of the MG rated current. Also, one can note that only VCM converters contribute to the reconnection current, and they return to the previous condition in less than $0.2s$.

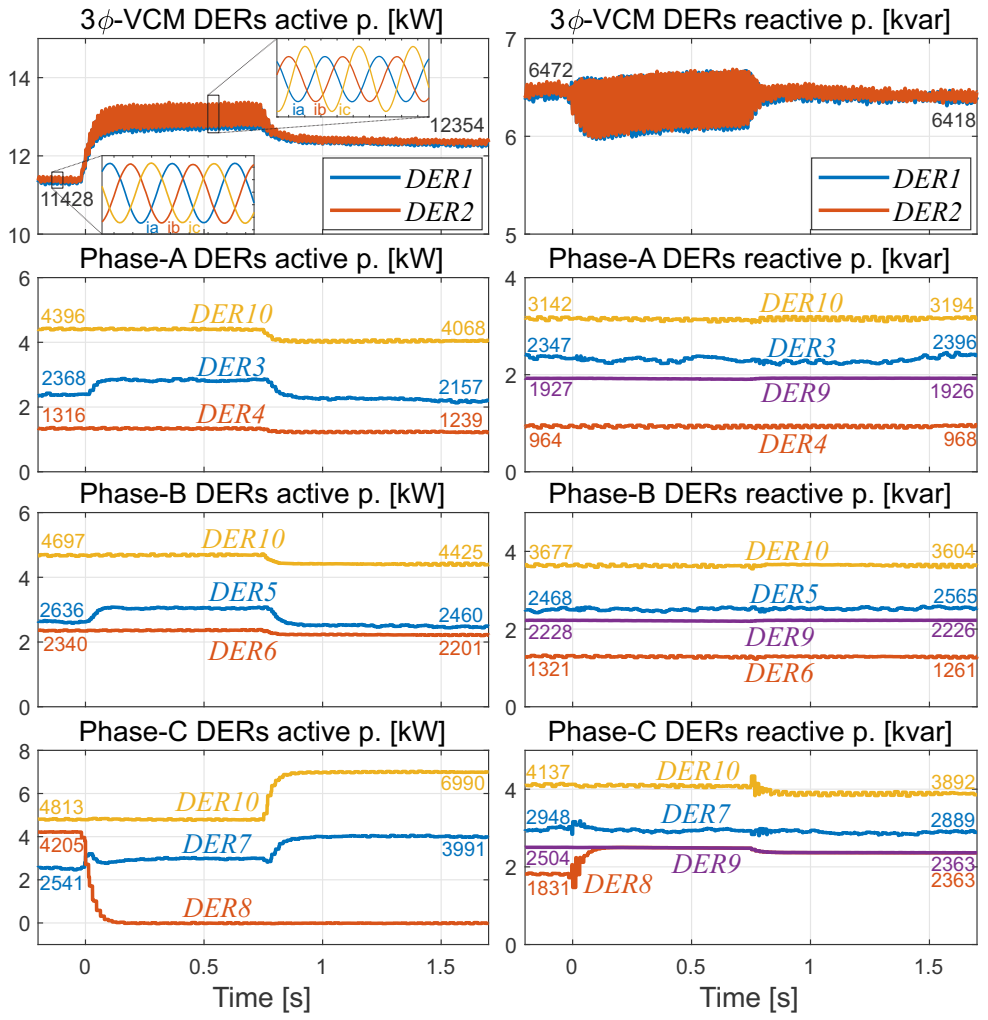

Figure 4.16: HIL Results: Islanded operation mode - PV withdraw.

4.6 Conclusions

In this chapter, it is proposed a complete control strategy for advanced microgrids capable of performing precise grid power flow control, converters power sharing, unbalance compensation and voltage/frequency restoration in both grid-connected and islanded modes. Smooth transitioning between operating modes is achieved without critical islanding detection. This strategy is a confluence of a centralized/hierarchical architecture and the droop-based power-loop for voltage-controlled converters developed in Ch. 3. Thus, two main points are highlighted: all objectives are accomplished without a central converter, and heterogeneous converters can participate in the coordinated control. Hardware-in-the-loop results show coordination of single- and three-phase converters, current- and voltage-controlled, and with self-imposed constraints in a low-voltage microgrid under several operating conditions.

Results support the conclusion that current-controlled converters are more accurate in power control and thus perform better power sharing. Voltage-controlled converters with an outer power-loop are able to provide controlled output power and participate in

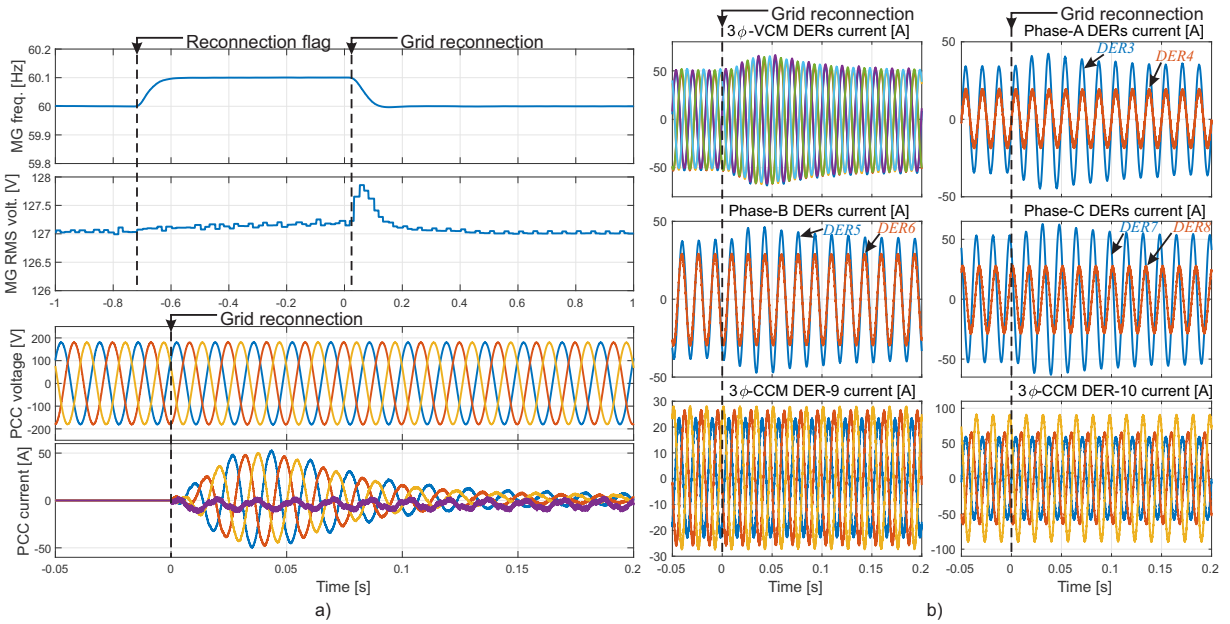

Figure 4.17: HIL Results: Transition from islanded to grid-connected mode; a) PCC quantities; b) DERs quantities.

power sharing. Besides, they are fundamental for islanded operation and for providing load transients. Furthermore, it was shown that only voltage-controlled converters contribute with the transient current in the reconnection state.

Chapter 5

Harmonic Voltage Synchronization for Grid-connected Converters

5.1 Introduction

As introduced in Section 2.4, when a VCI with purely sinusoidal voltage is connected to a grid with distorted voltage, an harmonic current flows between the two sources, due to the different voltage harmonic content. The VCM converter control developed in Ch. 3, and also used in Ch. 4, provides a sinusoidal voltage reference for the voltage loop of the VCI. In the previous chapters, the grid voltage is considered purely sinusoidal, thus, there is no harmonic current circulation.

In this chapter, the VCI is connected to a distorted grid. For this reason, it is proposed a novel strategy to synthesize, at the output of the VCI, the same harmonic voltage detected at the PCC. The harmonic voltage reference for the VCI is synchronized with the PCC harmonic voltage using GPS modules and its phase synchronization information and amplitude are broadcast through low-bandwidth communication.

The control proposed herein considers the synchronized harmonic voltage compensation for grid-connected converters without using the PCC voltage directly in the control loop. The proposed control is developed in a hardware-in-the-loop experimental setup, and is compared against conventional droop-control with outer power loop, and with the harmonic rejection approach. The results show that the proposed control is effective in improving the grid current and the load-voltage THD, and in reducing the circulating current and the power losses. The proposed strategy can be potentially applied for enhancing other existing control functions, like, for example, the one in [110] related to the sharing of harmonic currents between distributed converters.

5.2 Theoretical Background

The proposed control aims to synthesize at the output capacitor of the inverter the same harmonic voltages detected at the PCC of the grid subsection to which it is connected. To this end, the harmonic components to be compensated must have the same amplitude and phase, that is, they must be synchronized. However, the PCC may be physically distant from the converter, as shown in typical environments, like, for example, in [146]. This makes it challenging to measure PCC voltage in real-time and use it in a converter control loop.

A solution to feasibly achieve the desired features with existing, possibly, low-bandwidth communication means, consists in communicating only dc variables between the control agents. This section gives the theoretical background exploited to represent a time-varying phasor using dc variables that can be communicated to a different location and then allow a subsequent reconstruction of the original signal.

Consider the h-th harmonic component $v_h = V_h \sin(h\omega t)$ superimposed to a distorted grid voltage, where V_h is the amplitude of the harmonic and ω is the fundamental grid-voltage frequency. Also consider two unitary orthogonal signals, $v_{\parallel,h} = \cos(h\omega t + \phi)$ and $v_{\perp,h} = \sin(h\omega t + \phi)$, with the same frequency of the harmonic component, but not necessarily the same phase. Be ϕ the related phase-difference between the harmonic and the orthogonal voltages.

By multiplying the harmonic component by twice the voltage $v_{\perp,h}$, it yields:

$$\begin{aligned} \widetilde{v}_{qh} &= 2 \cdot v_h \cdot v_{\perp,h} = 2 \cdot V_h \sin(h\omega t) \cdot \sin(h\omega t + \phi) = \\ &= V_h \left[\cos\phi - \cos\left(2h\omega t + \phi\right)\right] , \end{aligned} \tag{5.1}$$

where the former component is constant and is related to the amplitude of the h-th harmonic projected along $v_{\perp,h}$, the latter is an oscillatory component at frequency $2h\omega$. Then, by appropriate filtering, it yields:

$$v_{qh} = V_h \cos\phi \,. \tag{5.2}$$

The same procedure considering the signal $v_{\parallel,h}$, gives:

$$\begin{aligned} \widetilde{v}_{dh} &= 2 \cdot v_h \cdot v_{\parallel,h} = 2 \cdot V_h \sin(h\omega t) \cdot \cos(h\omega t + \phi) = \\ &= V_h \left[-\sin\phi + \sin\left(2h\omega t + \phi\right)\right] \end{aligned} \tag{5.3}$$

$$v_{dh} = -V_h \sin\phi \tag{5.4}$$

Then, the dc terms v_{dh} and v_{qh} can be communicated to other remote converters and allow to reconstruct a replica v_h^* of original signal v_h, if the base $v_{\perp,h}$, $v_{\parallel,h}$ is known,

as:

$$\begin{aligned} v_h^* &= v_{qh} \cdot \sin(h\omega t + \phi) + v_{dh} \cdot \cos(h\omega t + \phi) \\ &= V_h \cos\phi \, \sin(h\omega t + \phi) - V_h \sin\phi \, \cos(h\omega t + \phi) \\ &= V_h \sin(h\omega t) \end{aligned} \tag{5.5}$$

Notably, the reconstructed harmonic voltage in (5.5) is virtually identical to the original signal v_h, thus, it can be used as a reference to synthesize that harmonic voltage at the converter output.

Of course, the signals $v_{\perp,h}$, $v_{\parallel,h}$ should be uniquely and autonomously determined by both the sender and the receiver of the terms (5.2) and (5.4). To this end, different approaches may be adopted. The use of a GPS synchronization means is proposed and explored herein, as explained in details in Sect. 5.3.

5.2.1 Phase-mismatch influence in parallel voltage-sources

The connection of a VCI to an electric grid can be simplified as two voltage-sources connected by a series impedance as shown in Fig. 5.1, where V_{ch} is the converter h-harmonic voltage amplitude, V_{gh} is the grid h-harmonic voltage amplitude, θ_h is the phase-difference between the harmonic voltages, R and L are the impedance resistance and inductance, respectively. The harmonic circulation current between the two sources can be computed as:

$$\dot{I} = \frac{V_{ch}e^{i\theta_h} - V_{gh}}{R + i\omega_h L} \tag{5.6}$$

Assuming equal amplitudes for the harmonics, that is, $V_{ch} = V_{gh}$, and $\theta_h = \omega_h t$, (5.6) can be rewritten as:

$$\dot{I} = \frac{V_{ch}(e^{i\omega_h t} - 1)}{R + i\omega_h L}\,, \tag{5.7}$$

which is represented in Fig. 5.2 normalized by the term:

$$I_0 = \frac{V_{ch}}{R + i\omega_h L} \tag{5.8}$$

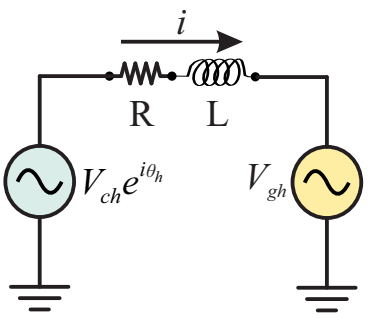

Figure 5.1: Simplified model of a grid-connected converter.

Fig. 5.2 shows the influence of the synchronization accuracy with respect to the harmonic current suppression. The current amplitude is reported in *p.u.* and the synchronization error in terms of number of samples, considering a sample frequency of 12 kHz. Notably, if both voltages are perfectly synchronized there is no current flow between the sources. However, a small error (e.g., two samples) is sufficient to cause a considerable current flow depending on the grid parameters (5.8). Moreover, higher-order harmonics are more sensitive to synchronization accuracy. These kind of considerations are important in order to design the accuracy of the synchronization equipment (e.g., GPS module) or the sample frequency of the controller, in relation to the targeted impact on current suppression.

5.3 GPS-based Harmonic Voltage Synchronization

The proposed strategy is performed based on two main players that are equipped with GPS modules:

- PCC measurement system (PMS), which estimates the parameters (amplitude and phase) of the main grid voltage, and
- VCI distributed within the considered sub-grid, like, a microgrid.

An application example of the proposed control is shown in Fig. 5.3.

The PMS is responsible for detecting the harmonic components of the PCC voltage v_{dqh}, and for calculating the time interval t_{PCC} between the GPS signal and the first positive zero crossing of the PCC voltage. The quantities are then sent to the dispersed VCI by low-bandwidth communication. Details of the PMS are described in Sect. 5.3.1.

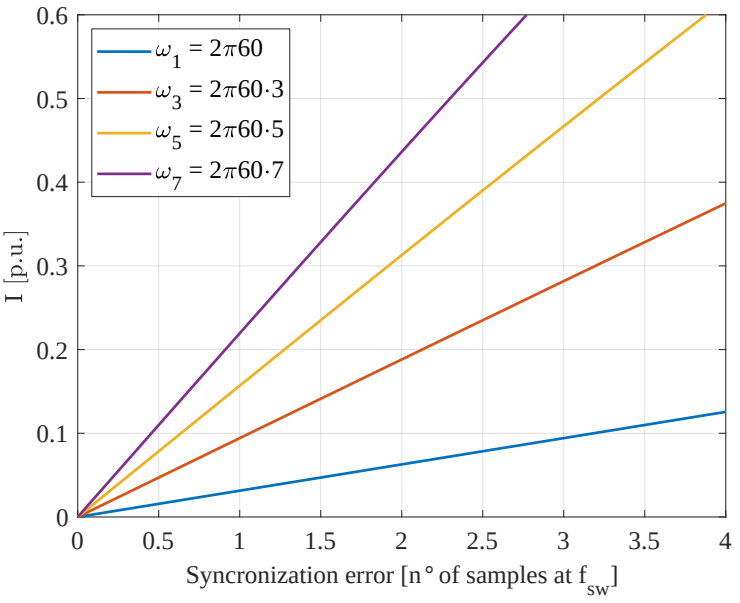

Figure 5.2: Normalized relations between synchronization error and current flow.

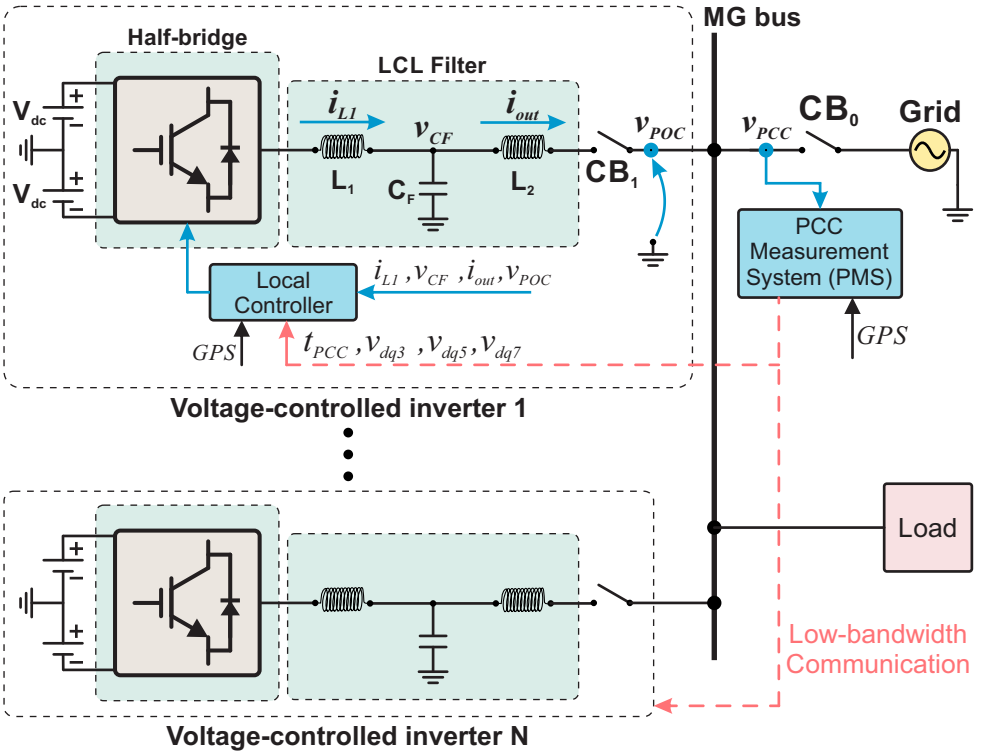

Figure 5.3: Application example of the proposed control.

The local controllers of VCI receive the quantities sent by the PMS and, based on their local GPS signals, they generate an harmonic voltage reference of the same amplitude and phase of the corresponding harmonic voltage at the PCC. The fundamental voltage reference is provided by a droop-based controller. The VCI control is discussed in more details in Sect. 5.3.2.

Each GPS module produces an IRIG-B output signal [147] that is synchronized with the other GPS modules. The IRIG-B signal is commonly used for transferring timing information, but it is also used as a precision trigger for time coordinated testing, event initiation, or other control functions. A sample of an IRIG-B signal is shown in Fig. 5.4b. Two consecutive pulses lasting 8 ms, referred to as "*Ref.*", occur once per second and indicate the beginning of a new time frame. Herein, only the rising edge of the first pulse after *Ref.* is used as synchronized trigger for both PMS and VCIs.

5.3.1 PCC Measurement System

The PMS scheme is shown in Fig. 5.4a. Two main tasks are performed in the PMS: *i)* calculate the amplitude (i.e., v_{dh} and v_{qh}) of the PCC harmonic voltages of interest; and *ii)* calculate the time interval t_{PCC} between the GPS signal and the PCC voltage at zero crossing, required for synchronization.

The amplitude of the h-th harmonic components (e.g., $h = 3, 5, 7$) is calculated independently in the, so called, "Harmonic Detection block", shown in Fig. 5.4c. To this

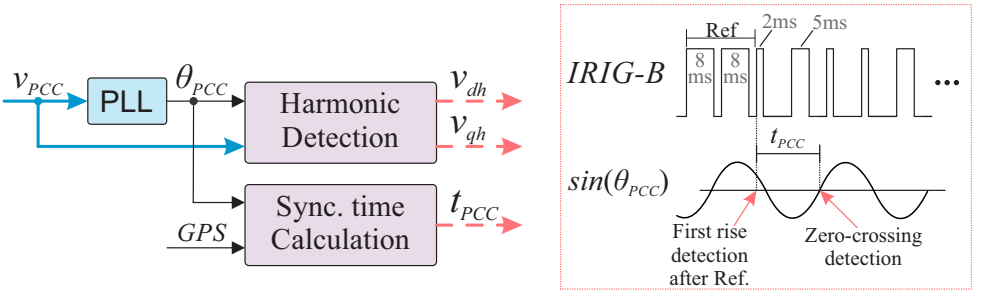

a) PMS scheme b) Sync. time calculation

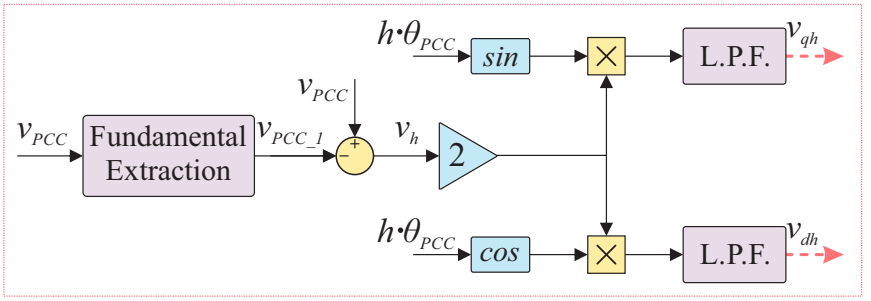

c) Harmonic detection block detailed

Figure 5.4: PCC Measurement System structure.

end, the fundamental component of the total PCC voltage, indicated as v_{PCC_1}, is firstly obtained and subtracted from the PCC voltage, in order to consider only the harmonic content. Two orthogonal voltages at the specific h-th harmonic component (i.e., $v_{\perp,h}$ and $v_{\parallel,h}$ in Sect. 5.2) are then created and multiplied by the PCC harmonic components. After processing the result through a low-pass filter (LPF), the direct (i.e., v_{dh}) and quadrature (i.e., v_{qh}) amplitudes are obtained and broadcast to the distributed converters. The time interval t_{PCC} between the GPS signal and the PCC voltage at zero crossing is also calculated, as shown in Fig. 5.4b. This information is broadcast to the VCI and used for the synchronization of the harmonic components.

5.3.2 Voltage-controlled inverter control

The control scheme at VCI side is shown in Fig. 5.5a. The control is composed of three cascade loops, that is, power, voltage, and current, that generate the PWM pulses to the gate driver of the converter. The outer power-loop is the same as the one in Ch. 3, and defines the fundamental component of the voltage. By this control, the converter is capable of providing controlled active and reactive power. The voltage-loop uses ordinary proportional-resonant controllers for each harmonic that should be compensated, while the current-loop uses a proportional controller.

The harmonic voltage reference v_h^* is defined by the "Harmonic Compensation" block, detailed in Fig. 5.5b. First, the GPS signal is used to calculate the time delay t_{POC} between the zero-crossing of the POC fundamental voltage v_{POC_1} and the first rising

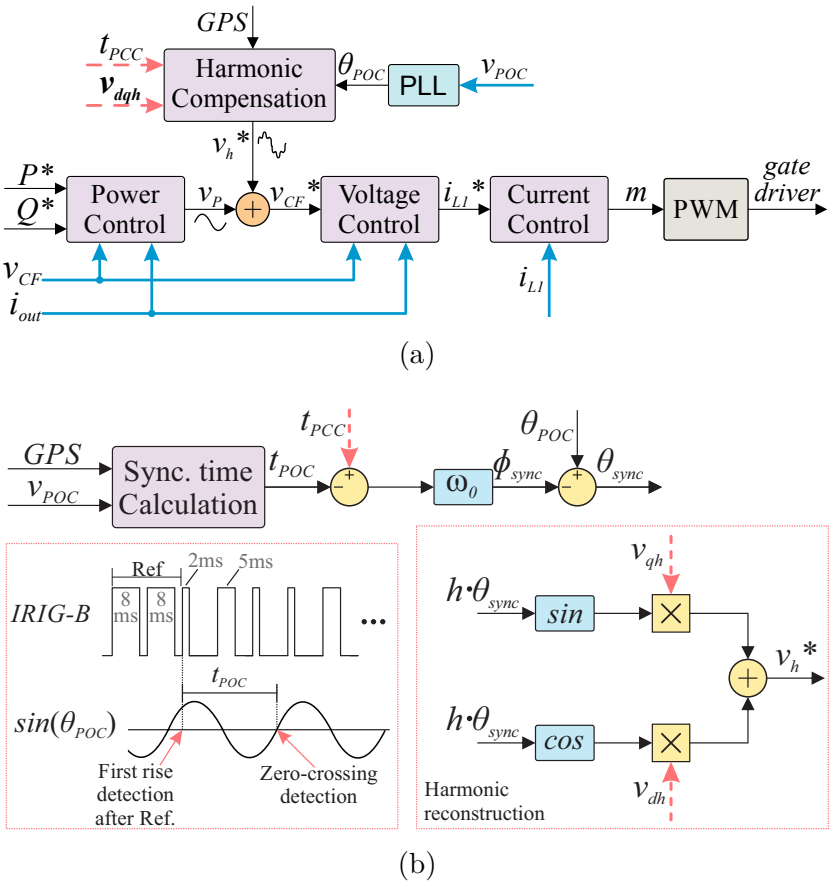

Figure 5.5: a) VCI control structure; b) Harmonic compensation block detailed.

edge after *Ref.* pulses from the local GPS signal, analogously to what is described in Sect. 5.3.1 for the PMS. Based on the received t_{PCC} broadcast by the PMS, and the local measurements t_{POC} and θ_{POC}, a synchronized phase θ_{sync} that estimates the phase of the PCC voltage θ_{PCC} can be computed as shown in Fig. 5.5b:

$$\begin{aligned}\theta_{sync}(t) &= \theta_{POC}(t) - \phi_{sync}(t) = \\ &= \underbrace{\omega_0 t - \omega_0 t_{POC}}_{\theta_{POC}(t)} - \underbrace{\omega_0 \left(t_{PCC} - t_{POC}\right)}_{\phi_{sync}} = \\ &= \omega_0 t - \omega_0 t_{PCC} = \theta_{PCC}(t)\end{aligned} \tag{5.9}$$

that is used for harmonic synchronization. Thereby, based on the harmonic amplitudes v_{qh} and v_{dh} transmitted by the PMS, it is possible to rebuild the harmonic voltage v_h^* that was detected at the PCC. The signal v_h^* can be finally given as reference to the converter voltage controller to reproduce at its output terminals the same harmonic content of the PCC voltage.

As a final remark, the proposed concept for harmonic synchronization can be potentially implemented with other synchronization mechanisms than the GPS technology considered herein.

5.4 Real-time Hardware-in-the-loop Results

Fig. 5.6 shows the HIL experimental setup used to validate the proposed control. The electrical circuit of Fig. 5.7, representing the the power stage, is implemented in Typhoon hardware-in-the-loop (HIL). The scenario consists of a VCI connecting a DER to the main grid with different loading conditions considered to evaluate the proposed method performance, including RL load, RC load, and non-linear load. The PMS and the VCI control are deployed in two different *Imperix B-Board* controllers, which generate the PWM control signals based on the measured currents and voltages of the converter emulated in the HIL system. The PMS communicates the control quantities to the VCI by Ethernet UDP protocol. The communication line is processed through a dedicated network emulator *NE-ONE* to emulate realistic conditions in terms of, for example, bandwidth, congestions, latencies, and packet loss. Each *B-Board* controller is connected to an independent *SEL-2401* GPS module, which provides the IRIG-B output with ±100 ns timing accuracy.

The results are evaluated considering three VCI control approaches: *1)* conventional control of the VCI, without harmonic compensation, v_h^* is set to zero; *2)* harmonic rejection in the converter output current, v_h^* is defined based on v_{POC} measurement instead of v_{PCC}, so the converter synthesizes a voltage v_{CF} with harmonics equal to those of v_{POC}, avoiding any harmonic current circulation at the output; and *3)* with the harmonic compensation proposed in this chapter, with v_h^* defined as in Fig. 5.5.

Four different case studies are considered to verify the effectiveness of the proposed control. The first three cases consider distorted grid voltage with linear loads, while the last case considers a pure sinusoidal grid-voltage with a non-linear load. System parameters, including line impedance values, grid voltage harmonic content, are listed in Table 5.1. The considered parameters are typical for low-voltage distribution networks (see, e.g., [146]).

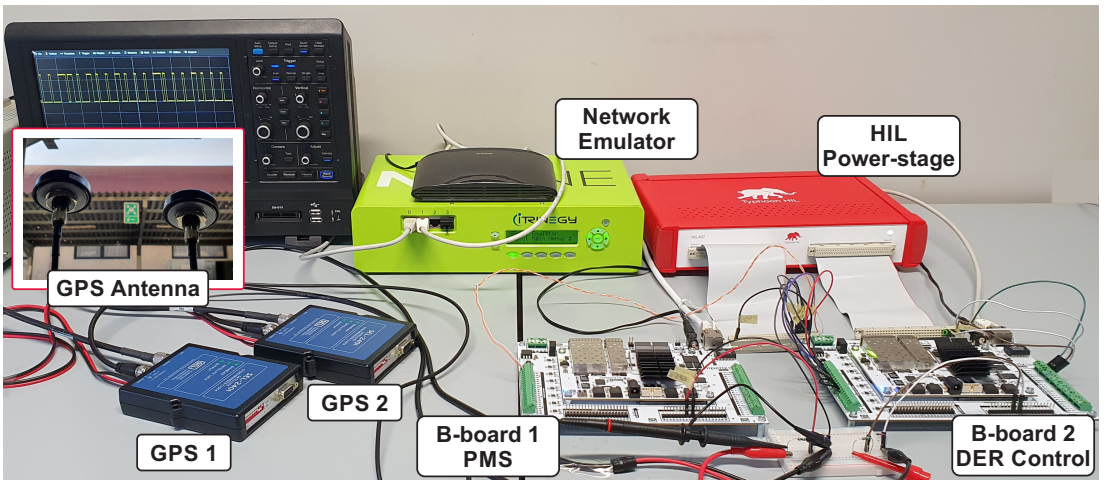

Figure 5.6: Experimental setup for the proposed method validation.

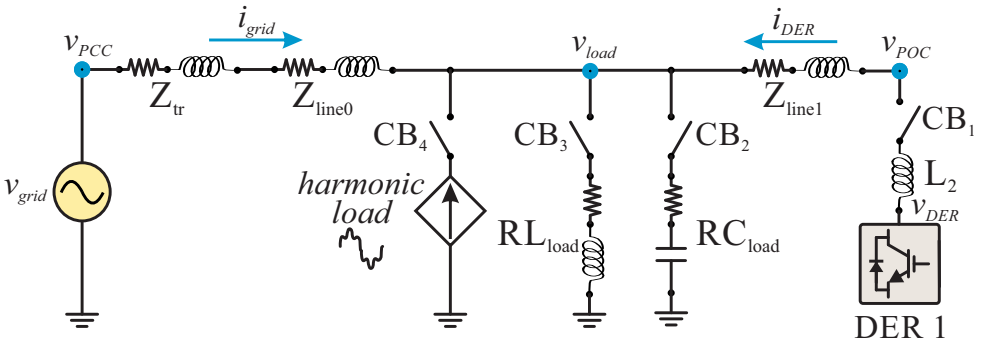

Figure 5.7: Electrical circuit implemented in HIL.

Table 5.1: System parameters

Parameter	Value	Parameter	Value
Grid frequency (ω_0)	$2\pi 60$ rad/s	DER power (Sn)	8.48 kVA
Grid voltage (V_0)	$127\sqrt{2}$ V	Inductor L_1	4.5 mH
3-rd harmonic	$5\%V_0\angle 15\,^\circ$	Capacitor C_F	140 μF
5-th harmonic	$4.5\%V_0\angle 25\,^\circ$	Inductor L_2	62.5 μH
7-th harmonic	$4\%V_0\angle 35\,^\circ$	Switching frequency	24 kHz
Grid voltage THD	7.83 %	R_{RC} load	0.19 Ω
Z_{tr}	$(9.5\text{m} + j\omega 62.5\mu)$ Ω	C_{RC} load	15.3 mF
Z_{line0}	$(30\text{m} + j\omega 10\mu)$ Ω	R_{RL} load	0.33 Ω
Z_{line1}	$(30\text{m} + j\omega 10\mu)$ Ω	L_{RL} load	0.89 mH

5.4.1 Distorted grid voltage—No load

The situation with VCI connected to a distorted grid voltage but without any load connected (i.e., CB_2-CB_4 in Fig. 5.7 open) is considered first. The grid voltage and current waveforms are shown in Fig. 5.8, where the distorted grid voltage is clearly noticed by its non-sinusoidal shape. When the conventional control is employed, the DER output voltage tries to be kept sinusoidal, which produces a noticeable circulating current between the grid and the converter, as shown in Fig. 5.8a.

When the proposed harmonic compensation is employed, the DER voltage presents the same harmonic content as the grid voltage measured at the PCC, as shown in Fig. 5.8c. Thus, the grid circulating current is drastically reduced from 89 A to 1.05 A, and the line impedance losses decreased from 118 W to 0.08 W. In this case study scenario (no load), there is no phase-shift between PCC and POC voltages, so the implementation of harmonic rejection performs similarly to harmonic compensation, as shown in Fig. 5.8b.

5.4.2 Distorted grid voltage—RC load

The second case study considers the RC load in Fig. 5.7 connected (i.e., CB_2 closed). In this way, the situation in which the POC voltage is phase-shifted from the PCC voltage is evaluated. In this particular case, POC fundamental voltage is 10° lagged

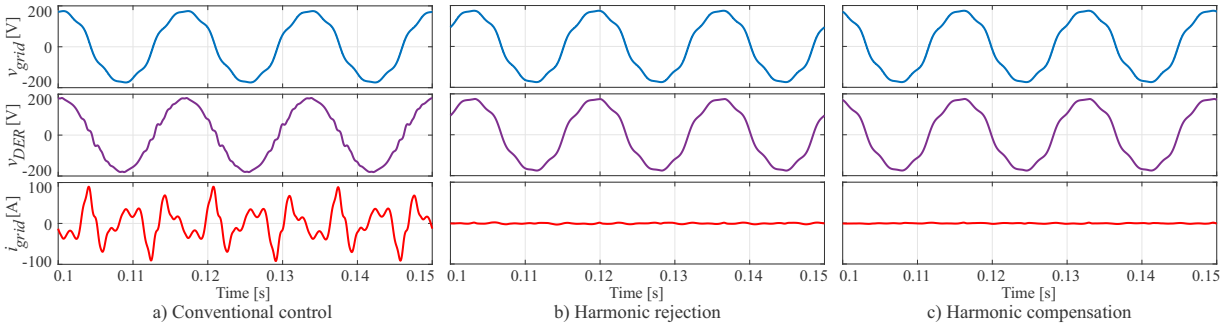

Figure 5.8: Results for distorted grid voltage and no load.

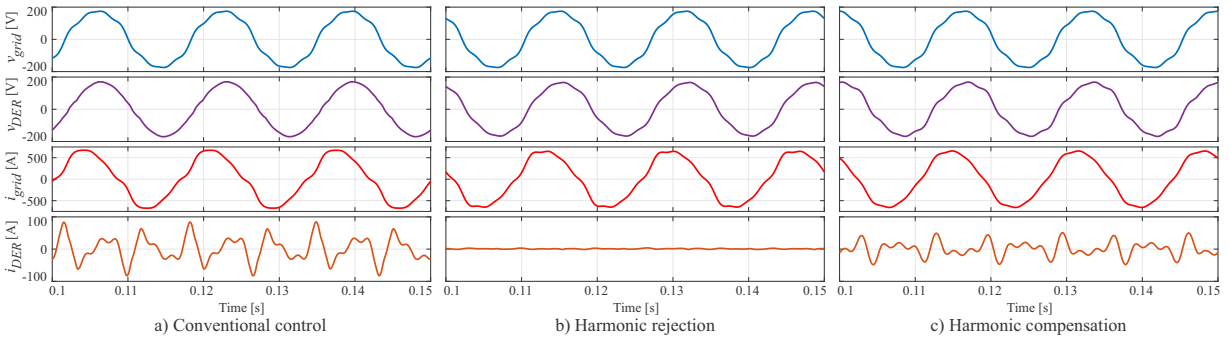

Figure 5.9: Results for distorted grid voltage and RC load.

from the PCC voltage. Other network configurations with different load and generation conditions could cause similar effects. The results are shown in Fig. 5.9.

The grid current without the DER (i.e., CB_1 open) shows a THD value of 9%. When conventional control is active, a high harmonic current flows from the DER to the grid, this situation deteriorates even more the grid current THD, which increases to 10.2%. The harmonic rejection strategy successfully inhibits the harmonic current flow keeping the grid current THD at 9.1%. The proposed harmonic compensation, instead, synthesizes the same PCC voltage in the converter output capacitor, this causes an harmonic current flow that contributes with the load harmonic current. In this last case, grid current THD improves to 5.7%.

Remarkably, this case study also shows that the use of the POC voltage instead of PCC voltage as an approximation for voltage compensation [116] could result in inappropriate compensation.

5.4.3 Distorted grid voltage—RL load

This section considers the RL load in Fig. 5.7 connected (i.e., CB_3 closed). When the DER is disconnected, the grid-voltage harmonics result in a correspondingly distorted load current, with THD value of 2.5%. In this case study, the DER is set to provide active and reactive power of 6 kW and 6 k*var*, respectively. Fig. 5.10a displays the obtained results by using a conventional control for the DER, in which a pure sinusoidal voltage is

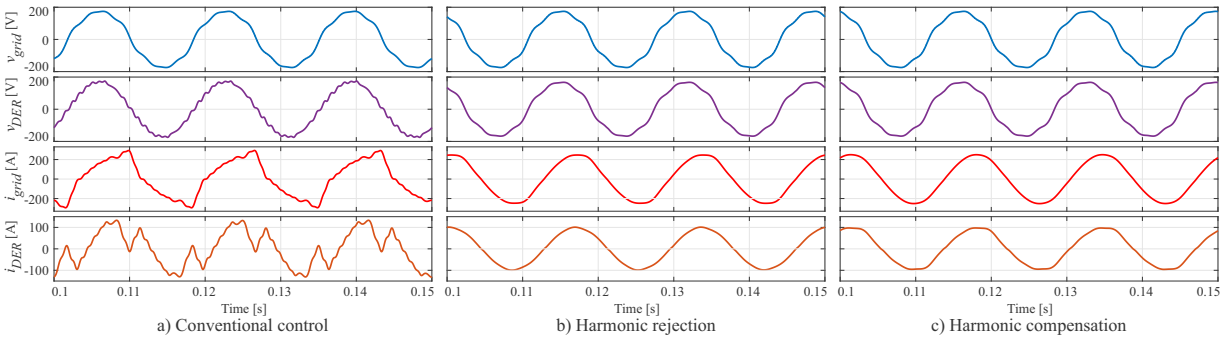

Figure 5.10: Results for distorted grid voltage and RL load.

given as reference to the converter voltage controller, as commonly done in classical droop control. In this case, the grid current shows a THD of 22.4%. Using the harmonic rejection approach, a substantial improvement is noted in the DER current (THD of 2.3%) but, on the other hand, a worse grid current (THD of 3.7%) than the situation without DER, as shown in Fig. 5.10b.

The proposed harmonic compensation is implemented with a poor quality communication of a bandwidth of 0.512 Mbps, a latency of $35-60$ ms, and a 5% of packet loss. The results are shown in Fig. 5.10c, in which a better grid current shape is noted (THD of 1.9%), due to the DER harmonics contribution (THD of 5.7%). It can be noticed that the proposed approach does not interfere with the active and reactive power supply of the converter, and the poor quality communication does not affect the operation performance.

5.4.4 Sinusoidal grid voltage—Distorted load

This last case study considers the grid voltage as purely sinusoidal and a controlled current source as a load. The current source is set to drain only harmonic current (h=3,5,7), so that the voltage drop in the line impedance causes a distorted voltage at the point of connection of the load, with a voltage THD value of 6.5%. With the VCI switched off (i.e., CB_1 open), the total losses in the line impedance amount to 1683 W.

In Fig. 5.11a, it is shown the behavior of the system using the harmonic rejection approach. The output voltage of the DER has a similar shape of the load voltage. Thus, the DER does not provide current to the grid, and the load voltage THD is kept in 6.5%. Using the proposed harmonic compensation, the DER synthesizes a pure sinusoidal voltage (the same as the PCC), as shown in Fig. 5.11b. Hence, the DER automatically shares the load harmonic current, reducing the voltage drop across the line impedances, and improving the load voltage quality (THD of 3.5%). Moreover, the total line impedance losses are reduced to 1600 W.

Table 5.2 shows a performance comparison of the four case studies regarding the line impedance power losses, the THD value of the grid and DER currents, and the THD value of the load voltage. In general, the conventional approach is the worst, as expected.

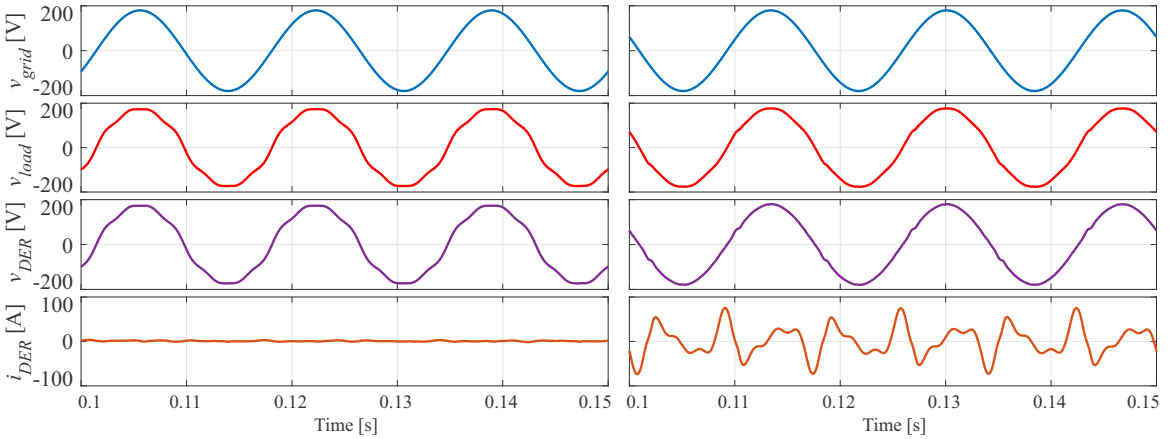

Figure 5.11: Results for sinusoidal grid voltage and distorted load.

Instead, the harmonic rejection approach is the best regarding the converter stress, as it presents the lowest THD for the DER current. Finally, the harmonic compensation strategy improves the power quality for both the load voltage and the grid current, and also presents the lowest overall line power losses.

Table 5.2: Performance comparison of the approaches

Case study	**no-load**	**RC-load**	**RL-load**		**nonlinear-load**	
Control adopted	Losses	THD i_{grid}	THD i_{grid}	THD i_{der}	Losses	THD v_{load}
Conventional control	118 W	10.2%	22.4%	55.5%	–	–
Harmonic rejection	0.1 W	9.1%	3.7%	2.3%	1683 W	6.5%
Harmonic compensation	0.08 W	5.7%	1.9%	5.7%	1600 W	3.5%

5.5 Conclusions

This chapter addressed the harmonic circulating current issue caused when a voltage-controlled inverter with a pure sinusoidal voltage output is connected to a grid with distorted voltage. To overcome this problem, an harmonic voltage compensation strategy is proposed, in which the voltage-controlled inverter synthesizes the same harmonic voltage detected at the PCC. Global positioning system (GPS) modules are exploited to perform the synchronization between the PCC and the voltage-controlled inverter harmonics. An experimental setup using hardware-in-the-loop with external controllers, together with GPS modules and a communication network emulator, was used to test the proposed approach. The proposed method was compared with two other approaches: 1) the conventional droop control with external power loop, and 2) with the harmonic rejection approach. Four case studies were conducted in order to verify the control performance

in different system conditions. The proposed harmonic compensation performs the best reduction in the grid current and load voltage THD, and in line power losses. However, the reproduction of the harmonics by the converter may increase the stress and losses inside itself, so, these issue needs to be further considered. The harmonic rejection approach, otherwise, is the best choice regarding the converter stress; it does not improve the grid current, as the harmonic compensation, but also does not deteriorate it, as the conventional control. Therefore, for a low investment implementation, the harmonic rejection is a better choice than the conventional control; but for the system overall operation, harmonic compensation presents the most beneficial choice.

Chapter 6

Conclusions and Research Perspectives

6.1 Conclusions

The advanced MG model is a promising grid application with technical, environmental and economical benefits. The grid power flow control feature is a feasible solution for 100% renewable generation and heavy integration of electric vehicles. It was presented some Brazil- and world-cases that already apply the MG model, benefiting from its flexibility and convenience. Some trends (e.g., the decrease in the prices of PV panels and battery packs, and the increase in energy tariff) indicate that in near future the MG implementation will become a more common reality. However, the technical development of a reliable MG is still in progress with some challenges to be solved. The main issue investigated in this dissertation is the development of a complete MG structure and control strategy that does not rely on a single grid-forming converter for the islanded operating mode. Nevertheless, such advanced MG strategy should be capable of: *i*) performing precise grid power flow control at its PCC; *ii*) operating in both grid-connected and islanded condition with smooth transitioning between modes; *iii*) regulating voltage and frequency during islanded mode; and *iv*) accomplishing proportional power sharing among all DERs.

With that clear objective, the first step, in Ch. 3, a control structure for grid-forming converter was investigated. It was proposed a control that uses a droop-based power loop with the insertion of saturators. The chapter main contribution is the proposal to use a frequency switch in the VCM converter control, so reconnection to grid-connected mode is automatic through slip frequency technique, without necessity of high-speed communication. The proposed control proved to be appropriate for synchronizing multiple VCM converters under circumstances such as intentional and unintentional islanding, since the MG voltage is not affected. Furthermore, the slip frequency technique is adequate for grid-reconnection of dispersed grid-forming converters. Results showed

that no critical voltage and current transition is observed in the reconnection process, even considering typical switch delays. The reconnection and synchrocheck function is part of MG secondary control, which must be embedded in a CC placed at MG PCC. Notably, MG transitions must be done smoothly, so that DERs do not get disconnected by their local islanding detection. Lastly, the proposed VCM converter control proved to be suitable for use in a centralized control, as desired.

Once the VCM converter control structure to substitute the central converter is defined, a secondary control is developed using such converter in Ch. 4. The power-based control is improved to consider this modification and also to include heterogeneous DERs. Such condition characterizes a more practical reality situation. All objectives are achieved transmitting only scaling coefficients from the CC to the DERs. The results support the conclusion that it is possible to obtain the same performance of a centralized control using dispersed grid-forming converters. The proposed strategy encourages the engagement of VCM converters and all DERs connected in MG in a coordinated control to achieve the common goals of MG. Thus, more power capacity will be available, and enhanced conditions of efficiency and power quality.

In Ch. 5, the scenario with distorted mains voltage is considered. Thus, a particular harmonic compensation for the VCM converter developed in Ch. 3 is proposed. The proposed method uses GPS modules to synchronize the harmonic output voltage of the VCM converter with the harmonics detected at the PCC. The results showed that the GPS module can be used for distributed harmonic compensation among VCM converters, reducing line impedances power losses, and improving overall power quality. It was observed that the compensation accuracy becomes more sensitive especially at higher frequencies. In addition, it was noticed that some factors influence the compensation accuracy, such as: the implemented digital low-pass filter, the converter control and PMS sample frequency, and the accuracy and jitter of the GPS module. Further investigation is needed to define such boundaries and the harmonic order limit for compensation. Moreover, the results support the conclusion that it is better for the overall electrical system that the converters contribute to harmonic currents locally, instead of only rejecting the harmonics.

Hardware-in-the-loop results with real digital controllers validate all proposed strategies, but still real MG testbeds are encouraged to verify real application aspects. Furthermore, all proposed strategies use only low-bandwidth communication, which makes their implementation feasible. This dissertation addressed several aspects and learning such as: control of power converters, power systems knowledge, implementation of digital control, implementation of communication, implementation of power meters in real hardware and signal conditioning. Finally, this dissertation contributes to the maturity of a centralized MG control, and several sorts of MGs can benefit from the proposed MG control structure, such as: commercial and industrial MGs, community MGs, utility MGs, institutions and campi MGs and military MGs.

6.2 Research Perspectives

The research developed in this dissertation opens up some challenges that require further investigation. Thus, the following topics are proposed as continuity perspectives:

- Further investigation of the communication issues for the PBC implementation. For example, define the maximum number of DERs that can participate at the coordinated control as function of the size of data packets that are sent and received and of the update rate of the coefficients;
- Investigate the use of integrative or derivative components in the calculation of the PBC coefficients to improve the control dynamics and steady-state error;
- Develop, in light of stability, a method to quantify the minimum power of a grid-forming converter for the islanded mode as a function of the total MG power, including CCM converters and loads;
- Investigate a method to specify the maximum reactive power that a three-phase unbalanced converter may provide as a function of the maximum ripple of the dc-link;
- Further investigate the use of GPS modules for harmonics compensation in power converters. Test the implementation boundaries and critical cases, such as desynchronization when multiple DERs perform compensation. Moreover, issues related to the use of digital low-pass filter that may affect harmonics components should be investigated.
- Implement the proposed strategies in a real experimental setup to verify the control performance under conditions closer to practical reality.

Bibliography

[1] J. R. Martí, "The ac electrical grid: Transitions into the twenty-first century." in *Energy Transitions in History: Global Cases of Continuity and Change*, R. W. Unger, Ed. RCC Perspectives, 2013, pp. 75–82.

[2] IEA, "International Energy Agency - Global Energy & CO2 Status Report," Available: https://www.iea.org/geco/electricity/, 2019, last accessed 01 October 2019.

[3] M. Diesendorf and B. Elliston, "The feasibility of 100% renewable electricity systems: A response to critics," *Renewable and Sustainable Energy Reviews*, vol. 93, pp. 318–330, 2018.

[4] P. Technology, "Fossil fuel free by 2050: Danish energy minister martin lidegaard explains how," Available: http://https://www.power-technology.com/analysis/featurefossil-fuel-free-2050-denmark-wind-power/, 2012, last accessed 29 August 2022.

[5] E. Commission, "2030 climate and energy framework," Available: https://ec.europa.eu/clima/eu-action/climate-strategies-targets/2030-climate-energy-framework_en, 2014, last accessed 29 August 2022.

[6] M. Child, C. Kemfert, D. Bogdanov, and C. Breyer, "Flexible electricity generation, grid exchange and storage for the transition to a 100% renewable energy system in europe," *Renewable energy*, vol. 139, pp. 80–101, 2019.

[7] P. Tenti and T. Caldognetto, "Generalized control of the power flow in local area energy networks," *Energies*, vol. 15, no. 4, p. 1416, 2022.

[8] A. Hoke, J. Giraldez, B. Palmintier, E. Ifuku, M. Asano, R. Ueda, and M. Symko-Davies, "Setting the smart solar standard: Collaborations between hawaiian electric and the national renewable energy laboratory," *IEEE Power and Energy Magazine*, vol. 16, no. 6, pp. 18–29, Nov 2018.

[9] K. L. Anaya and M. G. Pollitt, "A social cost benefit analysis for the procurement of reactive power: The case of power potential," *Applied Energy*, vol. 312, p. 118512, 2022.

[10] R. H. Lasseter, "Microgrids," in *2002 IEEE Power Engineering Society Winter Meeting. Conference Proceedings (Cat. No.02CH37309)*, vol. 1, Jan 2002, pp. 305–308 vol.1.

[11] D. I. Brandao, L. S. Araujo, A. M. S. Alonso, G. L. dos Reis, E. V. Liberado, and F. P. Marafão, "Coordinated control of distributed three- and single-phase inverters connected to three-phase three-wire microgrids," *IEEE Journal of Emerging and Selected Topics in Power Electronics*, vol. 8, no. 4, pp. 3861–3877, 2020.

[12] G. Valverde, D. Shchetinin, and G. Hug-Glanzmann, "Coordination of distributed reactive power sources for voltage support of transmission networks," *IEEE Transactions on Sustainable Energy*, 2019.

[13] L. S. Araujo, D. I. Brandao, S. M. Silva, and B. J. Cardoso Filho, "Reactive power support in medium voltage networks by coordinated control of distributed generators in dispatchable low-voltage microgrid," in *2019 IEEE 28th International Symposium on Industrial Electronics (ISIE)*. IEEE, 2019, pp. 2603–2608.

[14] J. R. S. Junior, D. I. Brandao, N. T. Fernandes, W. Uturbey, and B. Cardoso, "Multifunctional dispatchable microgrids," *Applied Energy*, vol. 282, p. 116165, 2021.

[15] D. E. Olivares, A. Mehrizi-Sani, A. H. Etemadi, C. A. Canizares, R. Iravani, M. Kazerani, A. H. Hajimiragha, O. Gomis-Bellmunt, M. Saeedifard, R. Palma-Behnke, G. A. Jimenez-Estevez, and N. D. Hatziargyriou, "Trends in microgrid control," *IEEE Transactions on Smart Grid*, vol. 5, no. 4, pp. 1905–1919, July 2014.

[16] R. M. Kamel, "New inverter control for balancing standalone micro-grid phase voltages: A review on mg power quality improvement," *Renewable and Sustainable Energy Reviews*, vol. 63, pp. 520–532, 2016.

[17] T. S. Ustun, C. Ozansoy, and A. Zayegh, "Recent developments in microgrids and example cases around the world – a review," *Renewable and Sustainable Energy Reviews*, vol. 15, no. 8, pp. 4030–4041, 2011.

[18] A. Hirsch, Y. Parag, and J. Guerrero, "Microgrids: A review of technologies, key drivers, and outstanding issues," *Renewable and sustainable Energy reviews*, vol. 90, pp. 402–411, 2018.

[19] G. Y. Morris, C. Abbey, S. Wong, and G. Joós, "Evaluation of the costs and benefits of microgrids with consideration of services beyond energy supply," in *2012 IEEE Power and Energy Society General Meeting*, July 2012, pp. 1–9.

[20] J. V. Caracas, "Uso da Energia Solar no Maranhão – Caso de sucesso Ilha dos Lençóis." Available: http://www.seme.ma.gov.br/files/2016/11/SEME-Semin%

C3%A1rio-Renov%C3%A1veis-Jo%C3%A3o-Caracas-Case-das-ilhas-do-MA.pdf, 2016, last accessed 13 November 2019.

[21] L. A. S. Ribeiro, O. R. Saavedra, S. L. de Lima, and J. de Matos, "Isolated microgrids with renewable hybrid generation: The case of lençóis island," *IEEE Transactions on Sustainable Energy*, vol. 2, no. 1, pp. 1–11, Jan 2011.

[22] R. V. Ferreira, S. M. Silva, D. I. Brandao, H. M. Antunes, and N. T. Fernandes, "Assessment of energy storage viability for a pv power plant injecting during peak load time," in *2017 IEEE 8th International Symposium on Power Electronics for Distributed Generation Systems (PEDG)*. IEEE, 2017, pp. 1–6.

[23] W. Hermsdorff and D. Oliveira Filho, "Geração independente na ponta," in *Proceedings of the 3. Encontro de Energia no Meio Rural*. SciELO Brasil, 2000.

[24] P. Asmus, A. Forni, and L. Vogel, *Microgrid Analysis and Case Studies Report. California, North America, and Global Case Studies*, ser. California Energy Commission. Navigant Consulting, Inc. 2017, 2018, publication Number: CEC-500-2018-022.

[25] ANEEL, "Tarifa branca - aneel," Available: www.aneel.gov.br/tarifa-branca, 2019, last accessed 13 November 2019.

[26] Ambiente Energia, "Linhas de financiamento aproximam energia solar do campo." Available: http://www.ambienteenergia.com.br/index.php/ 2017/09/linhas-de-financiamento-aproximam-energia-solar-campo/32693, 2017, last accessed 13 November 2019.

[27] M. A. I. Martins, C. Q. Pica, V. Maryama, B. Pacheco, M. L. Heldwein, and J. N. R. da Silva Junior, "Design and implementation of a microgrid power management unit using a back-to-back converter in a residential condominium connected at medium voltage," in *2015 IEEE 13th Brazilian Power Electronics Conference and 1st Southern Power Electronics Conference (COBEP/SPEC)*, Nov 2015, pp. 1–5.

[28] Aalborg University, "Microgrid technology research and demonstration," Available: https://www.et.aau.dk/research-programmes/microgrids/ activities/microgrid-technology-research-and-demonstration/, 2017, last accessed 13 November 2019.

[29] N. C. Foureaux, H. M. A. Antunes, S. M. Silva, B. de Jesus Cardoso Filho, F. M. R. Júnior, and J. A. de Souza Brito, "Decisoes de projeto da usina experimental fotovoltaica tesla engenharia de potencia," in *VI Congresso Brasileiro de Energia Solar*, 2016.

[30] Microgrid Knowledge, "Military microgrid: Fort bliss case study," Available: https://microgridknowledge.com/military-microgrid-fort-bliss/, 2014, last accessed 13 November 2019.

[31] Enerdata, "World power consumption - electricity domestic consumption," Available: https://yearbook.enerdata.net/electricity/electricity-domestic-consumption-data.html, 2019, last accessed 16 November 2019.

[32] IBGE, "Indicador 7.1.1 - percentagem da população com acesso à eletricidade," Available: https://indicadoresods.ibge.gov.br/objetivo7/indicador711, 2018, last accessed 14 November 2019.

[33] EBC, "No ano internacional da luz, 1,5 bilhão de pessoas vivem no escuro pelo mundo," Available: http://www.ebc.com.br/tecnologia/2015/06/no-ano-internacional-da-luz-15-bilhao-de-pessoas-vivem-no-escuro-pelo-mundo, 2015, last accessed 21 June 2017.

[34] 180graus, "Qualidade da energia na zona rural de teresina é discutida no ministério público," Available: https://180graus.com/geral/qualidade-da-energia-na-zona-rural-de-teresina-e-discutida-no-ministerio-publico-423312, 2011, last accessed 14 November 2019.

[35] C. Rural, "Falta de energia elétrica causa prejuízos à agropecuária em santa catarina," Available: https://canalrural.uol.com.br/noticias/pecuaria/falta-energia-eletrica-causa-prejuizos-agropecuaria-santa-catarina-24800/, 2014, last accessed 14 November 2019.

[36] A. Tortelli, "Subcomissão para tratar da qualidade da energia elétrica rural," http://www.al.rs.gov.br/FileRepository/repdcp_m505/SubQualidade_Energia_E_Rural/RF_qualidade_energia_e_rural.pdf, 2011, last accessed 14 November 2019.

[37] H. Lamin, "Qualidade da energia elétrica fornecida ao meio rural brasileiro," Agência Nacional de Energia Elétrica, Brasília - DF, Available: http://www2.camara.leg.br/atividade-legislativa/comissoes/comissoes-permanentes/capadr/audiencias-publicas/audiencias-publicas-2015/audiencia-publica-15-de-setembro-de-2015-aneel, 2015, last accessed 14 November 2019.

[38] G. Media, "Storage once again becoming a 'big deal' for solar," Available: http://midwestenergynews.com/2014/06/17/storage-once-again-becoming-a-big-deal-for-solar/#pq=XtyJ55, 2014, last accessed 14 November 2019.

[39] W. J. Cole, C. Marcy, V. K. Krishnan, and R. Margolis, "Utility-scale lithium-ion storage cost projections for use in capacity expansion models," in *2016 North American Power Symposium (NAPS)*, Sep. 2016, pp. 1–6.

[40] O. Schmidt, A. Hawkes, A. Gambhir, and I. Staffell, "The future cost of electrical energy storage based on experience rates," *Nature Energy*, vol. 2, no. 8, p. 17110, 2017.

[41] World Energy Council, *E-storage: Shifting from cost to value.* London, UK: World Energy Council, 2016, iSBN 978 0 946121 44 1.

[42] J. Gerdes, "The emerging power of microgrids - ensia," Available: https://ensia.com/features/the-emerging-power-of-microgrids/, 2014, last accessed 14 November 2019.

[43] Navigant Research, "Navigant research leaderboard: Remote microgrid players," Available: https://www.navigantresearch.com/reports/navigant-research-leaderboard-remote-microgrid-players, 2019, last accessed 14 November 2019.

[44] D. O. da Uniao, *Lei N. 14.300, de 6 de janeiro de 2022*, in portuguese, 2022. [Online]. Available: https://in.gov.br/en/web/dou/-/lei-n-14.300-de-6-de-janeiro-de-2022-372467821

[45] Ministério de Minas e Energia, "Programa de eletrificação rural," Available: https://www.mme.gov.br/luzparatodos/Asp/o_programa.asp, 2019, last accessed 14 November 2019.

[46] D. I. Brandao, P. Tenti, T. Caldognetto, and S. Buso, "Control of utility interfaces in low-voltage microgrids," *Brazilian Journal Of Power Electronics (SOBRAEP)*, vol. 20, no. 4, pp. 373–382, 2015.

[47] J. Matevosyan, B. Badrzadeh, T. Prevost, E. Quitmann, D. Ramasubramanian, H. Urdal, S. Achilles, J. MacDowell, S. H. Huang, V. Vital, J. O'Sullivan, and R. Quint, "Grid-forming inverters: Are they the key for high renewable penetration?" *IEEE Power and Energy Magazine*, vol. 17, no. 6, pp. 89–98, Nov 2019.

[48] O. Kulkarni, S. Doolla, and B. Fernandes, "Mode Transition Control Strategy for Multiple Inverter-Based Distributed Generators Operating in Grid-Connected and Standalone Mode," *IEEE Trans. on Ind. Apps.*, vol. 53, no. 6, pp. 5927–5939, 2017.

[49] K.-Y. Lo and Y.-M. Chen, "Design of a seamless grid-connected inverter for microgrid applications," *IEEE Trans. on Smart Grid*, vol. 11, no. 1, pp. 194–202, 2019.

[50] M. Ganjian-Aboukheili, M. Shahabi, Q. Shafiee, and J. M. Guerrero, "Seamless Transition of Microgrids Operation From Grid-Connected to Islanded Mode," *IEEE Trans. on Smart Grid*, vol. 11, no. 3, pp. 2106–2114, 2020.

[51] A. Vukojevic and S. Lukic, "Microgrid protection and control schemes for seamless transition to island and grid synchronization," *IEEE Transactions on Smart Grid*, vol. 11, no. 4, pp. 2845–2855, 2020.

[52] V. L. Srinivas, B. Singh, and S. Mishra, "Seamless mode transition technique for virtual synchronous generators and method thereof," *IEEE Trans. on Industrial Informatics*, vol. 16, no. 8, pp. 5254–5266, 2020.

[53] H. M. A. Antunes, S. M. Silva, D. I. Brandao, A. A. P. Machado, and B. d. J. C. Filho, "A new multifunctional converter based on a series compensator applied to AC microgrids," *International Journal of Electrical Power and Energy Systems*, vol. 102, no. February, pp. 160–170, 2018.

[54] P. Tenti, T. Caldognetto, S. Buso, and D. I. Brandao, "Control of utility interfaces in low-voltage microgrids," *Sobraep - Brazilian Journal of Power Electronics*, vol. 20, pp. 373–382, 2015.

[55] X. Huang, D. Chen, and L. Xu, "Microgrid design using folded P-f droop and new grid interface unit to minimize the need for communication," *International Journal of Electrical Power and Energy Systems*, vol. 130, no. January, p. 106949, 2021.

[56] S. Lissandron and P. Mattavelli, "A controller for the smooth transition from grid-connected to autonomous operation mode," in *2014 IEEE Energy Conversion Congress and Exposition (ECCE)*, 2014, pp. 4298–4305.

[57] X. Meng, Z. Liu, H. Zheng, and J. Liu, "A universal controller under different operating states for parallel inverters with seamless transfer capability," *IEEE Trans. Power Electron.*, vol. 35, no. 9, pp. 9794–9812, 2020.

[58] X. Meng, X. Liu, M. He, Z. Liu, and J. Liu, "A self-adaptive controller for inverter with seamless transfer and automatic pre-synchronization capability," *IEEE Access*, vol. 8, pp. 105 936–105 949, 2020.

[59] I. Ziouani, D. Boukhetala, A. M. Darcherif, B. Amghar, and I. El Abbassi, "Hierarchical control for flexible microgrid based on three-phase voltage source inverters operated in parallel," *International Journal of Electrical Power and Energy Systems*, vol. 95, pp. 188–201, 2018.

[60] M. Abadi and S. M. Sadeghzadeh, "A control approach with seamless transition capability for a single-phase inverter operating in a microgrid," *International Journal*

of Electrical Power and Energy Systems, vol. 111, no. October 2018, pp. 475–485, 2019.

[61] J. M. Guerrero, J. C. Vasquez, J. Matas, L. G. De Vicuña, and M. Castilla, "Hierarchical control of droop-controlled AC and DC microgrids - A general approach toward standardization," *IEEE Transactions on Industrial Electronics*, vol. 58, no. 1, pp. 158–172, 2011.

[62] G. Lou, W. Gu, J. Wang, J. Wang, and B. Gu, "A unified control scheme based on a disturbance observer for seamless transition operation of inverter-interfaced distributed generation," *IEEE Trans. on Smart Grid*, vol. 9, pp. 5444–5454, 2018.

[63] G. Lou, W. Gu, J. Zhu, P. Li, and X. Zhang, "A novel control strategy for the seamless transfer of microgrids based on disturbance observer," *International Journal of Electrical Power and Energy Systems*, vol. 118, no. December 2019, p. 105804, 2020.

[64] M. Gao, M. Chen, B. Zhao, B. Li, and Z. Qian, "Design of control system for smooth mode-transfer of grid-tied mode and islanding mode in microgrid," *IEEE Trans. Power Electron.*, vol. 35, no. 6, pp. 6419–6435, 2020.

[65] X. Hou, Y. Sun, J. Lu, X. Zhang, L. H. Koh, M. Su, and J. M. Guerrero, "Distributed hierarchical control of ac microgrid operating in grid-connected, islanded and their transition modes," *IEEE Access*, vol. 6, pp. 77 388–77 401, 2018.

[66] Y. Sun, C. Zhong, X. Hou, J. Yang, H. Han, and J. M. Guerrero, "Distributed cooperative synchronization strategy for multi-bus microgrids," *International Journal of Electrical Power and Energy Systems*, vol. 86, pp. 18–28, 2017.

[67] A. G. Alves, R. F. Dias, and L. G. Rolim, "A smooth synchronization methodology for the reconnection of autonomous microgrids," *Journal of Control, Automation and Electrical Systems*, pp. 1–10, 2020.

[68] W. R. Issa, A. H. E. Khateb, M. A. Abusara, and T. K. Mallick, "Control strategy for uninterrupted microgrid mode transfer during unintentional islanding scenarios," *IEEE Trans. Ind. Electron.*, vol. 65, no. 6, pp. 4831–4839, 2018.

[69] F. Tang, J. M. Guerrero, J. C. Vasquez, D. Wu, and L. Meng, "Distributed active synchronization strategy for microgrid seamless reconnection to the grid under unbalance and harmonic distortion," *IEEE Trans. Smart Grid*, vol. 6, no. 6, pp. 2757–2769, 2015.

[70] Y. Deng, Y. Tao, G. Chen, G. Li, and X. He, "Enhanced power flow control for grid-connected droop-controlled inverters with improved stability," *IEEE Trans. Ind. Electron.*, vol. 64, pp. 5919–5929, 2017.

[71] P. Rodríguez, C. Citro, J. I. Candela, J. Rocabert, and A. Luna, "Flexible grid connection and islanding of spc-based pv power converters," *IEEE Trans. Ind. Appl.*, vol. 54, no. 3, pp. 2690–2702, 2018.

[72] J. Rocabert, G. M. S. Azevedo, A. Luna, J. M. Guerrero, J. I. Candela, and P. Rodriguez, "Intelligent connection agent for three-phase grid-connected microgrids," *IEEE Trans. on Power Electronics*, vol. 26, no. 10, pp. 2993–3005, 2011.

[73] C. Blanco, D. Reigosa, F. Briz, and J. M. Guerrero, "Strategies for the connection of distributed power generation units to distorted networks," in *2014 IEEE Energy Conversion Congress and Exposition (ECCE)*, 2014, pp. 3378–3385.

[74] M. Karimi-Ghartemani, S. A. Khajehoddin, P. Piya, and M. Ebrahimi, "Universal controller for three-phase inverters in a microgrid," *IEEE J. Emerg. Sel. Topics Power Electron.*, vol. 4, no. 4, pp. 1342–1353, 2016.

[75] S. Sen and V. Kumar, "Microgrid control: A comprehensive survey," *Annual Reviews in control*, vol. 45, pp. 118–151, 2018.

[76] Y. Han, H. Li, P. Shen, E. A. A. Coelho, and J. M. Guerrero, "Review of active and reactive power sharing strategies in hierarchical controlled microgrids," *IEEE Transactions on Power Electronics*, vol. 32, no. 3, pp. 2427–2451, 2016.

[77] C. Ahumada, R. Cárdenas, D. Sáez, and J. M. Guerrero, "Secondary control strategies for frequency restoration in islanded microgrids with consideration of communication delays," *IEEE Transactions on Smart Grid*, vol. 7, no. 3, pp. 1430–1441, May 2016.

[78] Q. Sun, J. Zhou, J. M. Guerrero, and H. Zhang, "Hybrid three-phase/single-phase microgrid architecture with power management capabilities," *IEEE Transactions on Power Electronics*, vol. 30, no. 10, pp. 5964–5977, Oct 2015.

[79] Y. A. I. Mohamed and E. F. El-Saadany, "Adaptive decentralized droop controller to preserve power sharing stability of paralleled inverters in distributed generation microgrids," *IEEE Transactions on Power Electronics*, vol. 23, no. 6, pp. 2806–2816, Nov 2008.

[80] W. Yao, M. Chen, J. Matas, J. M. Guerrero, and Z. Qian, "Design and analysis of the droop control method for parallel inverters considering the impact of the complex impedance on the power sharing," *IEEE Transactions on Industrial Electronics*, vol. 58, no. 2, pp. 576–588, Feb 2011.

[81] C. Blanco, D. Reigosa, J. C. Vasquez, J. M. Guerrero, and F. Briz, "Virtual admittance loop for voltage harmonic compensation in microgrids," *IEEE Transactions on Industry Applications*, vol. 52, no. 4, pp. 3348–3356, July 2016.

[82] M. Zeraati, M. E. H. Golshan, and J. M. Guerrero, "Voltage quality improvement in low voltage distribution networks using reactive power capability of single-phase pv inverters," *IEEE Transactions on Smart Grid*, vol. 10, no. 5, pp. 5057–5065, Sep. 2019.

[83] A. Ranjbaran and M. Ebadian, "A power sharing scheme for voltage unbalance and harmonics compensation in an islanded microgrid," *Electric Power Systems Research*, vol. 155, pp. 153–163, 2018.

[84] Y. Wang, X. Wang, Z. Chen, and F. Blaabjerg, "Distributed optimal control of reactive power and voltage in islanded microgrids," *IEEE Transactions on Industry Applications*, vol. 53, no. 1, pp. 340–349, 2017.

[85] Q. Shafiee, V. Nasirian, J. C. Vasquez, J. M. Guerrero, and A. Davoudi, "A multifunctional fully distributed control framework for ac microgrids," *IEEE Transactions on Smart Grid*, vol. 9, no. 4, pp. 3247–3258, 2018.

[86] H. Zhang, S. Kim, Q. Sun, and J. Zhou, "Distributed adaptive virtual impedance control for accurate reactive power sharing based on consensus control in microgrids," *IEEE Transactions on Smart Grid*, vol. 8, no. 4, pp. 1749–1761, 2017.

[87] S. Y. Mousazadeh Mousavi, A. Jalilian, M. Savaghebi, and J. M. Guerrero, "Autonomous control of current- and voltage-controlled dg interface inverters for reactive power sharing and harmonics compensation in islanded microgrids," *IEEE Transactions on Power Electronics*, vol. 33, no. 11, pp. 9375–9386, Nov 2018.

[88] J. Zhou, S. Kim, H. Zhang, Q. Sun, and R. Han, "Consensus-based distributed control for accurate reactive, harmonic, and imbalance power sharing in microgrids," *IEEE Transactions on Smart Grid*, vol. 9, no. 4, pp. 2453–2467, 2018.

[89] N. Mohammed, A. Lashab, M. Ciobotaru, and J. M. Guerrero, "Accurate reactive power sharing strategy for droop-based islanded ac microgrids," *IEEE Transactions on Industrial Electronics*, 2022.

[90] F. Deng, X. Li, X. Zhang, and P. Mattavelli, "An iterative virtual impedance regulation strategy in islanded microgrids for enhanced balanced, unbalanced and harmonic current sharing," *IEEE Transactions on Sustainable Energy*, vol. 13, no. 1, pp. 514–526, 2021.

[91] V. Nasirian, Q. Shafiee, J. M. Guerrero, F. L. Lewis, and A. Davoudi, "Droop-free distributed control for ac microgrids," *IEEE Transactions on Power Electronics*, vol. 31, no. 2, pp. 1600–1617, 2016.

[92] J. W. Simpson-Porco, Q. Shafiee, F. Dörfler, J. C. Vasquez, J. M. Guerrero, and F. Bullo, "Secondary frequency and voltage control of islanded microgrids via distributed averaging," *IEEE Transactions on Industrial Electronics*, vol. 62, no. 11, pp. 7025–7038, 2015.

[93] W. Meng, X. Wang, and S. Liu, "Distributed load sharing of an inverter-based microgrid with reduced communication," *IEEE Transactions on Smart Grid*, vol. 9, no. 2, pp. 1354–1364, 2018.

[94] D. Zhao, C. Zhang, Y. Sun, S. Li, B. Sun, and Y. Li, "Distributed robust frequency restoration and active power sharing for autonomous microgrids with event-triggered strategy," *IEEE Transactions on Smart Grid*, vol. 12, no. 5, pp. 3819–3834, 2021.

[95] J. Jiang, S. Peyghami, C. Coates, and F. Blaabjerg, "A decentralized reliability-enhanced power sharing strategy for pv-based microgrids," *IEEE Transactions on Power Electronics*, vol. 36, no. 6, pp. 7281–7293, 2020.

[96] C. Huang, S. Weng, D. Yue, S. Deng, J. Xie, and H. Ge, "Distributed cooperative control of energy storage units in microgrid based on multi-agent consensus method," *Electric Power Systems Research*, vol. 147, pp. 213–223, 2017.

[97] J. Hu and A. Lanzon, "Distributed finite-time consensus control for heterogeneous battery energy storage systems in droop-controlled microgrids," *IEEE Transactions on Smart Grid*, vol. 10, no. 5, pp. 4751–4761, 2019.

[98] T. Caldognetto, S. Buso, P. Tenti, and D. I. Brandao, "Power-based control of low-voltage microgrids," *IEEE Journal of Emerging and Selected Topics in Power Electronics*, vol. 3, no. 4, pp. 1056–1066, Dec 2015.

[99] D. I. Brandao, T. Caldognetto, F. P. Marafão, M. G. Simões, J. A. Pomilio, and P. Tenti, "Centralized control of distributed single-phase inverters arbitrarily connected to three-phase four-wire microgrids," *IEEE Transactions on Smart Grid*, vol. 8, no. 1, pp. 437–446, Jan 2017.

[100] D. I. Brandao, L. S. de Araújo, T. Caldognetto, and J. A. Pomilio, "Coordinated control of three-and single-phase inverters coexisting in low-voltage microgrids," *Applied energy*, vol. 228, pp. 2050–2060, 2018.

[101] R. A. Otto, T. H. Putman, and L. Gyugyi, "Principles and applications of static, thyristor-controlled shunt compensators," *IEEE Transactions on Power Apparatus and Systems*, vol. PAS-97, no. 5, pp. 1935–1945, Sep. 1978.

[102] L. Monjo, L. Sainz, S. Riera, and J. Bergas, "Theoretical study of the steinmetz circuit design," *Electric Power Components and Systems*, vol. 41, no. 3, pp. 304–323, 2013.

[103] D. M. Ferreira, D. I. Brandao, G. Bergna-Diaz, E. Tedeschi, and S. M. Silva, "Distributed control strategy for low-voltage three-phase four-wire microgrids: Consensus power-based control," *IEEE Transactions on Smart Grid*, vol. 12, no. 4, pp. 3215–3231, 2021.

[104] T. Ackermann and V. Knyazkin, "Interaction between distributed generation and the distribution network: operation aspects," in *IEEE/PES Transmission and Distribution Conference and Exhibition*, vol. 2, 2002, pp. 1357–1362 vol.2.

[105] L. S. Araujo and D. I. Brandao, "Self-adaptive control for grid-forming converter with smooth transition between microgrid operating modes," *International Journal of Electrical Power & Energy Systems*, vol. 135, p. 107479, 2022.

[106] T. Caldognetto, H. Abedini, and P. Mattavelli, "A per-phase power controller for smooth transitions to islanded operation," *IEEE Open Journal of Power Electronics*, vol. 2, pp. 636–646, 2021.

[107] J. Lundquist, "On harmonic distortion in power systems," Master's thesis, Chalmeers University of technology, 2001.

[108] *IEEE Standard for Harmonic Control in Electric Power Systems*, IEEE Std 519-2022 (Revision of IEEE Std 519-2014), 2022.

[109] P. Tenti, A. Costabeber, P. Mattavelli, and D. Trombetti, "Distribution Loss Minimization by Token Ring Control of Power Electronic Interfaces in Residential Microgrids," *IEEE Transactions on Industrial Electronics*, vol. 59, no. 10, pp. 3817–3826, 2012.

[110] A. M. dos Santos Alonso, D. I. Brandao, T. Caldognetto, F. P. Marafão, and P. Mattavelli, "A selective harmonic compensation and power control approach exploiting distributed electronic converters in microgrids," *International Journal of Electrical Power & Energy Systems*, vol. 115, p. 105452, 2020.

[111] J. He and Y. W. Li, "Hybrid voltage and current control approach for dg-grid interfacing converters with lcl filters," *IEEE Transactions on Industrial Electronics*, vol. 60, no. 5, pp. 1797–1809, 2013.

[112] J. He, Y. W. Li, and F. Blaabjerg, "Flexible microgrid power quality enhancement using adaptive hybrid voltage and current controller," *IEEE Transactions on Industrial Electronics*, vol. 61, no. 6, pp. 2784–2794, 2014.

[113] J. He, Y. W. Li, and M. S. Munir, "A flexible harmonic control approach through voltage-controlled dg-grid interfacing converters," *IEEE Transactions on Industrial Electronics*, vol. 59, no. 1, pp. 444–455, 2012.

[114] X. Zhao, L. Meng, C. Xie, J. M. Guerrero, and X. Wu, "A unified voltage harmonic control strategy for coordinated compensation with vcm and ccm converters," *IEEE Transactions on Power Electronics*, vol. 33, no. 8, pp. 7132–7147, 2018.

[115] R. A. Mastromauro, M. Liserre, T. Kerekes, and A. Dell'Aquila, "A single-phase voltage-controlled grid-connected photovoltaic system with power quality conditioner functionality," *IEEE Transactions on Industrial Electronics*, vol. 56, no. 11, pp. 4436–4444, 2009.

[116] Y. W. Li and J. He, "Distribution system harmonic compensation methods: An overview of dg-interfacing inverters," *IEEE Industrial Electronics Magazine*, vol. 8, no. 4, pp. 18–31, 2014.

[117] M. Savaghebi, J. C. Vasquez, A. Jalilian, J. M. Guerrero, and T.-L. Lee, "Selective compensation of voltage harmonics in grid-connected microgrids," *Mathematics and Computers in Simulation*, vol. 91, pp. 211–228, 2013.

[118] T. Meyers and B. Mather, "Empirical evaluation of gps clock accuracy for isochronous droop-based inverters," in *2021 IEEE Energy Conversion Congress and Exposition (ECCE)*, 2021, pp. 390–395.

[119] A. Bellini, S. Bifaretti, and F. Giannini, "A robust synchronization method for centralized microgrids," *IEEE Transactions on Industry Applications*, vol. 51, no. 2, pp. 1602–1609, 2015.

[120] M. Litwin, D. Zielinski, and S. Stynski, "Remote synchronization of the microgrid to the utility grid without access to point of common coupling in the presence of disturbances," *IEEE Access*, vol. 10, pp. 27 819–27 831, 2022.

[121] M. S. Golsorkhi, M. Savaghebi, D. D.-C. Lu, J. M. Guerrero, and J. C. Vasquez, "A gps-based control framework for accurate current sharing and power quality improvement in microgrids," *IEEE Transactions on Power Electronics*, vol. 32, no. 7, pp. 5675–5687, 2017.

[122] M. S. Golsorkhi, D. D.-C. Lu, and J. M. Guerrero, "A gps-based decentralized control method for islanded microgrids," *IEEE Transactions on Power Electronics*, vol. 32, no. 2, pp. 1615–1625, 2017.

[123] H. Qian, Q. Xu, J. Zhao, and X. Yuan, "A robust gps-based control scheme for power sharing and quality improvement in microgrid," *International Journal of Electrical Power & Energy Systems*, vol. 123, p. 106324, 2020.

[124] H. Qian, Q. Xu, P. Du, Y. Xia, and J. Zhao, "Distributed control scheme for accurate power sharing and fixed frequency operation in islanded microgrids," *IEEE Transactions on Industrial Electronics*, vol. 68, no. 12, pp. 12 229–12 238, 2021.

[125] H. Qian, Q. Xu, Y. Xia, J. Zhao, and P. Du, "Analysis and implementation of virtual impedance for fixed-frequency control strategy in microgrid," *IET Generation, Transmission & Distribution*, vol. 15, no. 15, pp. 2262–2276, 2021. [Online]. Available: https://ietresearch.onlinelibrary.wiley.com/doi/abs/10.1049/gtd2.12176

[126] S. Patel, S. Chakraborty, B. Lundstrom, S. M. Salapaka, and M. V. Salapaka, "Isochronous architecture-based voltage-active power droop for multi-inverter systems," *IEEE Transactions on Smart Grid*, vol. 12, no. 2, pp. 1088–1103, 2021.

[127] N. Lidula and A. Rajapakse, "Voltage balancing and synchronization of microgrids with highly unbalanced loads," *Renewable and Sustainable Energy Reviews*, vol. 31, pp. 907–920, 2014.

[128] R. Rodrigues, Y. Du, A. Antoniazzi, and P. Cairoli, "A Review of Solid-State Circuit Breakers," *IEEE Trans. on Power Elec.*, vol. 36, no. 1, pp. 364–377, 2021.

[129] Greegoo, *Solid State Relays - 3 phase solid state relays*, Greegoo, 2020. [Online]. Available: https://www.greegoo.com/handler/download.ashx?url=/UploadFiles/solid-state-relays-GTH200.pdf

[130] R. Teodorescu, F. Blaabjerg, M. Liserre, and P. C. Loh, "Proportional-resonant controllers and filters for grid-connected voltage-source converters," *IEE Proceedings-Electric Power Applications*, vol. 153, no. 5, pp. 750–762, 2006.

[131] A. Etxegarai, P. Eguía, and I. Zamora, "Analysis of remote islanding detection methods for distributed resources," in *Int. conf. Renew. Energies power quality*, 2011.

[132] *IEEE Standard for Interconnection and Interoperability of Distributed Energy Resources with Associated Electric Power Systems Interfaces*, IEEE Std 1547-2018, 2018.

[133] K. Ogata and Y. Yang, *Modern control engineering*. Prentice hall India, 2002, vol. 4.

[134] ANEEL, *Electric Power Quality*, ANEEL PRODIST 8th Module, Rev.10, 2018, in Portuguese.

[135] M. A. Abusara, S. M. Sharkh, and J. M. Guerrero, "Improved droop control strategy for grid-connected inverters," *Elsevier Sustainable energy, grids and networks*, vol. 1, pp. 10–19, 2015.

[136] S. Golestan, M. Ramezani, J. M. Guerrero, F. D. Freijedo, and M. Monfared, "Moving Average Filter Based Phase-Locked Loops: Performance Analysis and Design Guidelines," *IEEE Trans. on Power Electronics*, vol. 29, no. 6, pp. 2750–2763, 2014.

[137] R. H. Lasseter and P. Piagi, "Control and design of microgrid components," *PSERC Publication 06*, vol. 3, 2006.

[138] I. V. Blagouchine and E. Moreau, "Analytic method for the computation of the total harmonic distortion by the cauchy method of residues," *IEEE Transactions on Communications*, vol. 59, no. 9, pp. 2478–2491, 2011.

[139] Schneider, *TeSys Catalogue 2020 - Innovative and connected solutions for motor starters*, Schneider Electric, 2020. [Online]. Available: https://www.se.com/ww/en/download/document/MKTED210011EN/

[140] T. Orłowska-Kowalska, F. Blaabjerg, and J. Rodríguez, *Advanced and intelligent control in power electronics and drives*. Springer, 2014, vol. 531.

[141] X. Pei, W. Zhou, and Y. Kang, "Analysis and calculation of dc-link current and voltage ripples for three-phase inverter with unbalanced load," *IEEE Transactions on Power Electronics*, vol. 30, no. 10, pp. 5401–5412, Oct 2015.

[142] ABB, *62Pak phase leg IGBT Module*, 5SNG 0150Q170300, 2016, datasheet. [Online]. Available: http://search.abb.com/library/Download.aspx?DocumentID=5SYA%201447&LanguageCode=en&DocumentPartId=&Action=Launch

[143] A. F. Cupertino, J. V. M. Farias, H. A. Pereira, S. I. Seleme, and R. Teodorescu, "Dscc-mmc statcom main circuit parameters design considering positive and negative sequence compensation," *Journal of Control, Automation and Electrical Systems*, vol. 29, no. 1, pp. 62–74, 2018.

[144] T. Tanaka, H. Wang, K. Ma, and F. Blaabjerg, "Reactive power compensation capability of a statcom based on two types of modular multilevel cascade converters

for offshore wind application," in *2017 IEEE 3rd International Future Energy Electronics Conference and ECCE Asia (IFEEC 2017-ECCE Asia)*. IEEE, 2017, pp. 326–331.

[145] W. M. Ferreira, I. R. Meneghini, D. I. Brandao, and F. G. Guimarães, "Preference cone based multi-objective evolutionary algorithm applied to optimal management of distributed energy resources in microgrids," *Applied Energy*, vol. 274, p. 115326, 2020.

[146] CIGRE Task Force C6.04.02, "Benchmark Systems for Network Integration of Renewable and Distributed Energy Resources," International Council on Large Electric Systems, Tech. Rep., 2014.

[147] IRIGB, *IRIG Standard 200-16 - IRIG Serial Time Code Formats*, Timing Committee Telecommunications and Timing Group, Range Commanders Council U.S. Army White Sands Missile Range, 2016.

[148] G. L. Reis, D. I. Brandao, J. H. Oliveira, L. S. Araujo, and B. J. Cardoso Filho, "Case study of single-controllable microgrid: A practical implementation," *Energies*, vol. 15, no. 17, 2022. [Online]. Available: https://www.mdpi.com/1996-1073/15/17/6400

[149] *IEEE Recommended Practice for the Planning and Design of the Microgrid*, IEEE Std 2030.9-2019, 2019.

[150] G. dos Reis, E. Liberado, F. Marafão, C. Sousa, W. Silva, and D. Brandao, "Model-free power control for low-voltage ac dispatchable microgrids with multiple points of connection," *Energies*, vol. 14, no. 19, 2021. [Online]. Available: https://www.mdpi.com/1996-1073/14/19/6390

[151] A. Giovinetto and A. Eller, "Navigant research: Comparing the costs of long duration energy storage technologies," National Grid Ventures, Available: https://www.slenergystorage.com/documents/20190626_Long_Duration%20Storage_Costs.pdf, 2019, last accessed 02 September 2022.

Appendix A

TESLA-UFMG Microgrid: A Practical Implementation

A.1 Introduction

This chapter presents the implementation of a single-controllable microgrid in the engineering school of the Federal University of Minas Gerais using commercial devices. Such a MG exchanges controllable active and reactive power terms with the upstream grid, proportionally shares active/reactive power among the battery-based DERs and endows the microgrid with the capability of operating in both grid-connected and islanded modes. The energy storage system is composed of three different battery technologies: lead-acid, lithium-ion and sodium-nickel, which are coordinately controlled according to their inherent features. The single-controllable MG is able to perform the following services: self-consumption, energy time shift, peak-shaving and reactive power support to the upstream grid. A coordinated secondary control, that is, the PBC, is applied into this setup and the services are validated by means of full-scale experimental results using commercial devices. The results demonstrate the MG capability of delivering ancillary services at the connection with the upstream grid, and proportionally exploiting the dispersed battery banks. In addition, the challenges of practical implementation were analyzed.

A.2 Microgrid Structure and Control

A.2.1 Microgrid structure

Fig. A.1 shows the centralized three-phase four-wire MG structure that has been running since July/2021. It consists of a centralized backup grid-forming system (full four-quadrant grid simulator TC.ACS); CB_1 and CB_2 breakers responsible for switching the MG operating modes, i.e., grid-connected (CB_1 closed and CB_2 open) and islanded (CB_1 open and CB_2 closed); CB_3 and CB_4 breakers to disconnect non-critical loads under island

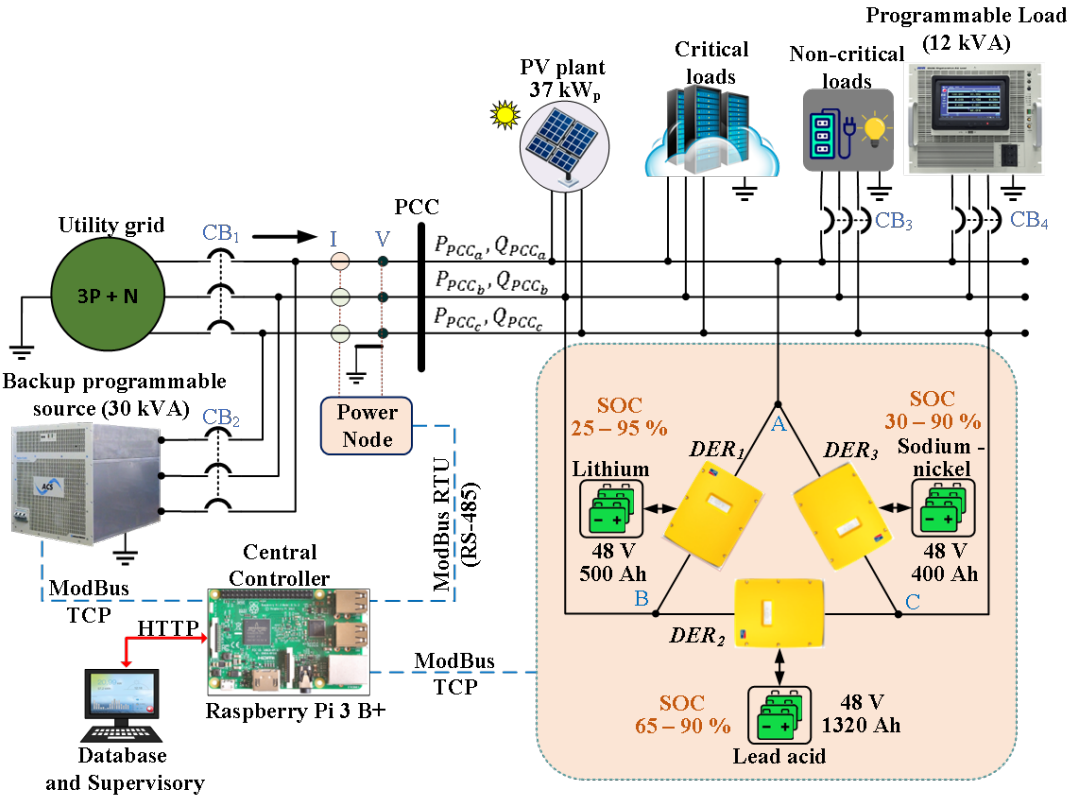

Figure A.1: Block diagram of the single-controllable microgrid.

mode; a PV power system with a 12-kilowatt three-phase inverter from PHB-PHB12KN-DT; a programmable power load (regenerative four-quadrant AC load NHR 9430); an AC bus for critical load connection (i.e., island operation transitioning); and three battery inverters of 6 kW each from SMA (sunny island 6.0 H), supplied by three different battery banks of about 5 kW/15 kWh of usable energy: lead-acid (48 V-1320 Ah)-six strings in parallel composed of four batteries in each of 12MS234 from Moura; lithium-ion (48 V-500 Ah)-five modules in parallel of UPLFP48 from Unipower; and sodium-nickel (48 V-400 Ah)-two modules in parallel of 48TL200 from FZSONICK. It is worth highlighting that the battery inverters are in delta connection due to their required voltage level (about 230 V). Such a MG is coordinated by means of a centralized controller, a Raspberry Pi B3+ embedded in a power node device in star connection at the MG PCC. The power node measures grid voltages and currents and computes the active and reactive powers, transferring them to the CC through a ModBus RTU (RS-485) communication link. It also performs non-critical load shedding (CB_3 and CB_4) during MG-islanded operation. The CC interoperability with the battery inverters is based on ModBus TCP. Finally, Fig. A.2 shows a picture of the actual installation at UFMG.

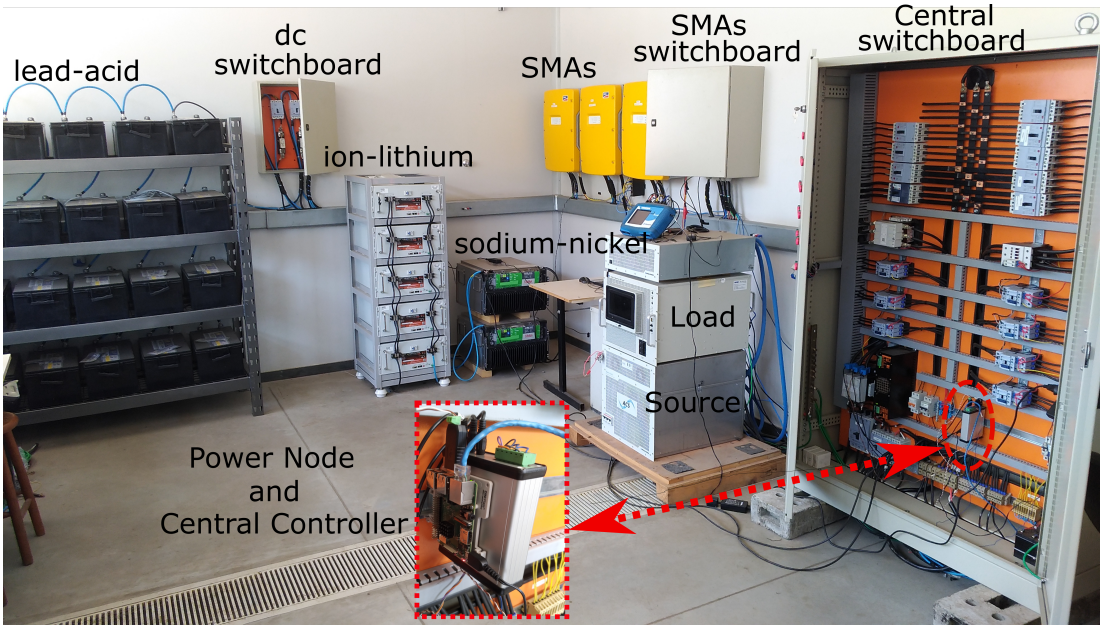

Figure A.2: Real installation of the single-controllable microgrid at UFMG, Brazil.

A.2.2 Control and Organization

The hierarchical MG architecture is adopted to coordinate the local operation of DERs, and to provide specific ancillary services to the single-controllable MG. The PBC is implemented at the CC [148], which uses a communication link to exchange data between DERs. The content of the data transmitted from DERs to the CC comprises the current status of output power as well as rated and generation capacities. The reverse path of communication is the scaling coefficients used to set the power references in the local controller of DERs.

A.2.3 Communication Infrastructure

Fig. A.1 shows the MG communication infrastructure. The DER units have a local communication interface, as recommended by IEEE Std. 1547-2018 [132]. The communication protocol used between the DERs and the CC is based on ModBus TCP, according to IEEE 2030.9-2019 [149]. The ModBus protocol paves the way for the interconnection of DERs from different manufacturers in a single-controllable MG. The communication between the power node device and the CC occurs via ModBus RTU (RS-485) at a baud rate of 115200 bits/s. Both Modbus protocols run with a polling rate of 5 s.

The Node-RED programming tool was used to develop the CC algorithm (i.e., modified power-based control-MPBC [150]). For the sake of stability, the secondary control must be processed at a lower rate than the traffic of data through the communication network. Then, the MPBC algorithm is executed once every minute because the SMA Sunny Island inverter inherits high latency in updating its output power after having

received a power command via the ModBus TCP port. Finally, communication between the database/supervisory and the CC is carried out once every minute via HTTP protocol, as shown in Fig. A.1. This ensures the interoperability of the MG with external agents, such as the MGO and/or DSO.

A.3 Single-Controllable Microgrid Operating Modes

The single-controllable MG performs different operating modes according to its targets, such as economical (self-consumption, energy time shift), electrical technical constraints (peak-shaving), reliable operation (island mode) and upstream power quality enhancement (grid operational support). The main operating modes are described as follows:

1. Self-consumption (SC): this mode minimizes the power flow exchanged between the MG and the upstream grid, thereby maximizing the use of renewables. Under normal operation of voltage, frequency and energy resources, the grid power flow is zero and the MG operates in a manner that is virtually disconnected from the mains, minimizing the impact on the upstream power system.

2. Energy time shift (ETS): this involves storing energy into the batteries when costs are low, and delivering energy when the costs are high. It maximizes the profit and shortens the payback period of DERs. In Brazil, the price of energy is about 3-4 times more expensive during 17-20 h (peak time) than for outside this range. Then, it is expected to store energy from the PV power plant and then self-supply the local loads between 17-20 h. The peak-shaving service is similar to ETS, but takes into account the peak load demand in order to alleviate the upstream feeders.

3. MG islanded operation (IO): this may occur intentionally or non-intentionally; the former is planned for MG stability, whereas the latter is used for continuous power supply during main grid absence. During the MG IO, the grid-forming converter provides voltage reference to the grid-following ones, and the non-critical loads are shed by means of remotely controlled breakers that are spread over the MG feeders.

4. Grid operational support (GOS): it enhances the power quality of the upstream grid based on active/reactive power responses as a function of frequency/voltage deviations. It is basically the freq/watt, volt/var and volt/watt functions applied to the MG PCC with the upstream grid. Moreover, it can also compensate for load imbalances by properly steering the phase-to-phase DERs.

A.4 Experimental Results - Energy time shift

As an application example, the service energy time shift is implemented with the setup of Fig. A.2. The challenge of this service is to completely deliver the energy during the 17-20 h period of costly energy prices, considering three different battery technologies: lead-acid, lithium-ion and sodium-nickel. In order to fully maximize the power delivery, the three battery banks must inject power that is proportional to the overall usable energy stored in the system, as well as consider their individual released capacities. Thus, this prevents a battery bank from reaching its minimum limit of SOC before the other battery banks. If this occurs, it will interrupt the ETS service or cause imbalances in power injected into the upstream grid. Fig. A.3 shows the output power, charged energy, discharged energy, SOC values of each battery bank and PCC power. The battery charging process begins at around 6 am with a power of 2.5 kW. As a result of the different battery technologies used, the charging process ends at different times. In addition, it is observed that the sodium-nickel battery reached its voltage limit twice during the charging process, and the central controller acted by reducing the power during charging. From the top graphic, one can see that the ETS service begins at 17 h and lasts up to 20 h, delivering about 5 kW per battery bank. At 17 h, the three battery banks show maximum SOC values, as shown in the fourth graphic. During the 3 h of ETS operation, the battery banks delivered power in proportion to their released capacities. One can see that the three battery banks achieved their minimum SOC values at 20 h. Thus, the three battery banks were fully exploited, independent of their technology and inner features. Finally, the round-trip efficiency is computed as the ratio between the discharging net energy delivered and the total charging energy consumed. Then, the round-trip efficiency for the battery banks are: lithium-ion, 93%; lead-acid, 89%; and sodium-nickel 88%. During the seven months of operation (from June to December of 2021), the average round-trip efficiency values were 93% (lithium-ion), 85% (lead-acid) and 81% (sodium-nickel). These numbers are in accordance with values found in literature that show 90-95% for lithium-ion, 80-85% for lead acid and 75-90% for sodium-nickel [151].

A.5 Conclusions

This chapter presented the practical implementation of a single-controllable MG based on commercial devices and open-source software. This approach creates possibilities for greater developments in MG labs at universities, allowing more interaction between researchers and students with technology. The setup was validated under typical operating conditions, highlighting its capability to provide ancillary services at the point of the MG connection with the upstream grid. The battery banks reached their minimum SOC values at about the same instant in time. The lithium-ion battery showed the best

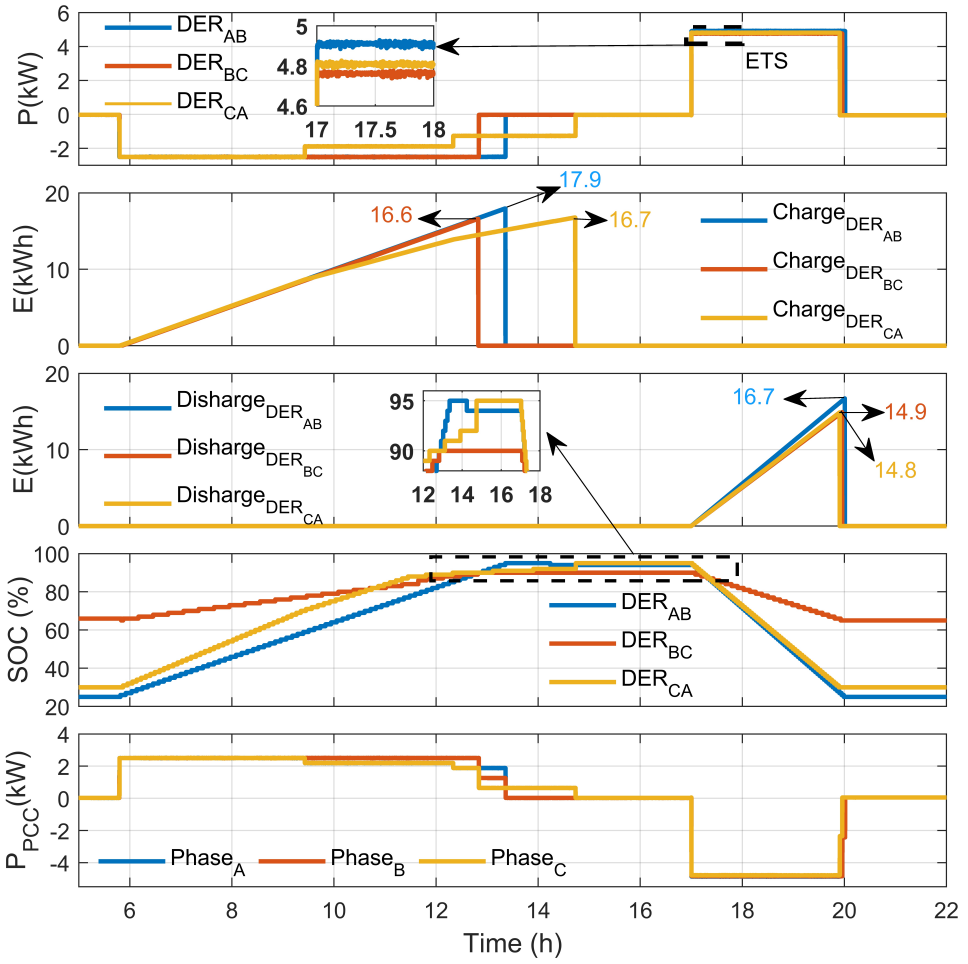

Figure A.3: Results of the energy time shifting operation: DER power, charged DER energy, discharged DER energy and SOC value during the energy time shift using three different battery banks: lithium-ion (DERab), lead-acid (DERbc) and sodium-nickel (DERca).

performance in terms of round-trip efficiency, 93% over 85% (lead-acid) and 81% (sodium-nickel). Lithium-ion battery technology also showed the best compromise between market availability, cost, energy density and usability. The centralized MG controller based on the MPBC was deployed using the Node-RED programming tool in a Raspberry PI. This combination made possible a relatively fast prototyping of the microgrid central controller and the supervisor, as well as easy interaction with the Modbus communication protocol. However, for applications that require greater processing power as well as reliability and redundancy in the central control, the use of programmable logic controllers (PLCs) appears to be a good option. In order to update the power variables through the ModBus communication port, the SMA Sunny Island inverter inherits a delay of about one minute. It limits the MG response time on the order of a few minutes, which is quite reasonable for services based on steady-state quantities, rather than on dynamic services as the reactive current support at the voltage level to create virtual inertia.